

THE TWO-DIMENSIONAL DEVELOPMENT AND ANALYSIS OF
BLADE PROFILES HAVING LARGE TURNING ANGLES

THE TWO-DIMENSIONAL DEVELOPMENT AND ANALYSIS OF
BLADE PROFILES HAVING LARGE TURNING ANGLES

by

RAMESH KUMAR MALHOTRA, B.Sc., B.Tech.

Submitted to the Faculty of Graduate Studies
in Partial Fulfilment of the Requirements
for the Degree
Master of Engineering

McMaster University

March 1971

MASTER OF ENGINEERING (1971)
(Mechanical Engineering)

McMASTER UNIVERSITY
Hamilton, Ontario.

TITLE: The Two-Dimensional Development and Analysis of Blade Profiles having Large Turning Angles.

AUTHOR: Ramesh Kumar Malhotra, B.Sc., B.Tech. (I.I.T., Madras).

SUPERVISOR: Professor J. H. T. Wade.

NUMBER OF PAGES: (ix), 127.

SCOPE AND CONTENTS:

The advances in gas turbine technology in recent years has focussed attention on problems associated with the attainment of high work output. This led to the consideration of high work output per blade, and thereby to the consideration of designing the blades with large turning angles.

A detailed step by step computational method is presented for the design of two dimensional blades of total turning angles 140° , $128^\circ-30'$, and 115° with a range of lift coefficients as defined by Zweifel of .8, 1.0, and 1.2 for each blade. The blade profiles thus obtained are based on the assumption of flow being irrotational, compressible, steady and the fluid being inviscid. The programme allows the calculation of the pressure distribution over both the suction and pressure surfaces and at any point in the passage. Considerable attention was given to the magnitude of the pressure gradient on the suction surface so as to reduce and where possible eliminate the possibility of separation. The blade's profile, pressure distribution, pressure gradients and velocity triangles are drawn for each set of blades. The theoretical performance of the blades has been examined over a range of incidence angles from zero to nine degrees.

ACKNOWLEDGEMENTS

My sincere gratitude and thanks are due to Dr. J. H. T. Wade for providing constant guidance and inspiration throughout the study. The author is grateful to Dr. D. A. J. Millar of Carleton University for his valuable suggestions.

The financial support provided through the National Research Council Grant A 1585 is gratefully acknowledged.

TABLE OF CONTENTS

	PAGE	
CHAPTER 1:	INTRODUCTION	1
CHAPTER 2:	Literature Survey	3
CHAPTER 3:	Performance and Design Considerations.	13
3.1	Turbine Losses	13
3.2	Preliminary Aspects of Design.	15
3.3	Blade Profile Shape.	19
3.4	Trailing Edge Thickness and Form.	25
3.5	Mechanical Design Aspects.	34
3.6	Materials for Turbine Blades.	36
CHAPTER 4:	Theoretical Analysis and Blade Profile Construction.	38
4.1	Design Procedure.	38
4.2	Method of Investigation in the Present Study.	40
4.3	Power Estimation from Velocity Triangles.	40
4.4	Profile Construction.	44
4.5	Pressure Distribution Analysis by the Method of Orthogonals.	54
4.6	Construction of the Orthogonals.	57
4.7	Analytic Solution of Momentum Equations.	60
4.8	Development of the Programme.	65
4.9	Loss Distribution along the Passage.	69
CHAPTER 5:	Results and Discussion.	71

		PAGE
CHAPTER 6:	CONCLUSIONS.	78
REFERENCES		80
ILLUSTRATIONS		
APPENDIX		
A.	Curvature Distribution as a Function of Blade Angles.	114
B.	Data Pertinent to Blades.	116
C.	Sample Calculations.	117
D.	The Computer Programme for Pressure Distribution.	118
D.1	List of Symbols Used.	119
D.2	Details of Programme.	121

NOMENCLATURE

<u>Arabic Symbols</u>	<u>Description</u>	<u>Units</u>
b	Axial Chord	inch
C	Curvature	1/inch
C_L	Lift Coefficient "defined by Zweifel" (See Page 6)	
c_p	Specific Heat at Constant Pressure	B.T.U./ °R Lb.
F_a	Axial force	Lbf
F_b	Bending force	Lbf
F_c	Centifugal force.	Lbf
g	Gravitational Constant	ft/sec ²
i	Incidence, Attack	degrees
J	Mechanical Equivalent of Heat	Lbf/B.T.U.
L.E.R.	Leading Edge Radius	inch
M	Mach Number	
m	Mass/Volume	Lbm/in ³
\dot{m}	Mass Flow Rate	Lbm/sec
n	Distance along Orthogonal Line	inch
n_o	Orthogonal Length	inch
O	Throat Opening	inch
p,P	Pressure	Lbf/in ²
r	Radius	inch
R	Radius of Curvature	inch
R_e	Reynolds Number (Based on axial chord length)	
R_g	Gas Constant	Lbf.ft/Lbm °R

s	Distance along Streamline	inch
S	Pitch	inch
T	Temperature	° R
T.A.	Turning Angle	degrees
T.E.R.	Trailing Edge Radius	inch
U	Blade Speed	ft/sec
V	Resultant Velocity	ft/sec
V_A, C_X	Axial Velocity	ft/sec
V_T, C_Y	Tangential Velocity	ft/sec
W	Relative Velocity	ft/sec
\dot{w}	Weight Flow Rate	Lbf/sec
x, y	Rectangular Co-ordinate Axis	
Y_p	Profile Loss Coefficient	
Z	Mass Flow Rate/Unit Area	Lbm/sec ft ²

Greek Symbols

ϵ	Trailing Edge Thickness	inch
ρ	Density	Lbm/ft ³
θ	Angular Position	degrees
α	Blade Angle	degrees
γ	Ratio of Specific Heats, $\gamma=1.40$.	
δ	Deviation Angle	degrees
ϕ	Potential Function	
ψ	Stream Function	

Subscripts

1	Inlet Section
2	Outlet Section
s	Suction Surface
p	Pressure Surface
o	Stagnation
mid	Midstream
rel	Relative
atm	Atmosphere

LIST OF FIGURES

- 2.1 Pressure distribution and velocities representation.
- 3.1 Representation of losses.
- 3.2 Variation in profile loss coefficient with incidence for typical turbine blades.
- 3.3 Blade nomenclature.
- 3.4 Variation of expansion-energy coefficient with design deflection angle.
- 3.5 Variation of incidence coefficient with incidence angle.
- 3.6 Variation of profile loss with Reynolds number.
- 3.7 Variation of blade loss with Mach number.
- 3.8 Effect of trailing edge thickness on flow direction.
- 3.9 Effect of trailing edge thickness on outlet deviation angle.
- 3.10 Calculated effect of trailing edge thickness on profile loss.
- 3.11 Effect of trailing edge curvature on profile loss.
- 3.12 Effect of trailing edge curvature on deviation.
- 3.13 Representation of blade forces.
- 4.1 Blade row and velocity triangles.
- 4.2 Thrust resolution.
- 4.3 Zweifel's blade nomenclature.
- 4.4 Construction of blade profile.
- 4.5 Variation of flow deviation with exit Mach number.
- 4.6 Plot of $\frac{b}{R_s}$ versus $\frac{x}{b}$.
- 4.7 Approximate channel width for curved channels.
- 4.8 Three dimensional orthogonal surface.
- 4.9 Construction of an orthogonal line.

1. Histogram showing the proposed variation of curvature of suction surface versus axial chord distance of turbine blade with turning angle 115° .
2. Histogram showing the proposed variation of curvature of suction surface versus axial chord distance of turbine blade with turning angle $128^\circ-30'$.
3. Histogram showing the proposed variation of curvature of suction surface versus axial chord distance of turbine blade with turning angle 140° .
- 4.(a,b,c) Blade profiles of turning angle 115° .
- 5.(a,b,c) Blade profiles of turning angle $128^\circ-30'$.
- 6.(a,b,c) Blade profiles of turning angle 140° .
7. Pressure distributions around blades of turning angle 115° .
8. Pressure distributions around blades of turning angle $128^\circ-30'$.
9. Pressure distributions around blades of turning angle 140° .
10. Variation of $\frac{dp}{ds}$ versus s of blade turning angle 115° .
11. Variation of $\frac{dp}{ds}$ versus s of blade turning angle $128^\circ-30'$.
12. Variation of $\frac{dp}{ds}$ versus s of blade turning angle 140° .
13. Velocity triangles of blade turning angle 115° .
14. Velocity triangles of blade turning angle $128^\circ-30'$.
15. Velocity triangles of blade turning angle 140° .
- 16.(a,b,c) Pressure distributions around turbine blade of turning angle 115° as a function of incidence angle for constant lift coefficient.
- 17.(a,b,c) Pressure distributions around turbine blade of turning angle $128^\circ-30'$ as a function of incidence angle for constant lift coefficient.
- 18.(a,b,c) Pressure distributions around turbine blade of turning angle 140° as a function of incidence angle for constant lift coefficient.
19. Pressure distribution along an orthogonal of blade with turning angle 115° , lift coefficient = .8.

CHAPTER 1

INTRODUCTION

The problem of increasing the power developed per blade involves the use of large deflection angle turbine blades. A large turning angle introduces the problem of flow over a rapid convergence of the contour of the annulus which has a pronounced effect upon the design of blade shape and flow passage. The axial velocity at the inlet section increases as the turning angle increases for symmetrical blades which cause excessively high local velocities in the flow passage. Experience has shown that the adverse pressure gradients occur over the suction surface of all blades regardless of turning angle but this problem becomes even more severe with large turning angle blades. Present trends show that large turning angle blades can be operated at high pressure ratios possibly as high as 6:1, but with the high pressure ratio one obtains regions of high Mach numbers, the opportunity of shock induced separation and the blade design, taking into account these further effects, is much more difficult.

This study is an extension of the potential flow analysis used in the design of small turning angle blades. It is understood that to solve the problem fully the boundary layer development around the blades needs to be taken into account. However, because of the physical size of these blades the boundary layer is assumed to be thin and a very good approximation of the passage shape can be made by neglecting the boundary layer displacement thickness.

The present programme allows the engineer to modify the pressure distribution over the blade surface as to achieve significant changes in both the magnitude and the fraction of the chord exposed to the adverse pressure gradient.

This thesis presents the theoretical design of turbine blades all of which are basically of the same family with turning angles 140° , $128^\circ-30'$ and 115° and in which the lift coefficients as defined by Zweifel was varied from .8 to 1.2.

CHAPTER 2

LITERATURE SURVEY

In the beginning, turbines were designed on the assumption of one-dimensional flow through the blade passages. The development of two-dimensional flow theories started in the 1920's when axial compressor blades began to be designed by considering each blade as an isolated airfoil. Tyler [1] and Howell [2] described the application of airfoil theory to propellers and fans and the development of theories of two-dimensional flow through cascades or airfoil lattices.

Turbine blades are normally designed by selecting the spacing by one or more of the empirical rules which have been evolved in the past, and then the turbine channels are designed.

Stodola [3], as early as 1891, suggested that the best spacing is given by $\frac{r}{2} \cos \alpha$, where r is the pressure side radius of curvature of the blade and α is the blade turning angle. He utilized the fact that the space or pitch/ axial chord = 0.5 in all his design work. His experimental results showed that this pitch/axial chord ratio could be increased without loss in performance.

Zweifel [4] observed that the losses from turbine blades were a function of tangential force coefficient. The tangential force coefficient (known also as blade loading coefficient or lift coefficient) was defined as the ratio of the tangential force (F_y) to the theoretical tangential force that could be achieved without adverse pressure gradient ($F_{y \text{ max}}$).

Fig. 2.1 indicates a typical pressure distribution around an isolated blade, curves P and S corresponding to the pressure (or concave) side and suction (or convex) side respectively. The pressures are projected parallel to the blade front such that the area enclosed between curves S and P represent the actual blade loading per unit height. With reference to Fig. 2.1 (c) which represents the velocities at both inlet and outlet sections, Zweifel [4] showed that tangential force (F_y) is given by the relation,

$$F_y = \rho S C_x (C_{y2} - C_{y1})$$

The conditions for the ideal load are fulfilled by p_0 acting over the entire P surface and p_2 acting over the entire S surface. Zweifel obtained an expression for ideal tangential force ($F_y \text{ max}$) given by the relation

$$F_y \text{ max} = \frac{1}{2} \rho w_2^2 b$$

The ratio of these two forces $\frac{F_y}{F_y \text{ max}}$ is defined as the lift coefficient and can be written as

$$\text{Lift Coefficient} = \frac{F_y}{F_y \text{ max}} = \frac{\rho S C_x (C_{y2} - C_{y1})}{\frac{1}{2} w_2^2 \rho b}$$

and using the trigonometric relations as described by Zweifel it can be shown that

$$C_x = w_2 \cos \alpha_2$$

$$C_{y2} = w_2 \sin \alpha_2$$

$$C_{y1} = w_1 \sin \alpha_1$$

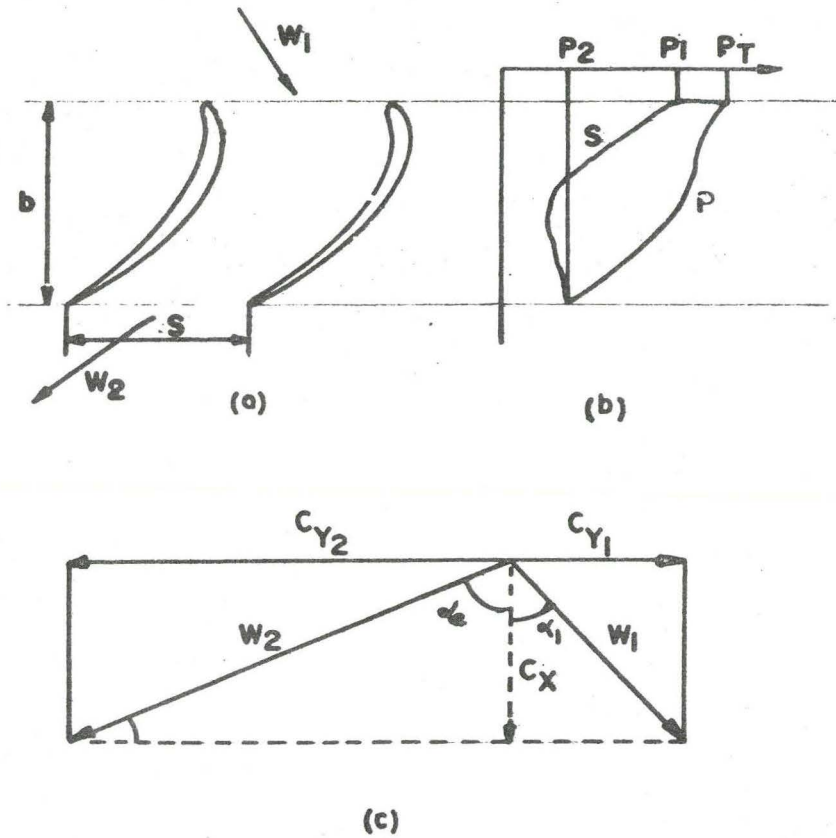


Figure 2.1. Pressure Distribution and Velocity Representation.

$$\therefore \text{Lift Coefficient} = 2 \frac{S}{b} \cos^2 \alpha_2 (\tan \alpha_2 - \tan \alpha_1)$$

or

$$C_L = 2 S/b \cos^2 \alpha_2 (\tan \alpha_2 - \tan \alpha_1)$$

Ainley and Mathieson [5] provided curves for the loss coefficient against pitch/chord ratio, fluid outlet angle and blade thickness/chord ratio. The profile loss coefficient in this paper is defined as the loss in stagnation pressure across the blade row, divided by the difference between stagnation and static pressures at blade exit section. Their work concluded that the loss coefficient for blades could also vary as the square of the fluid inlet angle. The various pitch/chord ratios were calculated by these authors from the experimental data obtained by a curve fitting technique for a wide range of inlet and outlet angles.

A review of the literature shows that early designs relied heavily on the use of experimental two-dimensional cascade results in which profiles of different shapes such as circular, parabolic (separately or in combination) or in fact modified NACA or ARC profiles were tested under a variety of conditions including changes in pitch/chord ratio, stagger angle and blade thickness. One might call this the phenomenological development of turbine design. The second method is essentially concerned with passage design in which an analysis is made of the potential flow through a lattice of two-dimensional turbine blade shapes.

Stanitz [6] method is useful for the solution of indirect problems which result in the accurate design of a blade cascade in compressible flow.

It consists of specifying the velocity distribution as a function of distance along the two channel walls and specifying the difference in stream function across the blade spacing. This is in effect a decision on the fluid flow through the blade channel. Finally, Stantiz solves the nonlinear equations by a relaxation technique, utilizing the boundary conditions for upstream and downstream of the flow passage.

Stantiz [7] is responsible for the development of another more rapid but approximate method. It represents the analysis generally for the compressible flow through turbomachines of varying annulus area, in which the meridional streamlines may change their radial position. It is interpreted for the two-dimensional compressible design of a turbine blade as follows: velocities on the blade suction and pressure surfaces are specified as a function of the axial co-ordinate "x". Using the energy equation and isentropic relations, the blade profile is fully developed as a first approximation using only the dependent variable "x".

In the second approximation it is assumed that the flow conditions vary linearly across the channel in the y-direction. The pitch/chord ratio is determined from the first approximation and streamlines are drawn. The mean tangential velocity distribution is again determined and finally the blade profile is developed by combining both the x and y solutions.

George R. Costello, Robert L. Cummings and John T. Sinnette, Jr. [8] have presented a method for computing blade profiles with prescribed velocity distributions based on the assumption that the pressure volume relationship is linear. The method uses the prescribed velocity distribution and compatible free-stream conditions to determine a mapping function. This transforms an incompressible flow about the unit circle into an exact compressible flow, with

a linear pressure-volume relationship, about a cascade of blades having the desired velocity distribution. In this method the relation between the actual fluid and the fluid with the linear pressure volume relation must be approximated so that the required velocity distribution and free stream conditions for the second fluid may be determined.

Another report [9] by the same authors has been presented in which the magnitude of the velocities in the two fluids are assumed to be proportional. The constant of proportionality is determined by the continuity equation using the same upstream and downstream flow angles for the two fluids. It includes adjustment of the prescribed velocity distribution to satisfy the restrictions on the mapping function.

A method which apparently offers a solution to both the direct and indirect problems of compressible flow past a cascade of arbitrary airfoils is presented by Chung-Hua Wu and Curtis A. Brown [10]. In both problems calculation is first made for the flow along a particular streamline in the channel formed by two neighbouring blades. (Preferably the mean streamline which divides the mass flow in the channel into two equal parts.) Here the close relationship between the shape of the blade camber line and the mean streamline of the passage and that between the variations in the channel width and the specific mass flow are employed. The flow is then extended in the pitch or "Y" direction by the use of Taylor series, where successive terms are obtained by the use of the equations of continuity and momentum.

In irrotational, incompressible flow the method of conformal transformation may be used to give solutions to the flow equations $\Delta^2 \psi$, $\Delta^2 \phi = 0$, where ϕ is the potential function and ψ is the stream function. If the complex potential $W = \phi + i\psi$ is known in a plane, the flow in the

physical plane can be determined if the transformation from the given plane to the physical plane is known. This is the general basis of all conformal transformations. Kraft [11] has also described his development of the laminar airfoil type turbine blade for impulse section using the conformal transformation technique. For a conventional turbine blade, as with a standard aerofoil section there is a pressure increase on the convex surface and a pressure decrease on the concave surface. The boundary layer faces the adverse pressure gradient over the rear part of the chord on the convex surface. For a small turning angle, Kraft designed a blade shape to produce substantially constant pressure over the suction surface.

The method of vortex singularities is useful for solving the indirect problem of incompressible flow through given sections of highly cambered blades. The potential function describing the flow associated with a distributed series of sources, sinks and vortices is found and combined with the uniform stream flow to give the flow past the airfoil shape. An elegant solution of the cascade problem was developed by Martensen [12] using vortex singularities. Vortices are distributed along the blade surface and the method is not limited to low cambers only. He formulated an integral equation of these sources, sinks and point vortices which describes the distribution of velocity on the blade surfaces. This equation was solved using a digital computer. In this method the problem lies in the determination of sources, sink and vortex distributions.

F. Baumgartner and R. Amsler [13] have presented a blade design method which was used to determine the shape of stationary nozzles and rotor blades for an axial flow type turbine. The main feature of the blade

design method consists of selecting a suitable airfoil and shaping it into a blade profile such that momentum requirements are satisfied, together with its predetermined requirements of optimum blade load distribution, flow rate and blade stress. However, the method is somewhat of a trial and error method unless one has a strong feeling for the proper blade proportions.

Horlock [14] describes a method to design a blade shape to give a specified velocity distribution. He describes the potential function and a stream function to represent the flow. He then finds the transformation function to describe the flow around the blade. The mathematics involved is complicated but the solution gives good results for the analysis of incompressible flow.

In the past, a free vortex flow pattern was in use for the design of blade shape. This type of flow requires the least amount of kinetic energy for a given flow rate and therefore represents the most stable flow condition. In a free vortex the tangential velocity components of the stream particles are inversely proportional to their radial distance from the centre line, the axial velocity components being constant across the whole flow area. This type of flow delivers equal amounts of work at any radial station. Analysis of turbine performance data based on the free vortex design approach indicated that it was desirable to adjust the airfoil designs at all radial stations in order to relieve the root and tip flow conditions.

T. E. Dorman, H. Welna, and R. W. Lindauf [15] have developed a design technique known as a controlled-vortex design system. The controlled

vortex design system permits the designer to alter and optimize each airfoil section designed by varying the main stream flow pattern. Controlled vortex turbines have demonstrated performance superior to equivalent free vortex turbines. The controlled-vortex design procedure has been applied to raise the root reaction without raising the tip reaction and without making significant changes in exit swirl distribution. Several experimental tests have been done with controlled vortex turbine which showed the efficiency requirements above those of free vortex turbines. It is now recognized that low root reaction is the fundamental cause of poor root performance because it causes localized root losses. Raising the reaction by means of controlled-vortex techniques can reduce these losses.

The literature survey indicates that methods to design the blade shape can be classified as follows:

- (i) Direct Method
- (ii) Indirect Method

Previous study shows that most of the blades are designed by the direct method. In this method the blade is started from standard airfoil shape and the performance is observed by conducting various experiments. The results of these experiments are analyzed and the blade shape is modified to get the desired output. This method is quite tedious, laborious and not a methodical one. Some of the authors have done work on the design of blades by the indirect method but encounter problems while defining the velocity distribution, the transformation function, the sources, sinks and vortices, etc. (which were very difficult to define). In other words, the different design procedures of all previous studies did not conform to the same "State of the Art". Hence it is

quite difficult to design a blade shape and then predict the performance.

The study done in this thesis is an extension of the free-vortex design but differs in that the blade's curvature distribution for pressure, suction surfaces and orthogonal lengths are defined properly as described in Chapter 4. Finally, the pressure distribution is computed by utilizing the compressible equations, satisfying the continuity equation and solving the momentum equations simultaneously at each and every station.

CHAPTER 3

PERFORMANCE AND DESIGN CONSIDERATIONS

3.1 Turbine Losses

The performance of a turbine is evaluated by the losses embodied within it. The main types of losses in turbines can be classified under the following headings:

- (1) Skin friction losses.
- (2) Profile losses associated with the effect of profile shape.
- (3) Secondary losses.
- (4) Separation losses.

Skin friction losses are directly due to shear stresses acting along the surface in the direction of the component of the fluid motion which is parallel to the blade. These stresses in turn depend on the local velocity conditions, and the nature of the surface of the blade in contact with the fluid. The Zweifel criteria is one method of determining the optimum pitch/chord ratio for keeping this loss to a minimum.

It is known that the gas passing through a stationary row of blades experiences some average loss in stagnation pressure caused by the blade wakes. If the blades are moving, a relative stagnation pressure can still be defined in terms of the pressure and relative velocity but radial streamline movements cause an increase in this relative stagnation pressure. The pressure loss may then be defined as the difference between the ideal frictionless relative stagnation pressure at the exit and the

actual value. In the case of axial flow machinery, it is usual to apply data from stationary blade tests to analyze rotating blade performance, the justification being that energy addition relative to the rotating row is small. Profile losses can be related to physical blade properties, such as blade pitch, thickness and throat opening and to gas incidence. They are also related more fundamentally to the form of velocity which controls the nature of the boundary layers which form the blade wake.

The nature of the secondary flow is illustrated in Fig. 3.1. Because of the turning of the stream, there is a pressure gradient across the blade passage to balance the centrifugal forces. There is a relatively high pressure on the lower surface and a low pressure on the upper surface of the blade. Near the walls the velocities are small so that the required pressure gradient is reduced, which gives, on the lower surface, a smaller pressure near the wall than in the middle of the blade passage with a resulting flow in the form of circulatory or eddy flow between adjacent blades. This is generally called secondary flow. The losses occurring with such type of flows are termed as secondary losses and are usually about the same magnitude as the profile losses. This loss is related most closely to mean acceleration of the gas in passing through the blades.

In the case of turbine blades, if the reaction blades or a combination of reaction and impulse are used, the pressure decreases up to the point of maximum curvature where velocity is also maximum and then the pressure starts increasing (i.e., the pressure gradient is positive in this region of the blade profile). Thus the fluid in the boundary layer is further retarded and, if the adverse pressure gradient is too severe, the fluid near the wall reverses its direction and separates from

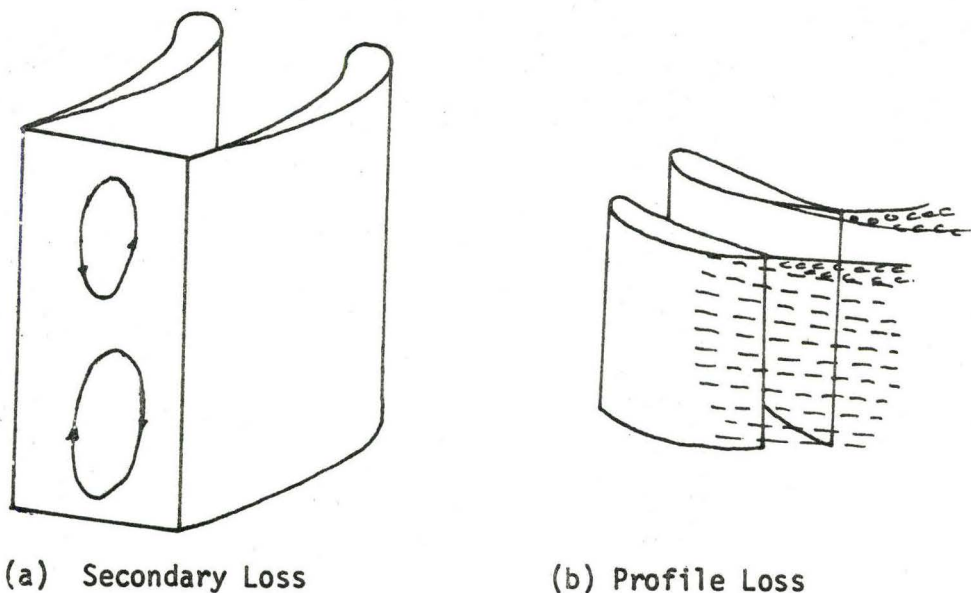


Figure 3.1. Representation of Losses.

the surface. The eddies and separation cause considerable loss of useful energy which is termed as separation loss. This loss is mostly dependent on the curvature distribution of the suction surface the pressure surface and the passage width.

3.2 Preliminary Aspects of Design

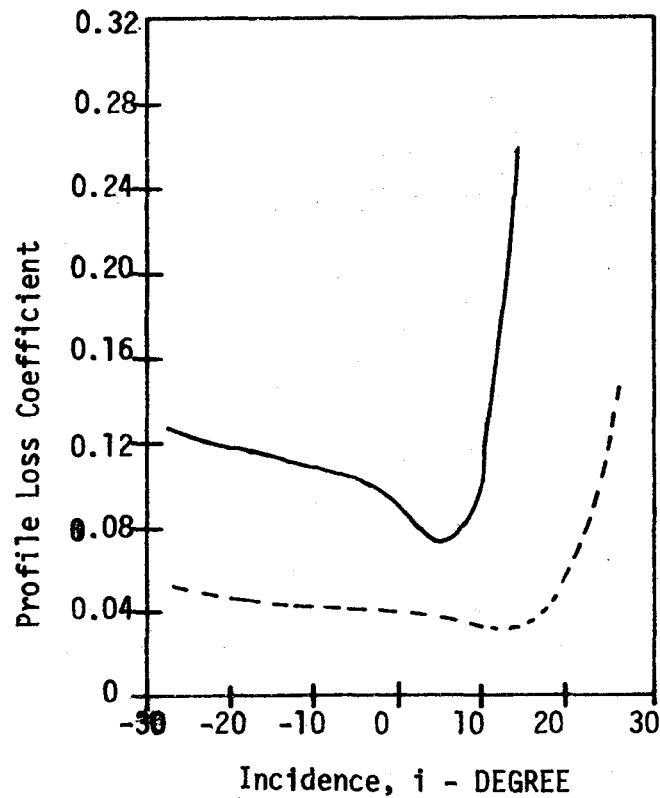
The questions that face a designer may be summarized broadly as follows:

- (1) What type of turbine, i.e., impulse or reaction turbine should be designed or combination of both?
- (2) What are the advantages of turbines equipped with blading of high or low deflection with varying degree of reaction?

- (3) What is the effect of blade profile form and pitch?
- (4) What effects do fluid compressibility and Reynolds numbers have on the aerodynamic characteristics?
- (5) What are the effects due to such factors as tip clearance, shrouding, axial spacing between blade rows, blade length/chord ratio, blade thickness from mechanical strength aspects?

One needs to know the effect of each variable on the performance of a turbine in order to design the blades to achieve the maximum attainable efficiencies. Some of these problems can be tackled only by experiment, unfortunately, the majority remain unsolved such as tip clearance, shrouding, etc. The results, used in the design of blades, are obtained from a tunnel which refers to a two-dimensional flow through a row of blades and are not necessarily immediately applicable to the vortex form of flow that actually occurs within a turbine. Nevertheless, the results help a designer to gain some idea of the merits and demerits of varying types of blades, and to design blades producing the particular gas flows, and deflexions thereof, which he requires.

D. G. Ainley [16] obtained the results from a typical test on an impulse section and on a high reaction section as shown in Fig. 3.2. The range of incidence over which both blades will operate without excessive variation in loss is quite large, but the reaction blades have the greater working range of incidence and the lowest loss. When a large family of turbine blade sections is tested, it is found that the minimum loss coefficient of a cascade invariably increases as the reaction of the blade is decreased (reaction in this sense is a qualitative



— Impulse blade
 - - - Reaction Blade

$$\text{Profile Loss Coefficient} = \frac{P_{\text{TOT.Inlet}} - P_{\text{TOT.Outlet}}}{P_{\text{TOT.Outlet}} - P_{\text{STAT.Outlet}}}$$

Figure 3.2 Variation in Profile Loss with Incidence for typical turbine blades (from Ainley [16]).

expression, and refers to the acceleration imparted to the gas as it flows through the blades and the accompanying drop in the static pressure). He also showed that the efficiencies of a reaction stage are likely to be considerably greater than those of an impulse turbine stage, particularly if the work output of the impulse stage, or the gas deflexion in the rotor blade is very high.

It is the shape of the blade which determines the form of the flow passages and the energy transferred from the fluid to the rotor is dependent chiefly on the nature of the flow through these passages. Then, clearly, it is important that careful attention be given to the development of the correct passage shapes.

The flow passages must also provide sufficient annular area to accommodate the entire flow of fluid. An adequate number of blades must be provided to ensure well defined flow passages. Yet the use of too many blades may increase unduly the resistance to flow. Special consideration must be given to the stresses imposed on the turbine blades by the pressures, temperatures, dynamic forces and rotational speeds encountered under all conditions of operation.

The arrangement of the flow passage has a marked effect not only on the efficiency of the turbine but on the manufacturing cost as well. The best design is a harmonious compromise between operating efficiency, size of unit and manufacturing cost. Although there is no reliable and rigid rule in making such a compromise, a great deal of information can be obtained from existing design procedures to assist in the desired aspect.

There is no rational method for laying out the profiles of such conventional reaction blades. However, a few observations are of some

value. The concave side may be nearly of constant radius, while the convex side is usually formed by faired circles in a shape that provides a passage which is always converging. It is of particular importance that the passage never becomes divergent in order to avoid eddy losses which accompany a diverging passage. Normally supersonic velocities are avoided in the flow passages to avoid shock losses, but occasionally it is necessary to introduce them in order to reduce the overall length of the turbine and to use them where high rotational speeds are acceptable.

The number of stages should be kept as small as possible because of weight consideration but should not be so small as to affect markedly the efficiency. Pressure ratios as high as 3:1 and 4:1 are used without seriously lowering efficiency according to design practices. If the average velocity leaving the passage does not exceed the sonic velocity by more than 50%, the convergent passage may be retained with only a slight drop in efficiency. If it is necessary to exceed these limits, then more stages must be employed.

3.3 Blade Profile Shape

For any blade, the required blade angles are fixed, the profile shapes that will most efficiently operate at these angles must be developed. As mentioned before, because of the requirements that dictate high turning angles and Mach number limits for exit and inlet velocities, most blades are of reaction or combination rather than the impulse type. Therefore, the remarks to follow apply more specifically to the reaction type blade. In addition, high turning angle blades with higher outlet blade angles require correspondingly higher chord lengths in order to provide a

sufficiently generous radius of curvature for the channel walls. The so called radius of curvature should be maintained so that the average Mach number over the passage width does not exceed that occurring at the blade throat. This is done in order to prevent local diffusion or adverse pressure gradient with losses and possibly separation. The main velocity in the channel should be constant or steadily increasing in order to avoid the possibility of diffusion in the passage.

An axiom commonly accepted by the aerodynamist asserts that energy losses associated with fluid flows in a curved passage are considerably less when an acceleration is imposed upon the flow than when the flow is accompanied by diffusion. Any diffusion of the flow through the turbine blade rows is particularly undesirable and must, at the design stage be avoided as far as possible. This is because the adverse pressure gradient (arising from the flow diffusion) coupled with large amounts of fluid deflection (usual in turbine blade rows), makes boundary layer separation more than merely possible with the result that large scale losses arise.

The shape of the inner and outer contours of the annulus should be such that a smooth and gradual decrease of annular area is provided in order to ensure against breakaway and excessive boundary layer thickness. The desired contour shape is obtained by minor adjustments of the curvatures at various points. The rapid change of curvature of the contour of the suction surface of the blade section reflects in the pressure distribution in the form of a sudden change of pressure.

It is worth pondering a little upon the effect of space/chord ratio in the turbine blade rows as this is a factor strongly affecting the efficiency. Now if the spacing between the blades is made small, the

fluid then tends to receive the maximum amount of guidance from the blades, but the friction losses will be very large. On the other hand, with the same blades spaced well apart, friction losses are small but, because of poor fluid guidance, the losses resulting from the flow separation are high.

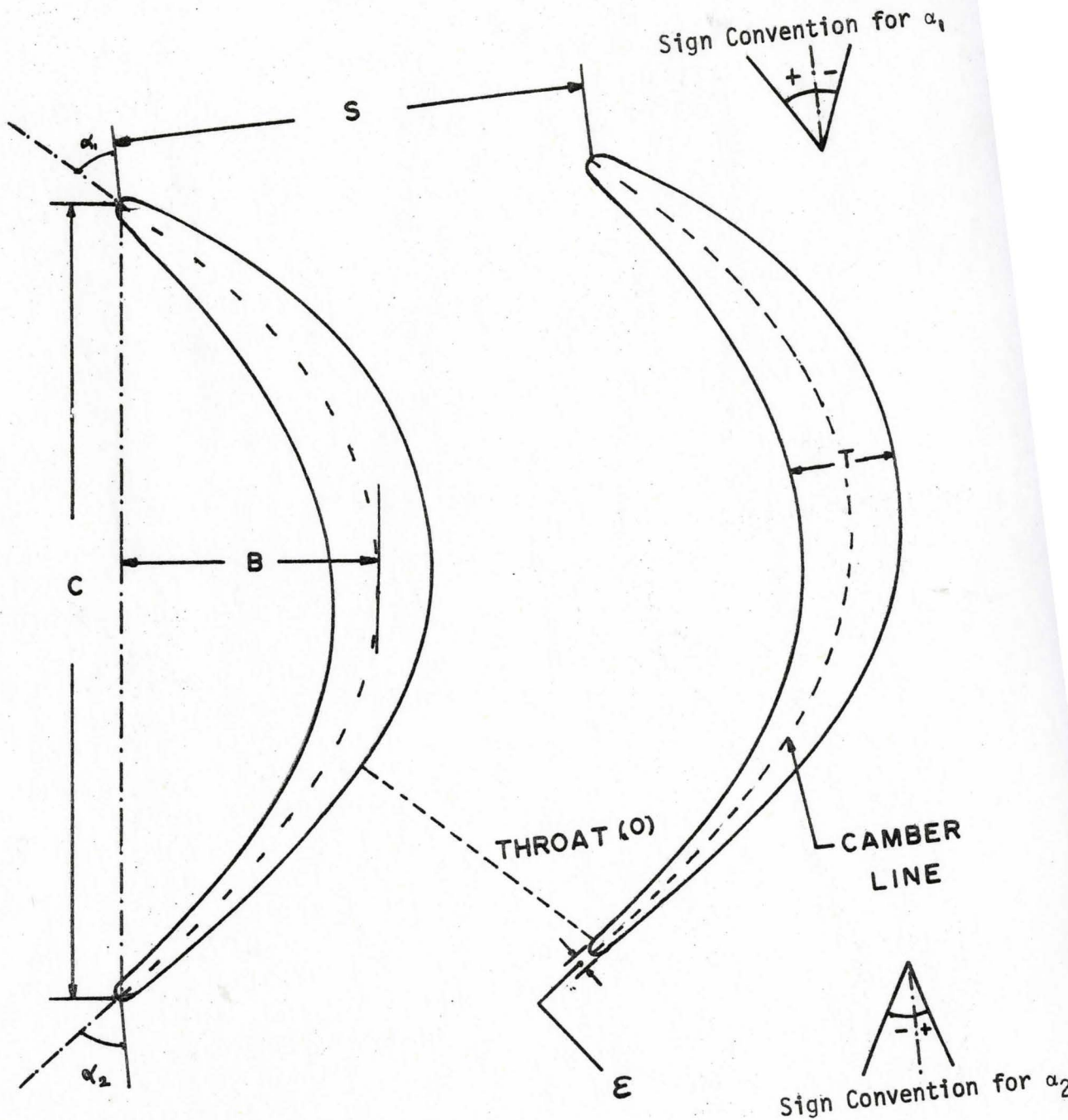
The basic variables in blade ring calculation observed by Emmert [17] are shown in Fig.3.3. The data apply to both fixed or moving blades, provided the velocity magnitudes and directions are taken relative to the blade ring under consideration. The most important quantity required in the blade ring analysis is the effective kinetic energy at the ring outlet. Emmert [17] computed the energy from the following relation.

$$\Delta h e_2 = \phi_\epsilon^2 (\Delta h S_2 + C_i \phi_v^2 \Delta h V_1)$$

where,

- ϕ_ϵ^2 - Expansion-energy coefficient
- C_i - Incidence coefficient
- ϕ_v^2 - Kinetic energy coefficient
- $\Delta h V_1$ - Kinetic energy at inlet
- $\Delta h S_2$ - Isentropic enthalpy drop
- $\Delta h e_2$ - Effective kinetic energy at outlet

The primary loss resulting from turbulence and wall friction within the blade passage is reflected by the expansion energy coefficient. It is observed that the effective energy obtained from a given amount of inlet kinetic energy is supplied by pressure drop. Kinetic energy coefficient is normally assumed to be equal to the expansion energy coefficient.



- S = Blade pitch
- B = Maximum Camber
- C = Chord
- O = Blade opening or throat
- ϵ = Trailing edge thickness
- α_1 = Blade inlet angle
- α_2 = Blade outlet angle
- T = Maximum thickness

Figure 3.3 Blade Nomenclature

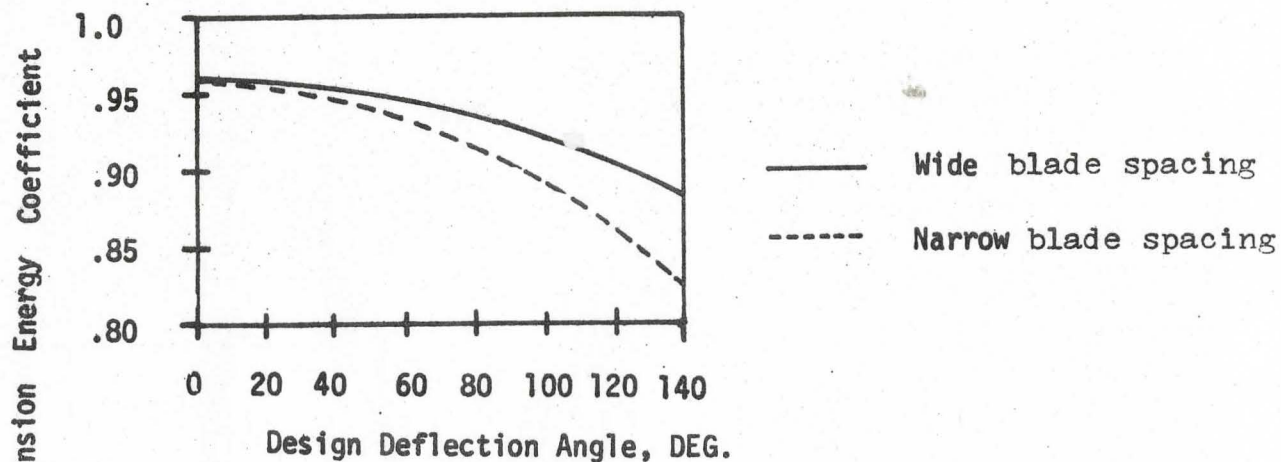


Figure 3.4 Variation of Expansion-Energy Coefficient with Design Deflection Angle (from Emmert [17]).

H. D. Emmert [17] obtained the graph of Expansion Energy Coefficient vs Design Deflection Angle as shown in Fig. 3.4. It can be concluded from this figure that the optimum blade pitch/chord ratio has to be used. When the inlet velocity vector forms a definite incidence angle with reference to the blade leading edge, an additional loss occurs which is evaluated by the Incidence coefficient. This coefficient is a function of the blade nose design.

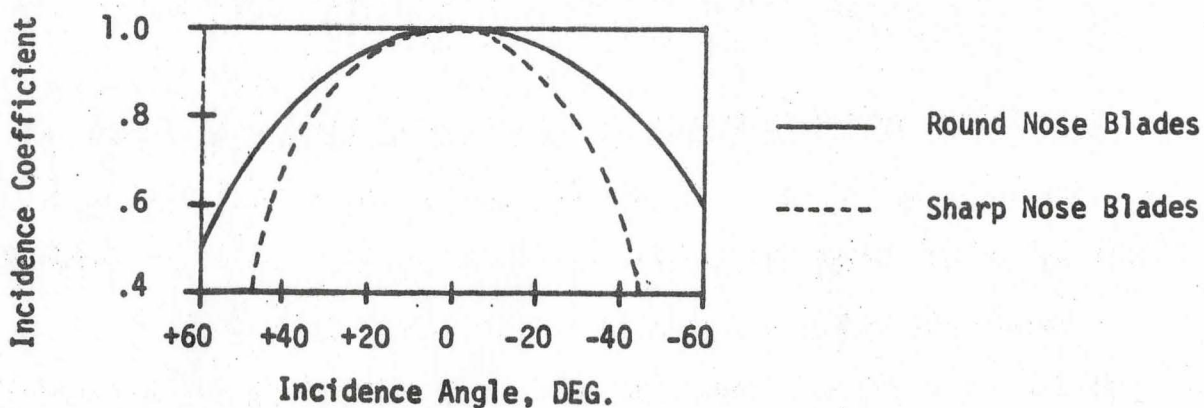


Figure 3.5. Variation of Incidence Coefficient with Incidence Angle (from Emmert [17]).

H. D. Emmert [17] studied the effect of incidence coefficient on the incidence angle as shown in Fig. 3.5. It can be concluded from the Fig. 3.5 that a round nose blade has the greater incidence coefficient than the sharp nose blade. Hence the blade designed should have a round nose to have less losses for equal incidence angles.

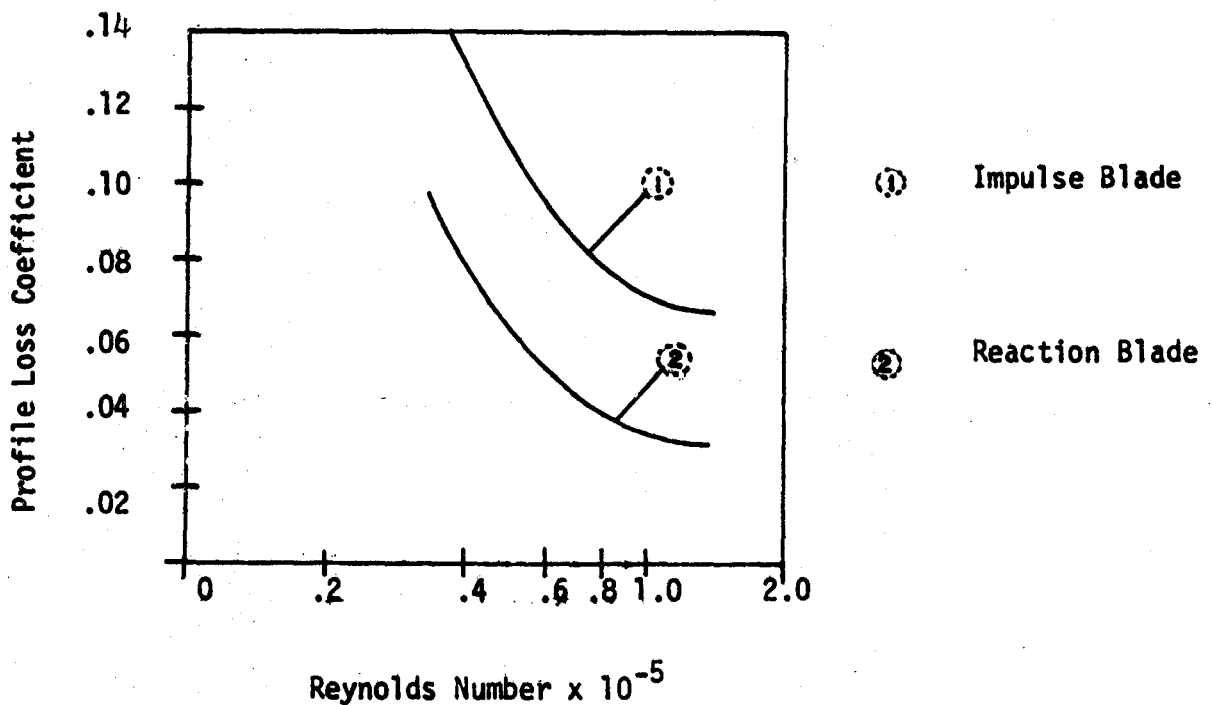


Figure 3.6. Variation of Profile Loss with Reynolds Number (from Emmert [17]).

Figure 3.6 indicates the variation of profile loss coefficient with respect to Reynolds number of the gas flow as obtained by D. G. Ainley [16]. At a fixed incidence the losses in the turbine increase rapidly as the Reynolds number is reduced below about 1.2×10^5 . It shows the proportional rate of increase of profile loss with reduced Reynolds number and when the Reynolds number is less than about 1.2×10^5 the profile

loss is approximately proportional to $Re^{-.5}$. At higher values of Reynolds number, the losses vary at a much lower rate. Hence while designing the blade the variation of losses with Reynolds number should be kept in mind.

3.4 Trailing Edge Thickness and Form

While designing a blade and passage we are faced with the problem of the deviation of the air from the actual blade angles specially at the exit section. To solve this deviation problem the flow pattern has to be analysed, but still further, the corrections such as overturning of the blade for this deviation, in order to be sure to get the work done, should be applied. However, overturning reduces the physical throat area, and if the throat Mach numbers are already close to one, a reduction in weight flow will be involved unless the blade height is increased. This blade height change means a lower axial velocity after the blade and thus affects the velocity diagram.

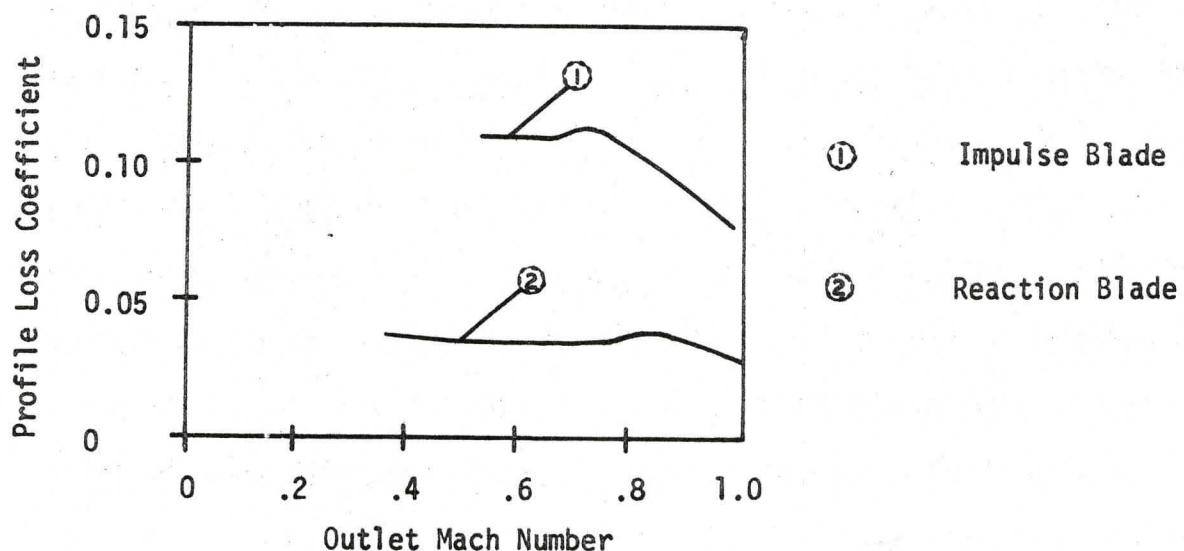


Figure 3.7. Variation of Blade Loss with Mach Number (from Ainley [16]).

As the outlet Mach number is increased the minimum profile loss coefficient varies only slightly until an outlet Mach number .7 to .8 is approached as studied by D. G. Ainley [16] and as shown in Fig. 3.7. At this point a small local shock wave appears on the convex surface of the blade inside the blade passage, causing a thickening of the boundary layers and a slight consequent increase in loss. As the Mach number increases further, the shock wave moves toward the trailing edge, with a corresponding decrease of the length of the blade surface exposed to the thickened boundary layer.

In determining the trailing edge thickness of turbine blades some compromise has to be made between the mechanical strength, reliability and ease of manufacture on one hand, and efficiency on the other. Maximum efficiency calls for as thin a trailing edge as possible, but too thin a trailing edge is particularly undesirable in gas turbine work when high local gas temperatures may easily burn away the very thin trailing edge. Trailing edge thicknesses have to be consistent with the particular manufacturing process to be used and vary from approximately 1 to 10% of throat opening, and leading edge thickness varies from 2 to 12% of pitch which is the common practice in industry [18]. The radius of trailing edges chosen in designing these blades is .011" and this is almost the minimum possible. With a smaller radius it becomes very difficult to hold for machining and even casting becomes very difficult. Moreover, if the trailing edge is too thin the blade trailing edge bends due to gas loads thus giving a wrong outlet angle.

Finite trailing edge thickness may be expected to give rise to pressure losses in much the same manner as a sudden enlargement of a pipe

through which fluid is flowing. The work capacity is closely related to the gas outlet angle and is usually correlated with the throat opening (O).

The following approximate relationship between blade geometry and gas outlet angle is often used as a guidance rule.

$$|\alpha_2| \cong \text{Cos}^{-1} \frac{O}{S} \quad (3.1)$$

where α_2 = gas flow outlet angle.

This relation is stated to be fairly accurate for most turbine blades when the Mach number at the blade exit is near unity. However, at low Mach numbers and large values of outlet angles this equation (3.1) represents considerable error. The actual gas outlet angle is conveniently recorded as a deviation angle (δ) from geometrical outlet angle ($\text{Cos}^{-1}O/S$). Using relation (3.1) and referring to Fig. 3.8

$$\delta = |\text{Cos}^{-1} \frac{O}{S}| - |\alpha_2|$$

$$\tan \alpha_2 = \frac{\tan \alpha_2'}{(1 - \frac{\epsilon'}{S})} \quad (3.2)$$

and

$$\tan \alpha_2' = \frac{\sqrt{(S - \epsilon')^2 - O^2}}{O} \quad (3.3)$$

Combining equations (3.2) and (3.3), the outlet angle can be written

$$\tan \alpha_2 = \frac{[(1 - \frac{\epsilon'}{S})^2 - (\frac{O}{S})^2]^{\frac{1}{2}}}{(1 - \frac{\epsilon'}{S}) \frac{O}{S}}$$

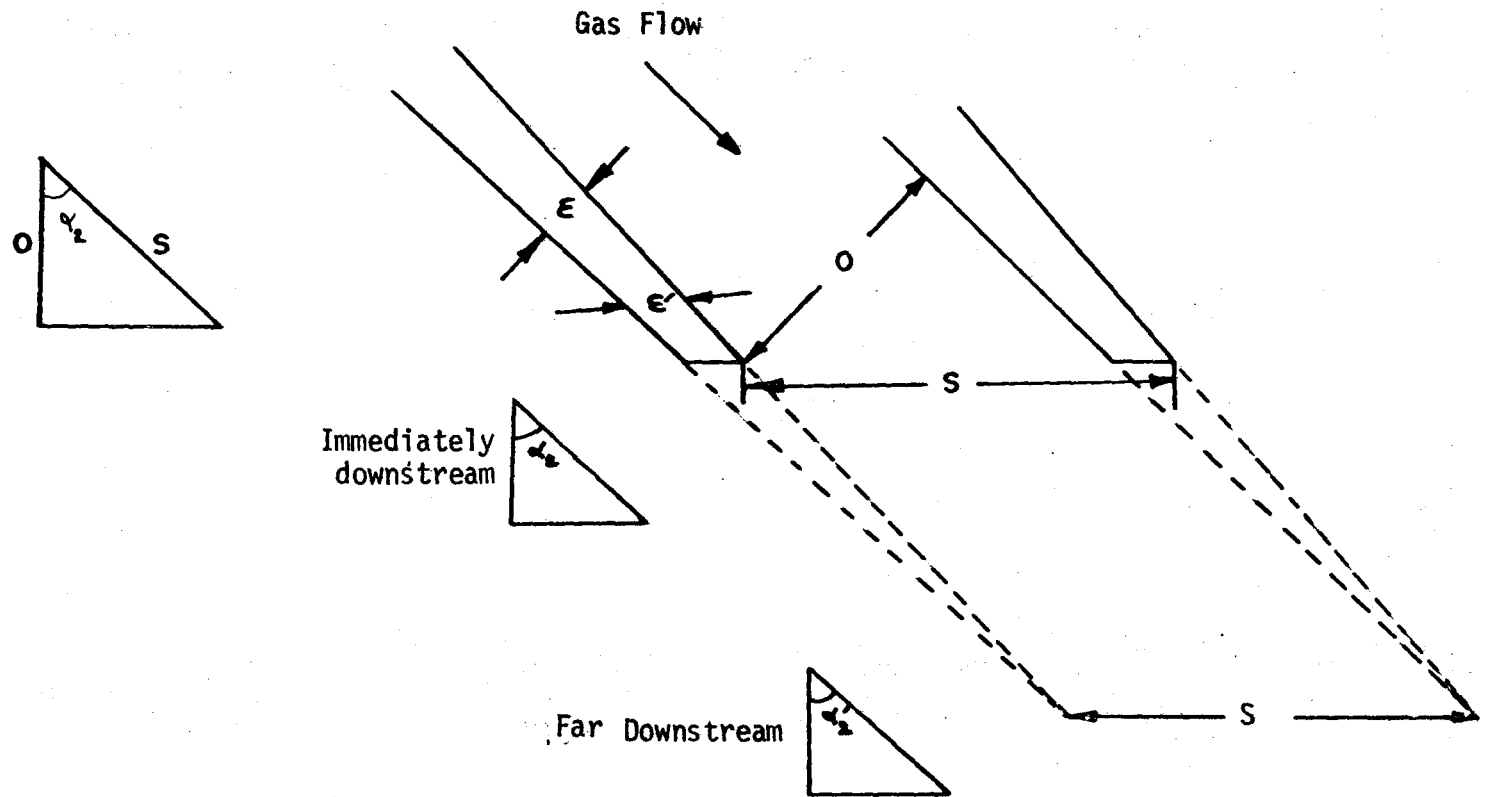


Figure 3.8 Effect of Trailing edge thickness on flow direction.

The deviation angle δ , defined by equation (3.1), then becomes

$$\delta = \cos^{-1} \frac{0}{S} - \tan^{-1} \frac{[(1-\epsilon'/S)^2 - (\frac{0}{S})^2]^{\frac{1}{2}}}{(1-\frac{\epsilon'}{S}) \frac{0}{S}} \quad (3.4)$$

A graph is plotted representing the effect of trailing edge thickness on outlet deviation. It can be seen from this graph that for minimum deviation (δ), the ratio ($\frac{\epsilon}{S}$) should be minimum and the losses encountered go on reducing as the outlet angle is increased. The relationship given by equation (3.4) is represented in the Fig. 3.9. Deviations are usually greater than these values because surface boundary layer presents a blockage to the flow which increases the effective trailing edge thickness of the blading.

Trailing edge thickness losses are deduced in a similar manner to the foregoing analysis.

$$y_p = \left(\frac{\epsilon}{S}\right)^2 \quad (\text{Ref. 19})$$

where y_p = Profile loss coefficient.

Early work has shown that loss increment due to trailing thickness is as presented in Fig. 3.10 by Hawthorne [19]. In this study the loss coefficient for the blades which have been designed has been kept at a minimum.

It has been found in general, that there is nothing to be gained in a practical sense by decreasing the blade trailing edge thickness

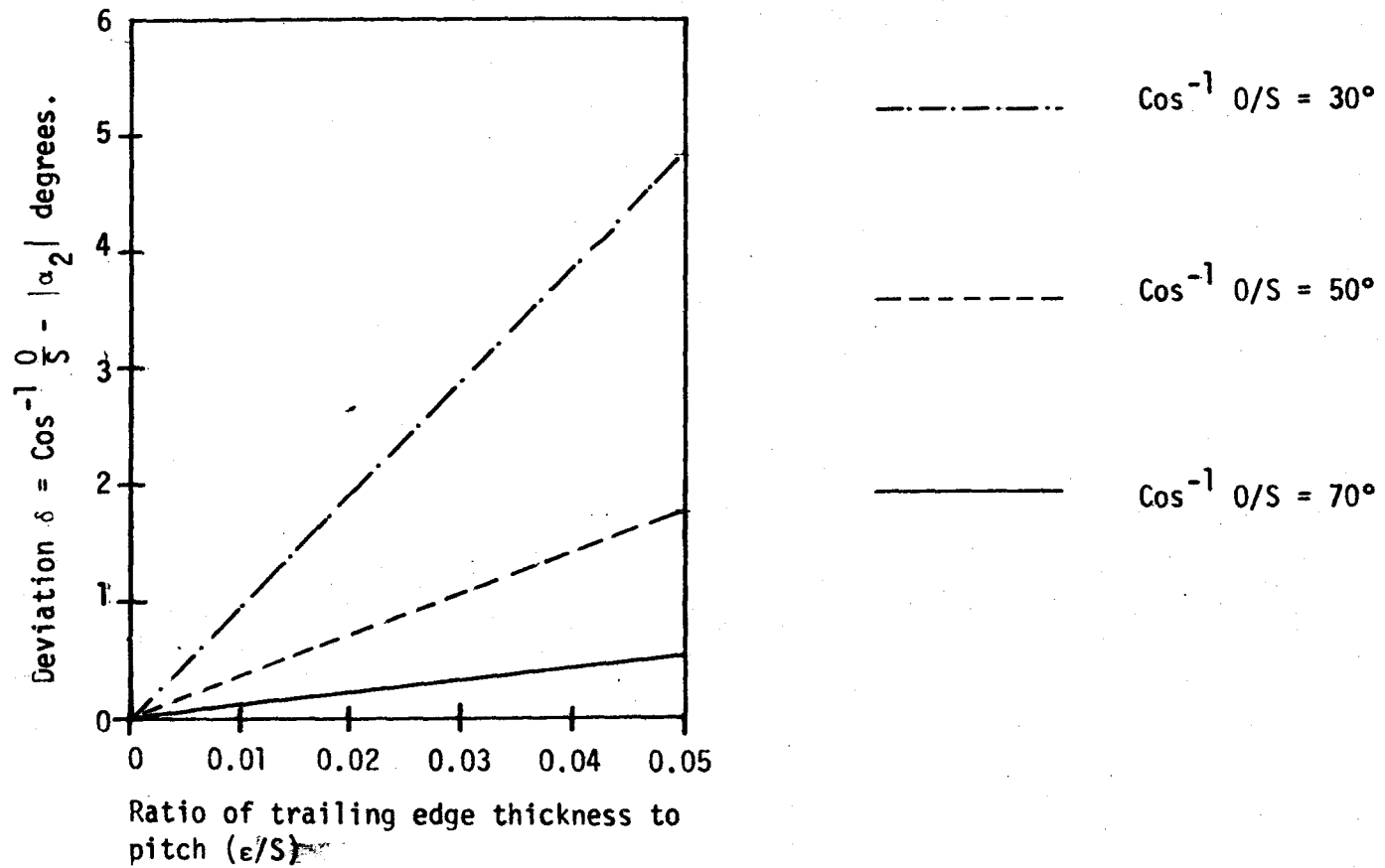


Figure 3.9. Effect of Trailing Edge Thickness on Outlet Deviation Angle.

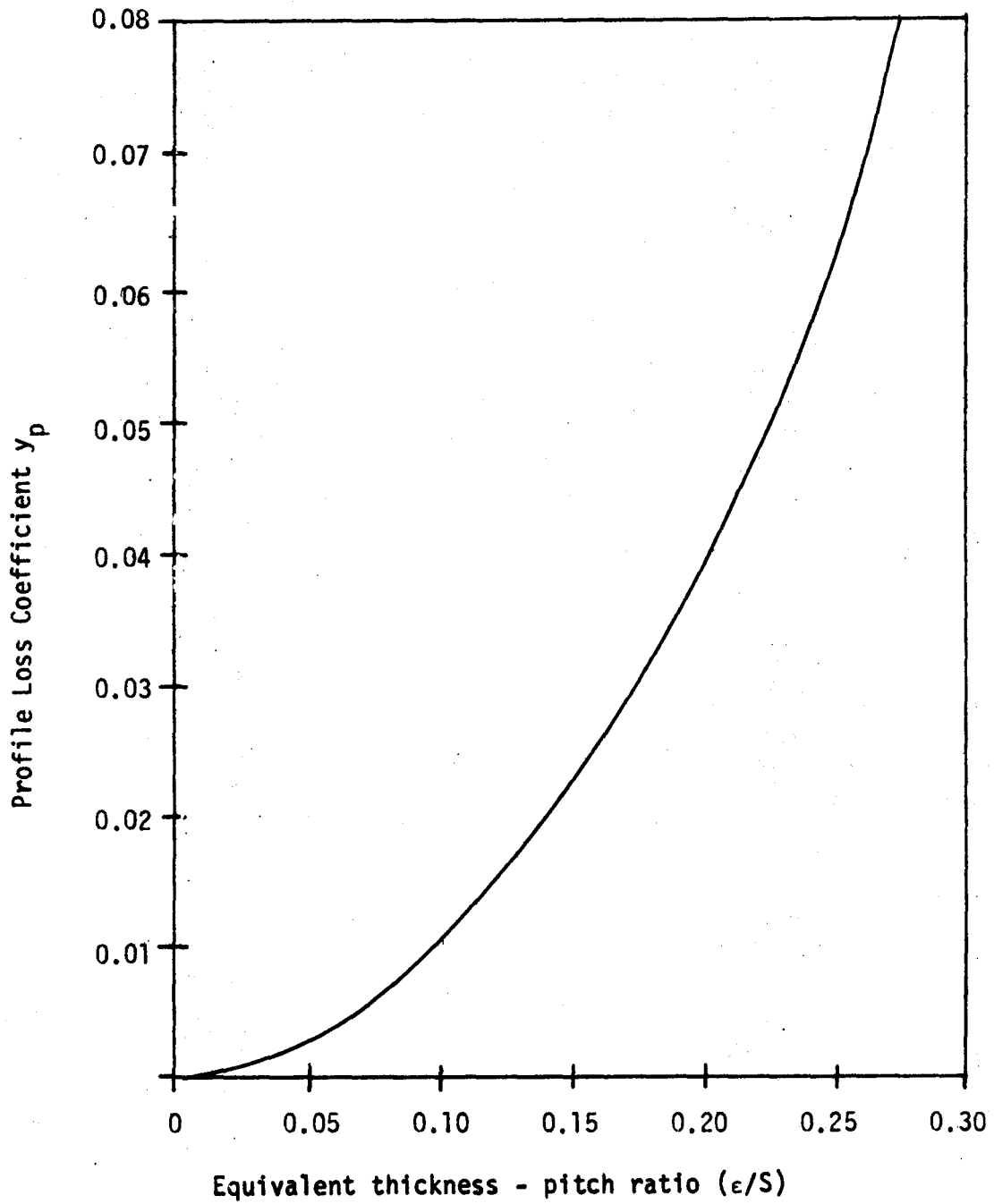


Figure 3.10. Calculated Effect of Trailing Edge Thickness on Profile Loss (from Hawthorne [19]).

below 1.3% of the blade chord as concluded by J. H. Horlock [20].

While designing the trailing edge portion of the blade the problem of controlling the radius of curvature is more severe. J. H. Horlock [20] concluded in his study that the straight backed blades show less efficiency than the blades with slight curvature. This factor can be quite clearly understood from the work presented by D. G. Ainley and G. C. R. Mathieson [21]. They presented a graph indicating the variation of profile loss coefficient versus the pitch/radius of curvature ratio for various outlet Mach numbers as shown in Fig. 3.11. It is found that the effect of curvature is more predominant in the flows which have outlet Mach numbers more than 0.6 or 0.7. It can be concluded that for outlet Mach numbers near unity or slightly higher, that the pitch/radius of curvature ratio should lie between 0 and .2 which indirectly means that the curvatures should be quite small approaching zero. The present study shows that the curvature should be slowly increasing in the direction from the trailing edge towards the leading edge.

Another effect of the curvature variation at or near the trailing edge concerns the actual gas path along the blade surface. This has to be carefully controlled in order to avoid further flow deviations from the surface in question. It might be expected, for instance, that the influence of the trailing edge curvature on the gas outlet angle is also strongly dependent on the outlet Mach number. Flow deviations based on experimental data are shown in Fig. 3.12 as suggested by Ainley and Mathieson [21] for low subsonic and sonic exit

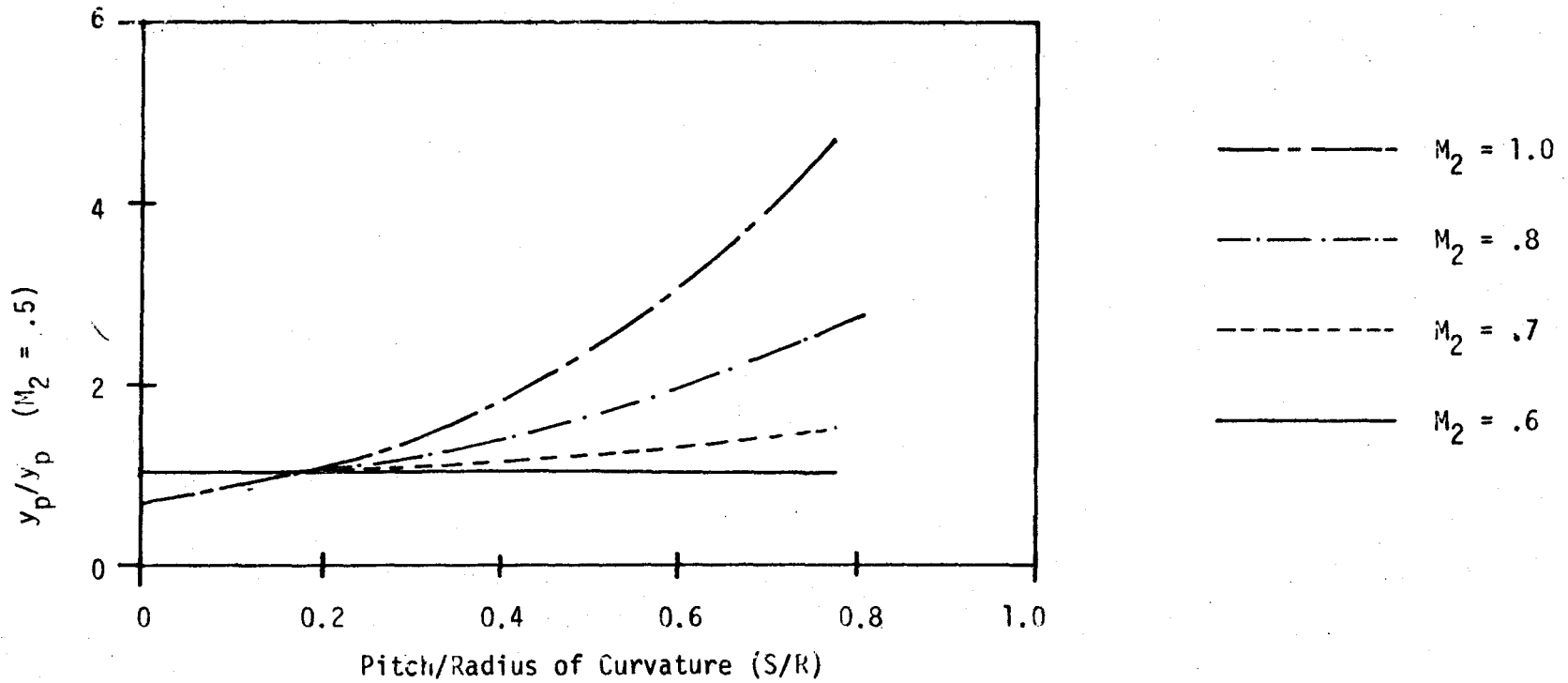


Figure 3.11. Effect of Trailing Edge Curvature on Profile Loss (from Ainley and Mathieson [21]).

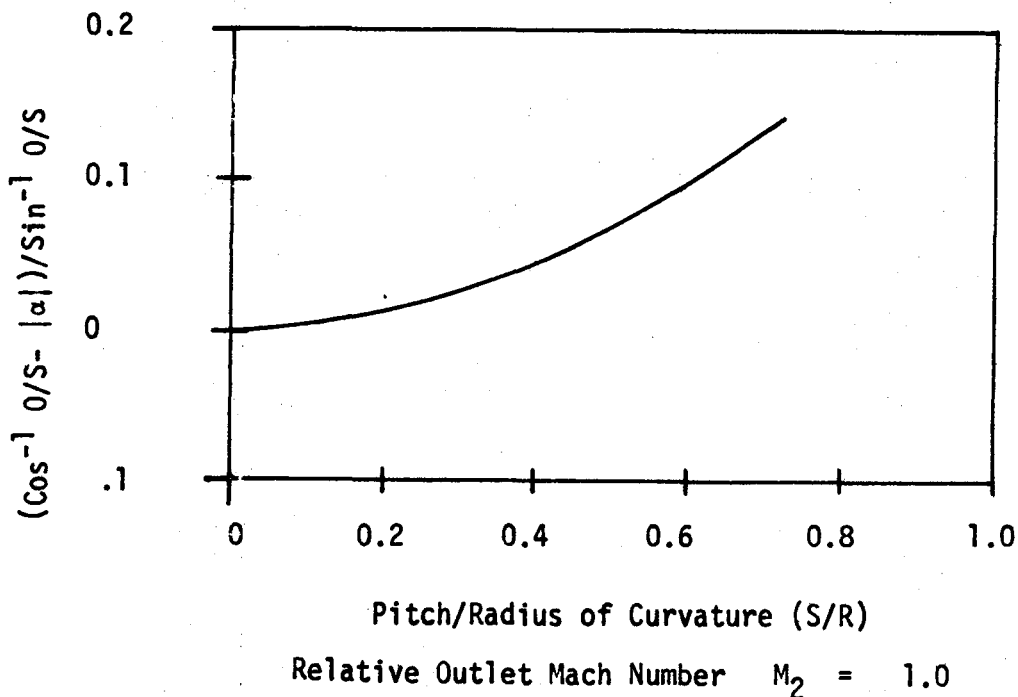


Figure 3.12. Effect of Trailing Edge Curvature on Deviation (from Ainley and Mathieson [21]).

velocities. At other relative Mach numbers some interpolation is necessary. Based on the above work the blade should have a Pitch/Radius of curvature ratio between 0 and .2 to have minimum possible deviations.

3.5 Mechanical Design Aspects

The mechanical design considerations also have an important effect on the performance. The aerodynamic forces may excite blade vibration and may also be responsible for some damping effect. The stresses produced due to blade vibrations cause fatigue failure at the root of the blade. A knowledge of the frequencies of vibration is required to properly analyze the root fittings. Sunder Rawtani [22]

has investigated the effect of the aspect ratio, the amount of pretwist, the speed of rotation, the disc radius and the setting angle on the natural frequencies and on the mode shapes. The above analysis helps in determining the relation of the blade thickness at the root to the tip thickness.

The upper limit of blade rotational speed is limited by root stresses. The determination of the blade stresses is a critical factor regardless of the type of blades being designed. Gas turbines blading is particularly important from the stress stand-point because of the high temperatures encountered.

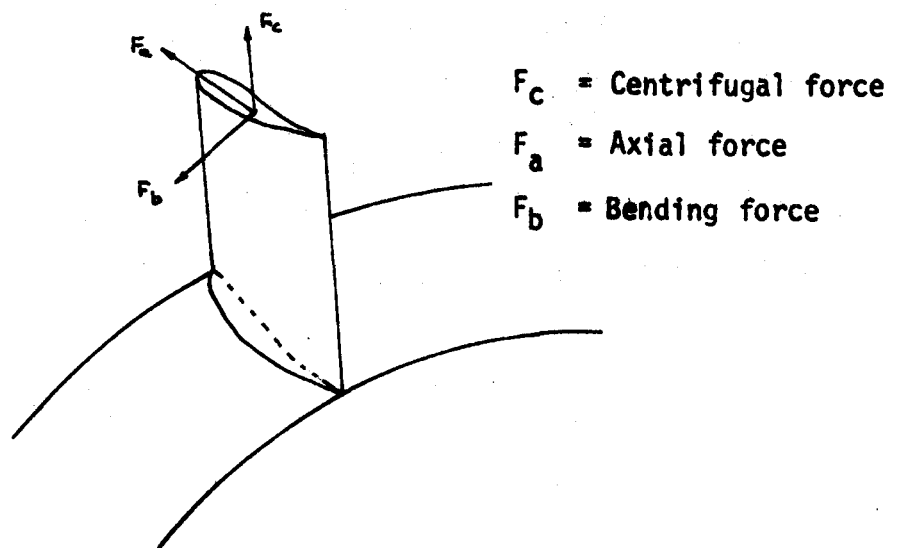


Figure 3.13. Representation of Blade Forces.

The severest stresses are imposed by centrifugal force, fluid pressure differences and vibration. Provision has to be made in the blade design to withstand all these stresses encountered in the operation as shown in Fig. 3.13.

Turbine blades are also subjected to resonant vibrations induced by irregularities in the fluid flow path resulting from such obstructions as struts, the non-symmetry of the stationary passages, disturbances due to the wake of earlier blade rows. The frequency of vibration is seen to depend on the stiffness and mass of the blade. References [23], [24] and [25] refer to recent work on the vibration analysis of curved blades.

3.6 Materials for Turbine Blades

For a given pressure ratio the higher the operating temperature of a gas turbine the greater the power developed. Specially for the airbourne field, weight consideration is very important. In many applications it is important to develop the most power for the least amount of hardware thus, it is desirable to be able to operate the gas turbines at high temperatures. This creates an important problem from the stand-point of suitable materials. In all metals the strength decreases and the creep rate increases with an increase of temperature.

In addition to the fundamental requirements of strength at high temperatures and a low creep rate, the material should have several

other important qualities such as adequate fatigue strength, strong resistance to corrosion, forgeability, weldability, and machinability.

Usually the materials used for turbine blades are S-816, S-590, Vitallium, the cemented hard carbides and ceramics. Carbides of tungsten, zirconium, molybdenum, tantalum and titanium are available with cobalt as the matrix. A particularly interesting cemented carbide is that of titanium with cobalt. The most promising material is a combination of ceramics and metals such as bonding alumina to steel for turbine blades or silicon carbide with iron and sintered aluminum oxide [26].

CHAPTER 4

THEORETICAL ANALYSIS AND BLADE PROFILE CONSTRUCTION

4.1 Design Procedure

The main requirement of the blade design was to obtain high pressure ratio and high output. The swirl was neglected and a low axial velocity was also assumed. The resulting design would therefore have a high pressure ratio, high enthalpy drop and high deflection of the flow.

The classical method of design for turbines is the free vortex design. Two assumptions are involved in this design,

- (i) The flow is assumed to be in radial equilibrium before and after all blade rows, so that

$$\frac{dp}{dr} = \frac{mv_T^2}{r}$$

- (ii) The tangential velocity distribution is required to be free vortex in which the product of tangential velocity and radius is constant that is $(r V_T) = \text{constant}$.

The main question to be answered is in what manner does the blade shape and setting vary along its height also when the velocities are high enough to introduce compressibility effects, the change of density from root to tip will vary as the flow passes through the blades. There will also be axial and radial velocities to be taken into account.

Whitehead [27] assumed that between the blade rows of a turbine the radial velocities and accelerations would quickly vanish and a condition of radial equilibrium would be established. He showed that the axial velocities would then be invariant with radius. Many turbines have been designed by this method and the blades in these turbines are termed free vortex blades. A disadvantage of the free vortex design is that a high degree of twist in the rotating blades is needed to accommodate the large changes in inlet and outlet angles. This leads to the problem of precise instrumentation and manufacturing difficulties which adds to the cost of the blade.

In other blade design methods, radial displacements of the streamlines have been eliminated or reduced by making the product of local density and axial velocity invariant with the radius. The resulting constant specific mass flow design, introduces radial variations of circulation and therefore are of use especially when the turbine pressure drop is sufficiently large.

Another method for the design of blades is based on more exact theory. This tends to lead to numerical solutions in the design of blade passage. The assumption of axially symmetric flow has accordingly been made and is the basis for the theoretical work which forms a useful improvement over the radial equilibrium theory. The theoretical calculations are laborious, however, and it has been found easier and more direct to describe the profile shape over the required range of turning angles and then designing the channel by varying the curvature at points on the profile to obtain the most favourable pressure distribution around the blade.

4.2 Method Of Investigation in the Present Study

This method is an extension of the last method as described in Section 4.1 but differs in that the blades are designed for a specific lift coefficient and therefore blade spacing. For comparison purposes the inlet and outlet angles are kept constant for each lift coefficient. The axial chord is also a constant in the design.

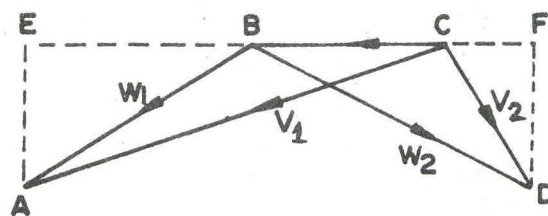
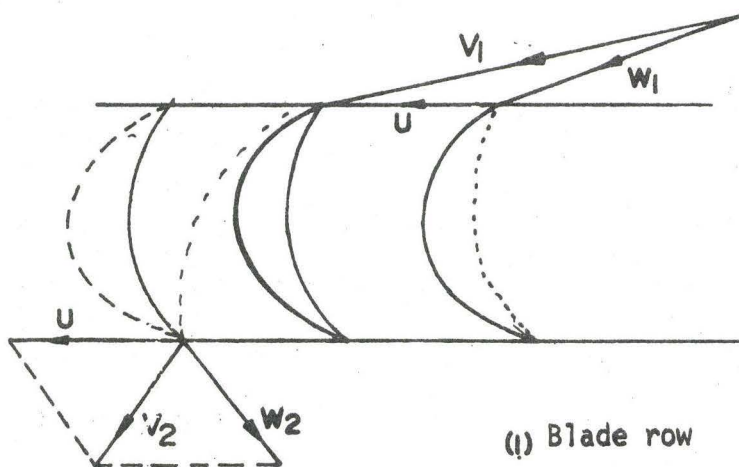
Probably the most important consideration in the design of the blade is the resultant pressure distribution around the blade. These are described later in this chapter. It should be noted that the pressure distribution is effected by every parameter of the blade.

4.3 Power Estimation from Velocity Triangles

In order to estimate the power available from the blade, one first calculates the tangential force induced by the action of the gas jet on the blade. The function of the blade is to change the direction of motion of the jet in as smooth a manner as possible. In changing its direction the jet experiences a change of momentum in the original direction of motion. Now Newton's Second Law states that when a body experiences a change of momentum, the rate of change of momentum is proportional to the force which produces the change. Since the blades cause a change in the momentum of the jet, they experience a force which is proportional to the rate of change of momentum.

Since the functioning of the turbine depends entirely upon the behaviour of the gas during its period of contact with the blades, it is

necessary to determine the variations in the inlet and outlet velocity of the gas. The velocity conditions can best be illustrated graphically in the form of a velocity diagram, giving a clear picture of the changes which take place.



(ii) Reaction velocity triangles

Figure 4.1. Blade Row and Velocity Triangles.

Figure 4.1 is a typical schematic diagram of a turbine blade row on which the inlet and outlet velocity triangles have been drawn. The notation is as follows.

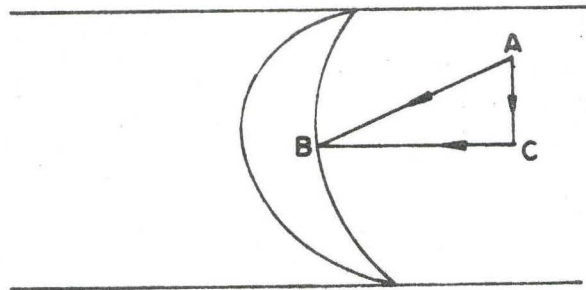
- W_1 = velocity of gas relative to blades at inlet.
- V_1 = absolute velocity of gas at blade inlet.
- W_2 = velocity of gas relative to blades at outlet.
- V_2 = absolute velocity of gas at blade outlet.
- U = peripheral velocity of blades.

It is the common practice to represent both the inlet and outlet triangles in a single diagram as shown in Fig. 4.1.(ii).

It is observed that when there is a reaction effect, the velocity at the outlet is increased.

If there is a reaction effect the total thrust on the blades is derived from two sources,

- (i) The impulse due to the change in momentum of the gas stream, produced by the deflexion caused by the curvature of the moving blades.
- (ii) The reaction generated by the change in momentum of the gas stream due to contraction in the moving blade passage.



- AB = Total Thrust
 AC = Axial Thrust
 BC = Tangential Thrust

Figure 4.2 Thrust Resolution.

Figure 4.2 represents the various thrusts coming into the picture on the blade surface. The total thrust can be resolved into two components. One parallel to the axis of the drum which is known as axial thrust and the other tangential thrust. The latter one provides the output power while the axial thrust has to be taken up by a suitable bearing. Referring to the velocity triangle diagram if the weight flow of the gas discharged over the blade per sec is \dot{w} Lb then

$$\text{Tangential thrust} = \frac{\dot{w}}{g} (BE + BF)$$

or the horsepower obtained from the blade is given by

$$\text{Horsepower} = \frac{\dot{w}}{g} (BE + BF) \frac{U}{550}$$

4.4 Profile Construction

The following procedure is necessary to produce blade profiles for compressible flow which have a favourable pressure gradient over a large percentage of the total blade area.

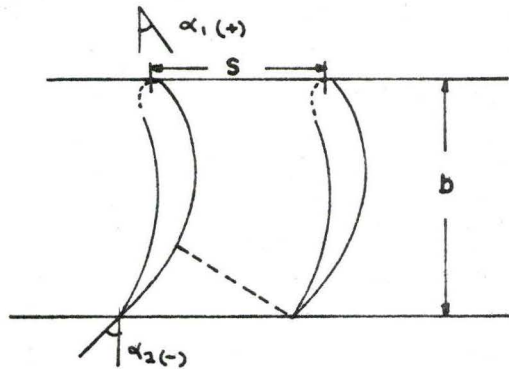
4.4.1 Selection of Pitch/Chord Ratio

Zweifel [4] as described in Chapter 2 suggested that

$$C_L = 2 \frac{S}{B} \cos^2 \alpha_2 (\tan \alpha_1 - \tan \alpha_2) \quad (4.1)$$

where C_L is the lift coefficient.

According to Zweifel a reasonable degree of symmetry must be observed for equation (4.1) to apply. In a study such as this it is obviously easy to have both the inlet and outlet angles the same and this simplifies the design. However, this equality is not a rigid requirement and blades have been designed using Zweifel's technique with differences in angles of the order of 15 - 20 degrees. In the work to be presented the lift coefficients had been chosen in the range of .8 to 1.2. Using these values in the equation, the corresponding values



Trailing edge radius = zero.

Figure 4.3. Zweifel's Blade Nomenclature.

of $\frac{S}{b}$ are calculated. Hence for some suitable value of Chord (b), the pitch (S) can be calculated.

4.4.2. Blade Layout

Figure 4.4 shows the mechanical design features on the drafting of a turbine blade.

- (a) On a suitable scale ($1'' = 10''$ is usually satisfactory) draw two lines parallel to each other at a distance $b + \text{T.E.R.}$ apart, representing the leading and trailing lines of the cascade.

- (b) One then marks out the pitch distance (S) on the trailing edge line and draws the trailing edge circles for the two blades and ensures that the trailing edge line is tangent to these circles.
- (c) The outlet throat (O) as shown in Figure 4.4 can be calculated from the trigonometric relation

$$\frac{O}{S} = \cos \alpha_2$$

The next step is to draw an arc of radius O + trailing edge radius with the centre located at the same point as the trailing edge circle. (Note that either circle can be chosen depending on the direction of motion of the the blade, here it is chosen to the right)

- (d) One then draws a tangent to the other trailing edge circle, at an angle $\beta_{2S} = \cos^{-1} \left(\frac{O}{S} - \Delta \cos \beta \right)$ where $\Delta \cos \beta$ depends on the exit plane Mach number (M_2). The plot of exit Mach number versus $\Delta \cos \beta$ is given in Figure 4.5. It should be recalled that the velocity diagram provides information regarding the exit plane Mach number so that once this is estimated the $\Delta \cos \beta$ can be obtained. A curve, effectively a straight line as a first approximation, starting from the trailing edge is drawn to the throat position. Blades having a straight line portion from the trailing edge to the throat position are termed flat-back

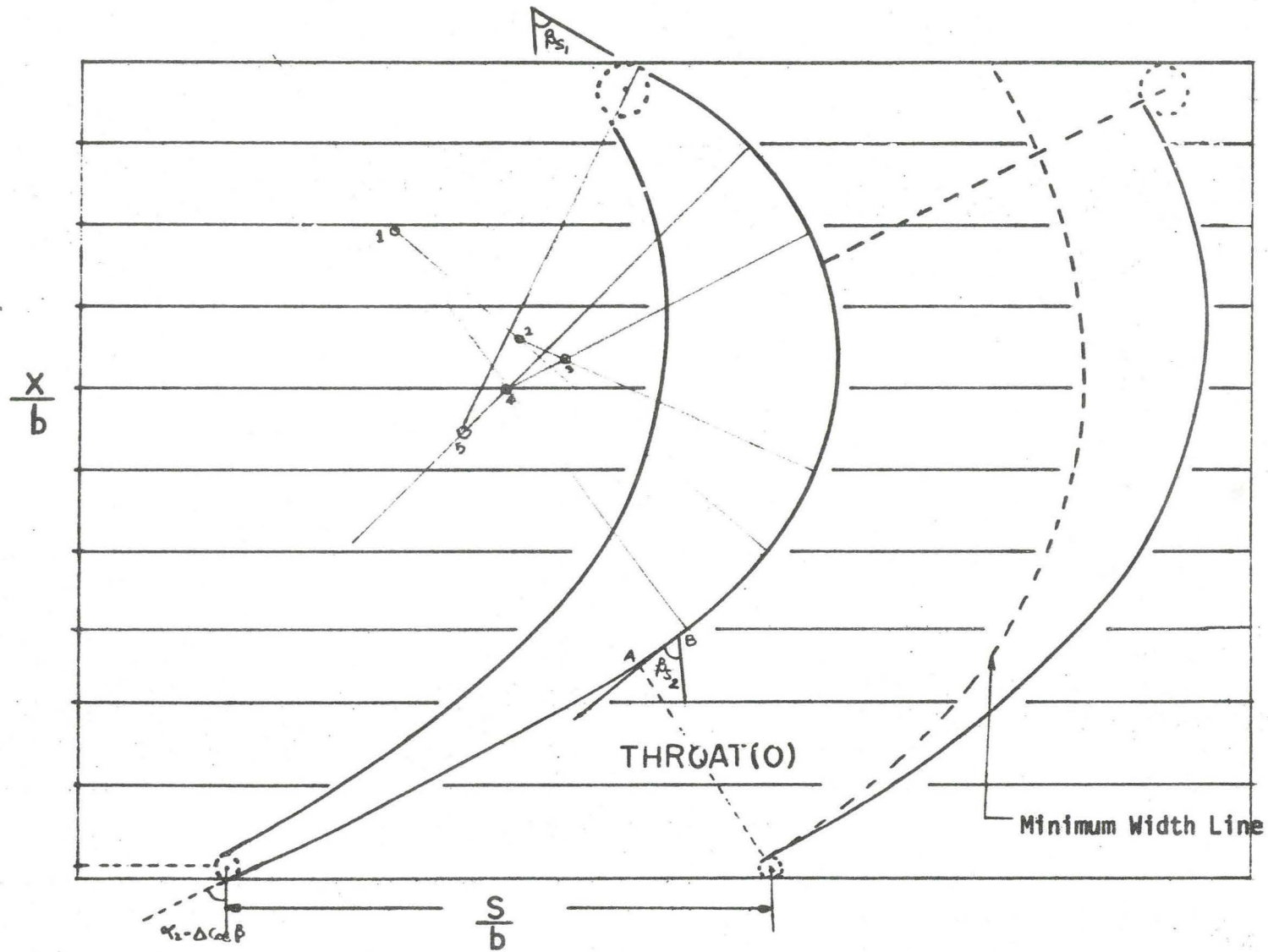


Figure 4.4. Construction of Blade Profile

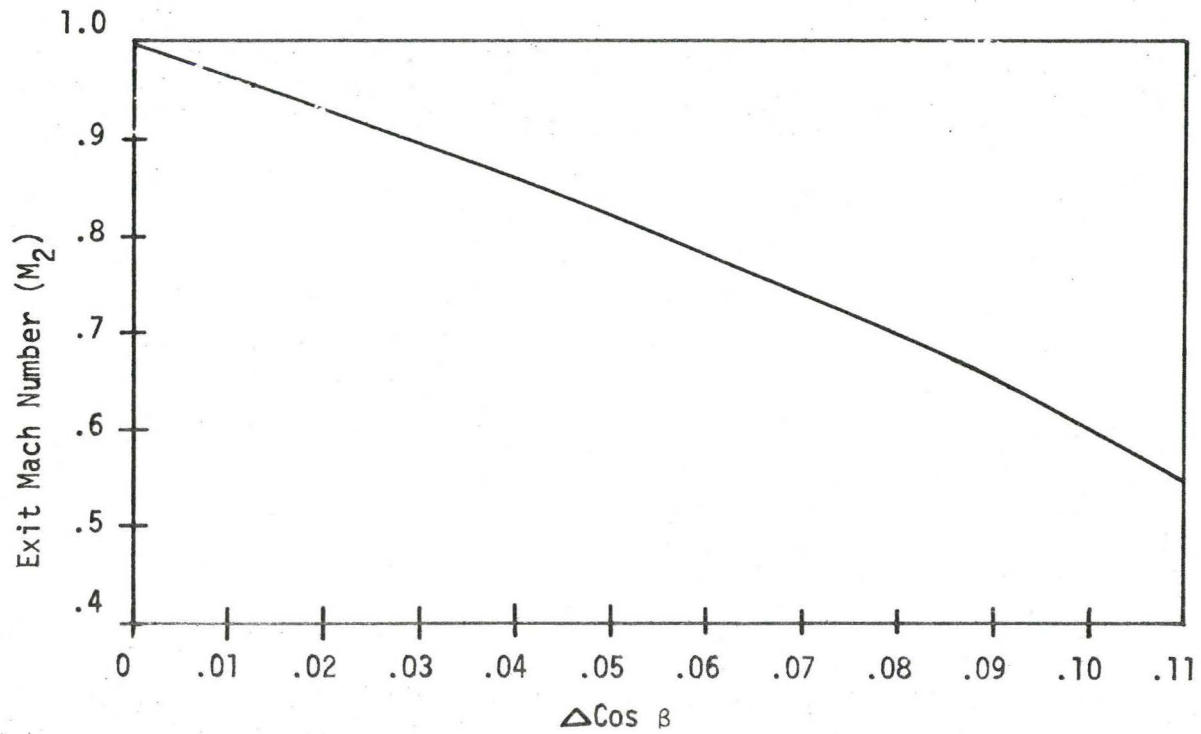


Figure 4.5 Variation of flow deviation with exit Mach number (from Reference [29]).

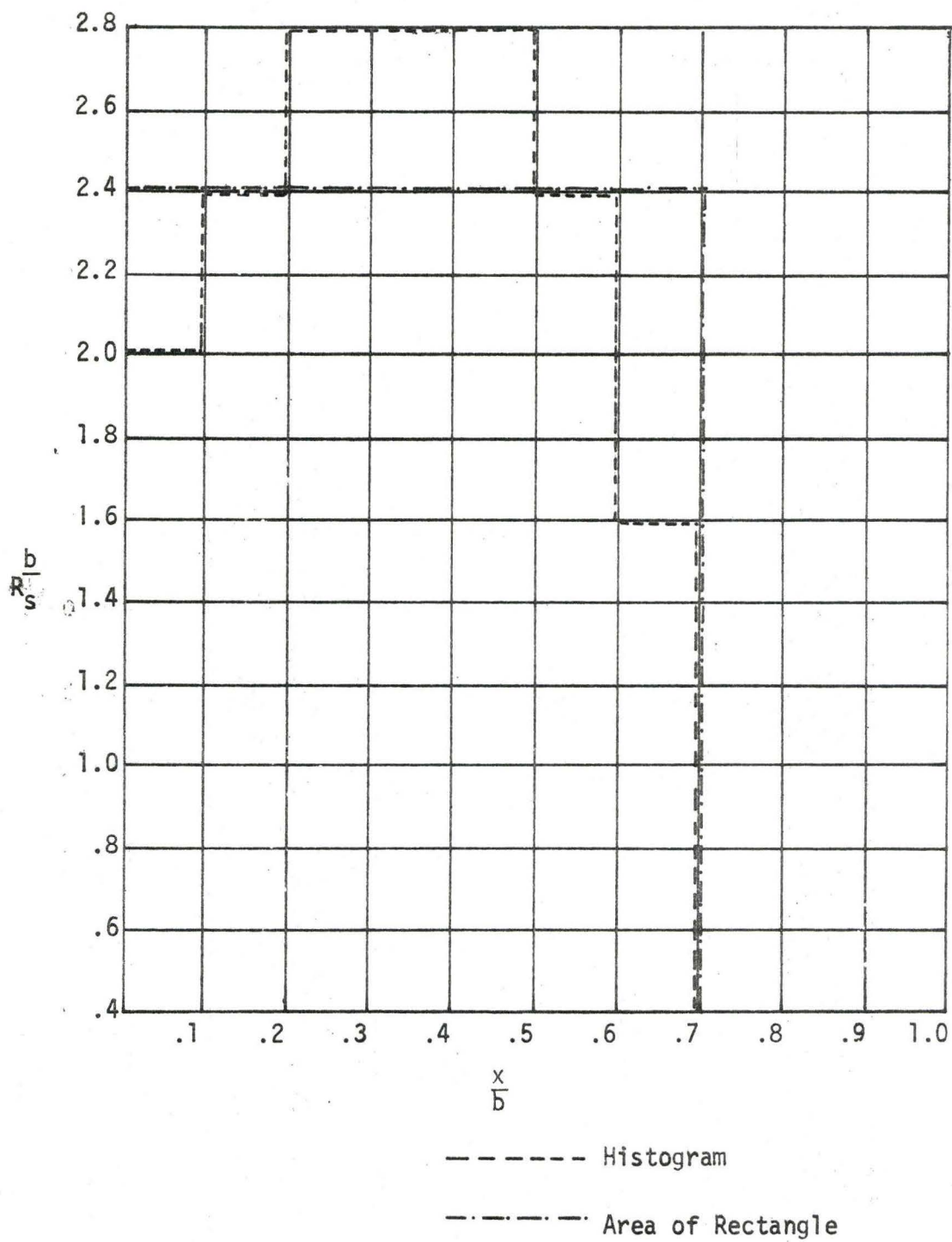
blades. In general a modification is usually presented to provide for a small degree of curvature to this section. In fact the small curvature in the vicinity of the throat is necessary to complete the computer programme.

- (e) One now determines the angle β_{S_1} at which the suction surface intersects the leading edge line (as determined by α_1). It is to be noted that the nose radius provides the extra included angle which has to be taken into consideration. Usually the angle β_{S_1} varies from $\alpha_1 + 20^\circ$ to $\alpha_1 + 15^\circ$, i.e., $\alpha_1 + i \text{ angle} + \text{nose angle} / 2.0$.

where $i \text{ angle} = 0 \text{ to } 5^\circ$ and

Nose angle $\cong 20^\circ$ (Reaction Blades)

- (f) After finding β_{S_1} one then finds β_{S_2} . The angle β_{S_2} is the angle made by the suction surface at the point B as shown in Figure 4.4. Usually the angle β_{S_2} varies from $\alpha_2 - 10^\circ$ to $\alpha_2 - 5^\circ$. After knowing β_{S_1} and β_{S_2} , one calculates $|\sin \beta_{S_1}| + |\sin \beta_{S_2}|$, also once the exit throat is drawn the value of x/b at the throat (point A) is known. A rectangle of area $|\sin \beta_{S_1}| + |\sin \beta_{S_2}|$ is then erected with the base value of x/b at the point B and $\frac{b}{R_s}$ on the Y-axis as shown in Figure 4.6.
- (g) On the rectangle erected, superimpose a histogram of equal area, with a peak value existing at some intermediate x/b value. This redefinition of the area described is, so far,

Figure 4.6 Plot of b/R_s Versus x/b

entirely optional but experience has shown that $\frac{b}{R_s}$ maximum should take place within the range of $0.2 < \frac{x}{b} < .55$. The main point to be noted here is that one is specifying the curvature over the suction surface and while the histogram is discontinuous for ease of analysis, the curvature cannot be.

- (j) Extend the radius of curvature line from point B as shown in Fig. 4.4 and mark off the centre at a distance $\frac{R_s}{b}$ taken from the histogram. One then draws arcs of circles (with common tangents at junctions) of radii $\frac{R_s}{b}$ values calculated from Fig. 4.6 which exist between the appropriate values of x/b as shown on the histogram. After drawing all the arcs from the exit throat to the leading edge, the suction profile is redrawn using a spline fitting technique.
- (k) Once the suction surface has been constructed one turns his attention to the development of the pressure surface. Since the blade passage area ratio has to converge from its entrance area as shown in Figure 4.7 to the throat location, steps are taken to ensure that this convergence is monotonically decreasing. Since both inlet and throat areas are known, a curve similar to that shown in Figure 4.7 can be drawn to provide the ratio of channel width/throat width as a function of R_s/R_s throat. Once these points have been established, a smooth curve fitted through the points establishes the pressure surface. The radius of curvature

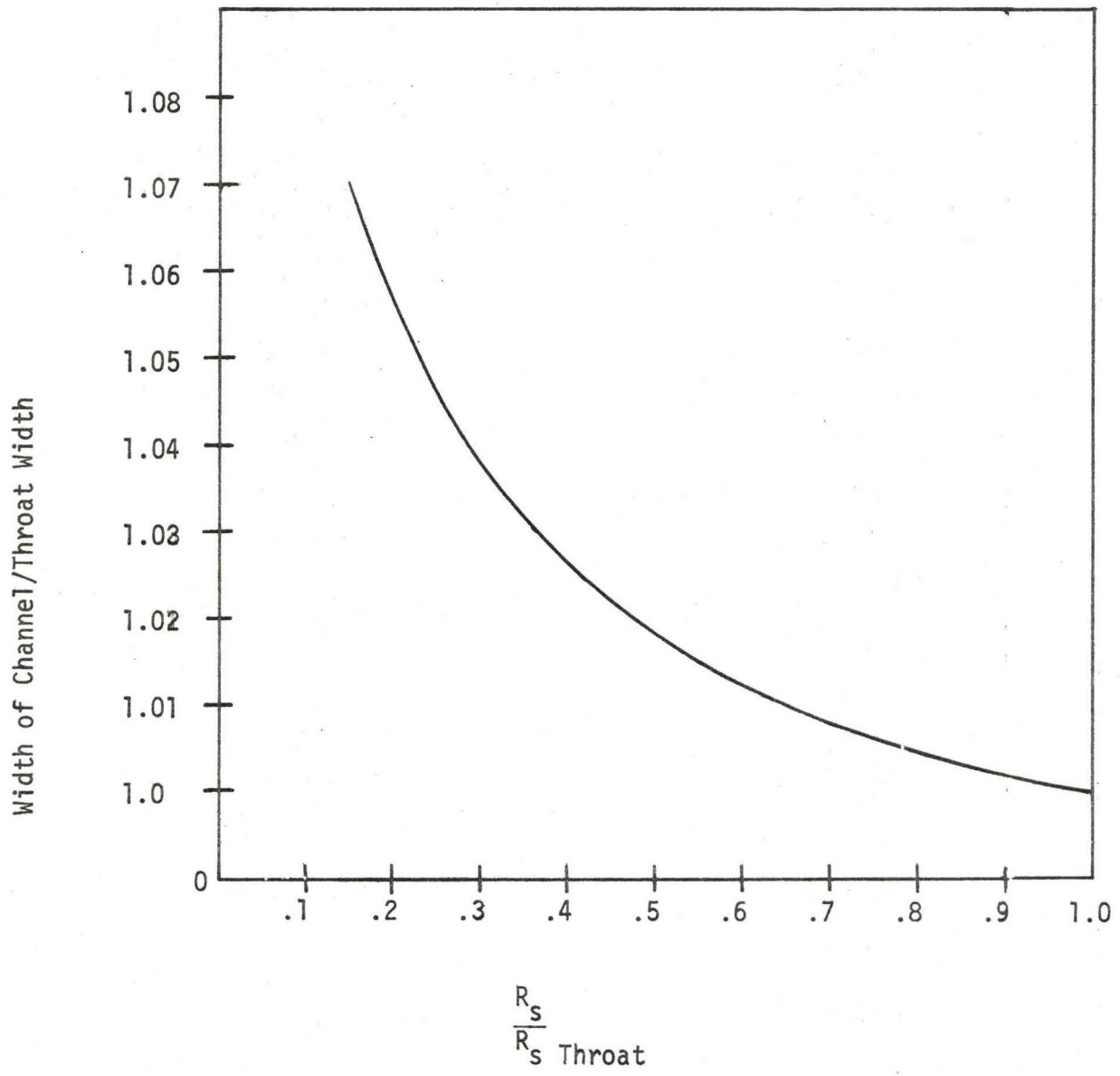


Figure 4.7 Approximate Channel Width for Curved Channels (from Reference [29]).

at each x/b on the pressure surface now have to be calculated and care must be taken to ensure that all radii of curvatures have the same sign.

- (l) Now one can draw in the two leading edge circles of appropriate radii. A comment has already been made in Chapter 3 regarding current practice with respect to leading and trailing edge radii.
- (m) One then combines the pressure surface profile with the suction surface profile to provide a complete blade outline and one examines the resulting blade profile for general features including the accuracy of inlet and outlet angles.
- (n) The next step is to draw in the equipotential lines across the channel at various stations and assuming a linear variation of either radius of curvature of suction surface (or of the curvature of the suction surface), one calculates the surface pressure distribution on the suction and pressure surfaces of the blade, utilizing the equipotential's length at various stations, by simultaneously satisfying the continuity equation and the momentum equations. It is normal procedure to examine the pressure distribution around the blade for regions of high adverse pressure gradients. If these are found to exist then changes can be made, starting with the histogram, to alleviate such conditions.

- (o) Finally, another factor which could influence the final profile concerns the thickness of the blade, which should be reasonable in order to withstand the various loads. One would normally check the blade proportions, blade spacing etc. for strength consideration and also ease of manufacture.

4.5 Pressure Distribution Analysis by the Method of Orthogonals

This is a method of analyzing flow through a passage which is formed by two successive blades. An orthogonal is defined to be any curve that intersects every streamline at 90 degrees between the flow boundaries exactly once. Figure 4.8 shows the three-dimensional orthogonal surface. The streamlines and their normals are drawn to establish a grid for the flow solution. The first step in this method is to obtain a two-dimensional solution on an assumed mean stream surface between the blades. In cases where the distance between blades is great and there is a large change in flow direction within the passage, the normals vary considerably in length and direction. Therefore, it becomes difficult to obtain a direct solution of the flow passage without resorting to intermediate steps. The use of normals makes it possible to obtain a direct solution by the use of a set of arbitrary curves or streamlines from one blade surface to the other blade surface. The orthogonal remains fixed regardless of the number of streamlines used. By using this technique, it is possible to obtain a computer solution

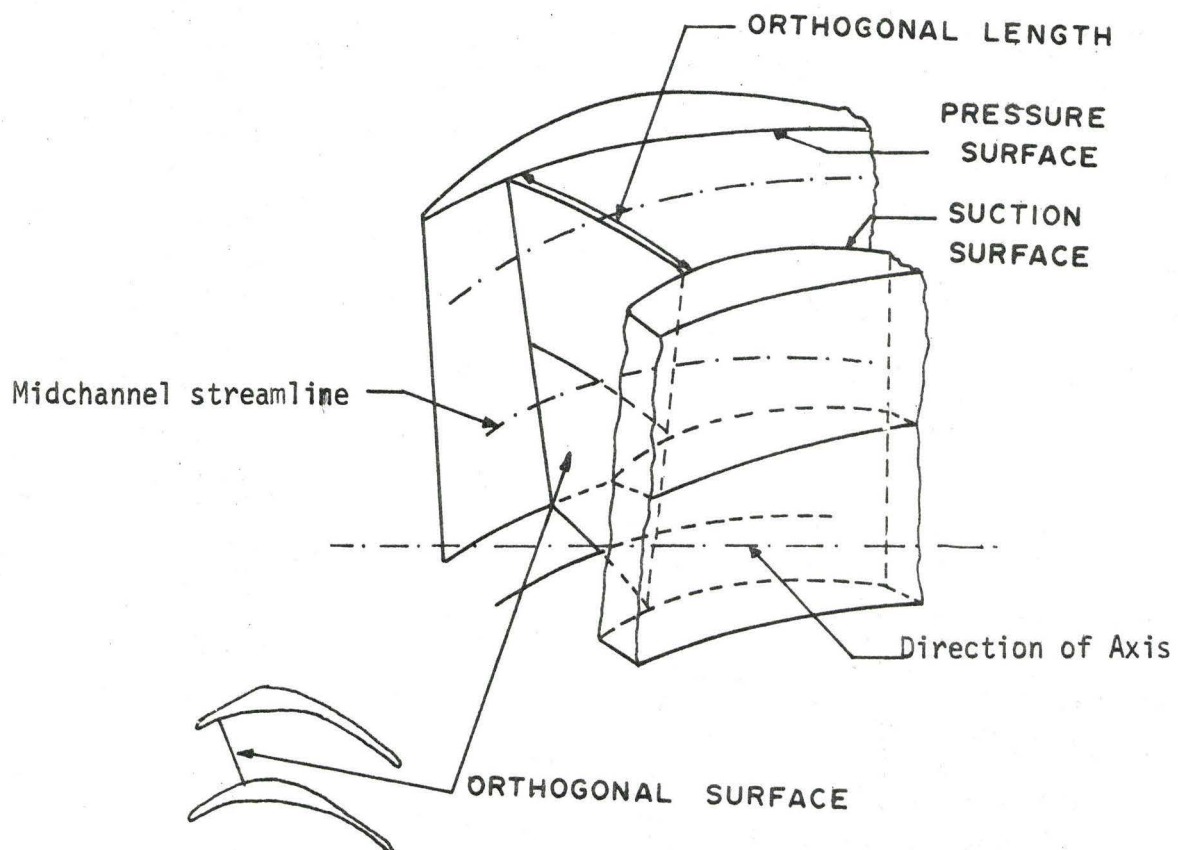


Figure 4.8. Three-Dimensional Orthogonal Surface

to the two-dimensional problem which would be a numerical solution to the general equation which allows the calculation of flow properties along both the streamlines and orthogonals even with significant changes in both area ratio and flow direction.

Assumptions:

- (i) The fluid is considered inviscid but compressible.
- (ii) Flow is steady.
- (iii) Flow has no radial component.

The continuity equation for the flow through any orthogonal can be written as

$$\dot{m} = \int_0^{n_0} \rho V dn \quad (4.2)$$

while the momentum equation has the familiar form

$$\rho \cdot V \cdot V \cdot \frac{\partial \theta}{\partial S} = \frac{\partial p}{\partial n} = \frac{\rho V^2}{R} \quad (4.3)$$

where θ is the deflection angle,

and $\frac{\partial \theta}{\partial S}$ is by definition the curvature at a point on the streamline. Here n_0 is the total length of the orthogonal line between the two boundaries. (i.e., the pressure surface and the suction surface). While V is the velocity along the streamline.

Equations (4.2) and (4.3) can be numerically integrated along one of the orthogonals by assuming a velocity at either surface and then

calculating the pressure, density and velocity at the neighbouring point taking the assumed velocity for the initial calculations and using the known value of radius of curvature at the point in question. The procedure can be continued until the opposite surface is reached always moving along the orthogonal. Once the velocities and densities at each and every point along the orthogonal are known, the total mass flow rate can be calculated. This mass flow rate is then compared with the design mass flow rate which of course is based on a unit height of the blade. If a difference exists between these mass flow rates, the assumed velocity is corrected to finally obtain the correct mass flow rate.

From the same set of equations the velocities and pressures can be obtained provided that the curvatures of the streamlines at each and every point is known. It is obvious that a major point in the analysis remains the establishment of the radii of curvatures throughout the flow field. As a preliminary estimation it is usually assumed that either the curvature or radius of curvature varies linearly along the orthogonal from the suction surface to the pressure surface.

A computer program which has been developed to perform the above operations with the necessary assumptions is given in Appendix D and is further developed in the remainder of this chapter.

4.6 The Construction of the Orthogonals

Later in this section the method of finding the pressure distribution is described. The length and position of the orthogonal is

one of the input data required for the evaluation of the pressure distribution.

An orthogonal surface is perpendicular to all the streamlines which include the suction and the pressure surfaces of the blade. Very careful judgement and experience is necessary in the construction of the orthogonal lines and a sample of this construction is shown in Fig. 4.9 which shows a blade passage and a typical orthogonal.

The suction surface of the blade is drawn using a series of arcs of circles as defined by a histogram which in turn depends on the blade turning angle. Thus all the centres of curvatures are known of the suction surface. The orthogonal lines are not straight lines in general. To draw the orthogonal lines between the suction and pressure surfaces, consider a point B on the suction surface, join BD, where D is the centre of curvature of an infinitesimal length of arc near the point B. A point C is chosen on the pressure surface and a normal is drawn to the blade surface at the point in question. Produce it to intersect DB at E, such that $BE = CE$. Then E lies on the mean streamline. A smooth curve is drawn which has to be perpendicular to both surfaces as shown in Figure 4.9. In a similar fashion other points on the suction surface can be considered and the above procedure is repeated to construct orthogonal lines.

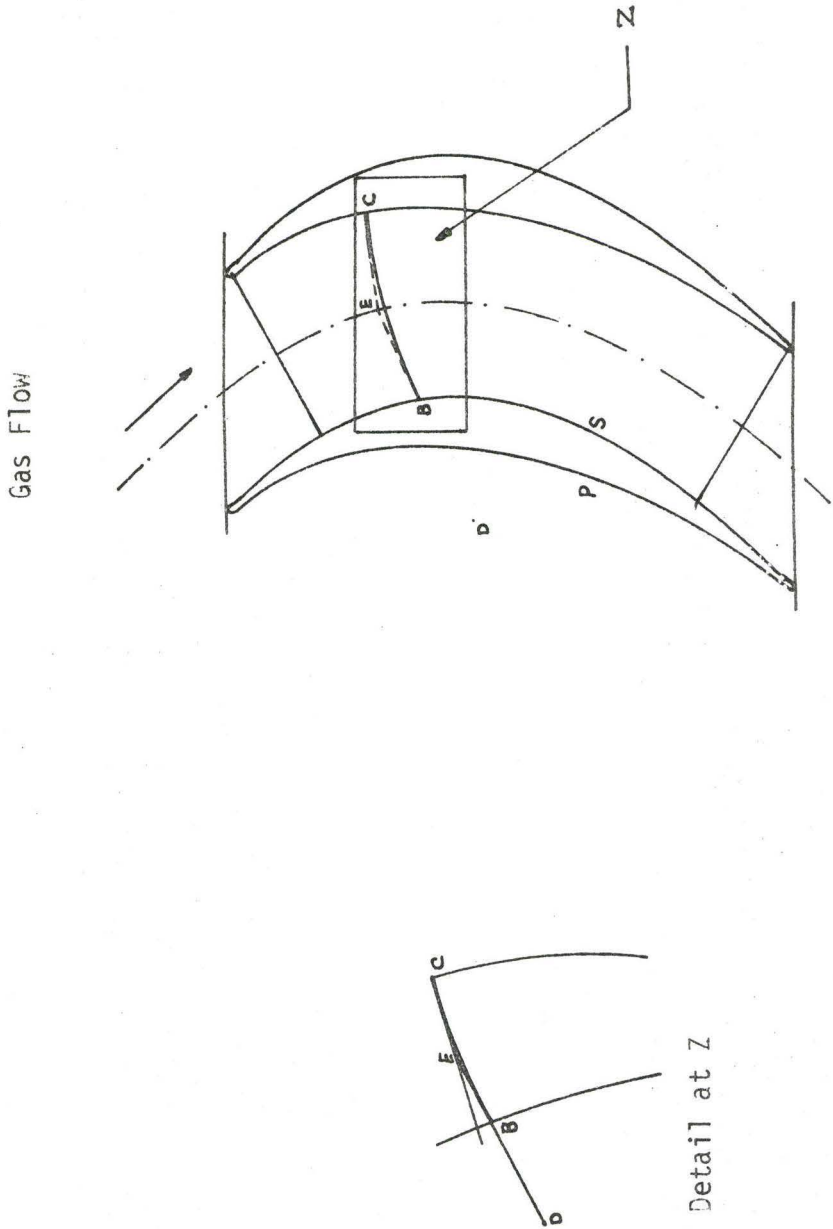


Figure 4.9 The Construction of an Orthogonal Line.

4.7 Analytic Solution of Momentum Equations

Momentum equations in the n, S co-ordinates system are given as

$$-\frac{1}{\rho} \frac{dp}{dn} = -\frac{v^2}{R} \quad (4.4)$$

$$-\frac{1}{\rho} \frac{dp}{dS} = v \frac{dv}{dS} \quad (4.5)$$

In the solution of these equations further assumptions are made as follows:

- (i) The flow is isentropic.
- (ii) Either the curvature of the streamlines varies linearly along the orthogonal from the suction to the pressure surface or alternatively the radius of curvature varies linearly from the suction to the pressure surface.
- (iii) The mid-passage line is defined as a streamline and is referred to in this thesis as the midstream.

Corresponding to the alternative conditions in item (ii) above, there exist two solutions which are given below.

From equation 4.5 at a point on a streamline

$$\frac{dp}{\rho} = -v dv \quad (4.5a)$$

Substituting the value of $\frac{dp}{\rho}$ from equation 4.5a into 4.4 one obtains the relation

$$v \frac{dv}{dn} = - \frac{v^2}{R}$$

or

$$\frac{dv}{v} = - \frac{dn}{R}$$

$$\therefore \frac{dv}{v} = - \frac{dn}{R} \quad (4.6)$$

or using the definition of curvature this equation can be written as

$$\frac{dv}{v} = - C dn \quad (4.7)$$

Since the curvature is assumed to vary linearly along the orthogonal one can write

$$C = C_S + (C_p - C_S) \frac{n}{n_0} \quad (4.8)$$

Where C_p and C_S are curvatures at the pressure and suction surfaces respectively, n_0 is the length of the orthogonal line between the two surfaces, and n is the distance along the orthogonal measured from the blade suction surface.

Differentiating equation (4.8) one obtains

$$dc = 0 + (C_p - C_S) \frac{dn}{n_0}$$

and substituting the value of dn into equation (4.7) one arrives at the relation

$$\frac{dv}{V} = - \frac{C (n_o)}{C_p - C_s} dc$$

$$\log V = \frac{-n_o}{C_p - C_s} \times \frac{C^2}{2}$$

or

$$V = e^{-\frac{n_o}{2(C_p - C_s)} \cdot C^2} \quad (4.9)$$

which defines the velocity at any point as a function of curvature.

The velocity at midstream is obtained as follows.

$$C_{(Mid)} = \frac{C_p + C_s}{2}$$

$$\therefore V_{(Mid)} = e^{-\frac{n_o}{2(C_p - C_s)} \left[\frac{(C_p + C_s)^2}{4} \right]}$$

therefore

$$\frac{V}{V_{(Mid)}} = e^{-\frac{n_o}{2(C_p - C_s)} \left[C^2 - \frac{(C_p + C_s)^2}{4} \right]}$$

which defines the velocity at any streamline in terms of $V_{(Mid)}$.

Eliminating C from the above equation one obtains the final result in the form

$$\frac{v}{V_{(Mid)}} = e^{-\frac{n_o}{2(C_p - C_s)} \left[[C_s + (C_p - C_s) \frac{n}{n_o}]^2 - \frac{(C_p + C_s)^2}{4} \right]}$$

which can be recast as follows

$$\frac{v}{V_{(Mid)}} = e^{n_o \left[C_s \left(\frac{3}{8} - \frac{n}{n_o} \right) + \frac{1}{8} C_p - \frac{1}{2} (C_p - C_s) \left(\frac{n}{n_o} \right)^2 \right]} \quad (4.10)$$

Thus the velocity at any point is known in terms of midstream channel velocity. The $V_{(Mid)}$ not only has to satisfy equation (4.10) but also the equation of continuity simultaneously. For the particular case when $C_p = C_s$ which may occur near the blade trailing edge, the blade equation (4.10) reduces to the form

$$\frac{v}{V_{(Mid)}} = e^{n_o \left(\frac{1}{2} - \frac{n}{n_o} \right) C_s} \quad (4.10a)$$

If on the other hand, variation of the radius of curvature is assumed linear from the suction to the pressure surface then

$$R = R_s + (R_p - R_s) \frac{n}{n_o}$$

$$\therefore dR = 0 + (R_p - R_s) \frac{dn}{n_o} \quad (4.11)$$

Substituting the value of dn from equation (4.11) into (4.6) one can obtain the following expression

$$\frac{dV}{V} = - \frac{n_o}{R_p - R_s} \frac{dR}{R} \quad (4.12)$$

Integrating (4.12) one finds

$$\log V = - \frac{n_o}{R_p - R_s} \log R \quad (4.13)$$

The radius of curvature at the midstream is given by

$$R_{(Mid)} = \frac{R_s + R_p}{2}$$

$$\therefore \log V_{(Mid)} = \frac{n_o}{R_p - R_s} \log \left(\frac{R_s + R_p}{2} \right) \quad (4.14)$$

Dividing equation (4.13) by equation (4.14) it can be seen that

$$\log \frac{V}{V_{(Mid)}} = \frac{n_o}{R_p - R_s} \times \log \left[\frac{R_s + \frac{R_p - R_s}{2}}{R_s + (R_p - R_s) \frac{n}{n_o}} \right]$$

when $R_S \neq R_p$, the above equation reduces to

$$\frac{V}{V_{(Mid)}} = \left[2 \left\{ \frac{C_p + (C_S - C_p) \frac{n}{n_0}}{C_p + C_S} \right\} \right]^{\frac{n_0 C_p \cdot C_S}{C_p - C_S}} \quad (4.15)$$

4.8 Development of the Programme

The theoretical derivation of the relations between midchannel streamline velocity and velocities at other streamlines across the same orthogonal surface are used in the computer programme developed in Ref[30]. The first part of the programme deals with the calculation of the design mass flow rate, calculation of relative stagnation temperature, relative stagnation pressure and iterated mass flow rate. The second part deals with calculations of static temperatures and pressures for zero degrees angle of attack (or incidence). The mass flow rate/unit height of the blade is given by

$$\dot{m} = \rho_1 * V_A * \frac{S}{12} \quad (4.8.1)$$

where

S is the pitch in inches

ρ_1 is the density of the gas

V_A is the axial velocity

Density is given by the perfect gas law in the form

$$\rho_1 = \frac{P_1 \times 144.0}{R_g T_1} \quad (4.8.2)$$

where

P_1 is the static pressure

R_g is the gas constant

and T_1 is the static temperature of the gas.

The static pressure is given by the isentropic relation

$$P_1 = P_{01} / (T_{01} / T_1)^{\frac{\gamma}{\gamma-1}} \quad (4.8.3)$$

where

P_{01} is stagnation pressure at the inlet

T_{01} is stagnation temperature

and T_1 is the static temperature at the inlet, given by the relation,

$$T_1 = T_{01} - \frac{V_1^2}{2g J c_p} \quad (4.8.4)$$

where

V_1 is the resultant velocity at the inlet defined by the expression

$$V_1^2 = V_A^2 + V_T^2$$

The relative stagnation temperature at inlet is obtained from the known total temperature and the blade speed in the following form

$$T_{01_{rel}} = (T_{01} - \frac{V_1^2}{2g J c_p}) + \frac{W_1^2}{2g J c_p} \quad (4.8.5)$$

where

W_1 is the relative velocity at inlet.

Relative stagnation pressure at the inlet is obtained by the isentropic relation

$$P_{01_{rel}} = P_{01} \left(\frac{T_{01_{rel}}}{T_{01}} \right)^{\gamma/\gamma-1} \quad (4.8.6)$$

Thus the relative total pressure at the outlet is given by

$$P_{02_{rel}} = P_{01_{rel}} - P_{loss}$$

To initiate the iteration process, a value of the midchannel streamline velocity is assumed. The orthogonal line is then divided into any number of equal parts the present program deals with eight subdivisions and each correspond to a channel between two streamlines. With the known value of suction and pressure surfaces curvatures and the length of the orthogonal (gauging), using equations 4.10, (4.10a) and (4.15)

the velocities at 9 points along each orthogonal are obtained. Static temperature based on the absolute velocity can be obtained from the relative stagnation temperature by using the energy equation. The static pressure is obtained by using the isentropic relation (see equation (4.8.3)).

also the density at each streamline is calculated by using the equation (4.8.1).

If $Z(I) = \rho(I) \times W(I)$, where $Z(I)$ is the mass flow rate/unit area.

Since $Z(1)$, $Z(2)$, ----- are known at all the 9 points, along the orthogonal line, then the total mass flow through the channel is given by the following [28].

$$\dot{m} = \{ .03489(Z(1)+Z(9)) + .20769(Z(2)+Z(8)) - .03273(Z(3)+Z(7)) + .37023(Z(4)+Z(6)) - .16014(Z(5)) \} * \frac{\text{Gauge}}{12.0}$$

The assumed velocity of the midstream $V_{(Mid)}$ channel is iterated to obtain a mass flow rate equal to the initially calculated mass flow rate at the inlet section within the desired accuracy. For the programme at hand the deviation was programmed to be of the order of 0.01%. Once the stream tube mass flow rate has been established then the average velocity can be calculated using either of the two expressions

which were arrived at on the assumption of a linear variation of either the curvature or radius of curvature. (See equations (4.10, 4.10a, and 4.15)).

Finally, the Mach number at each and every station is calculated based on the velocity as given above and the speed of sound based on the static temperature at the point in question. Once the correct value of midstream velocity is obtained the iteration stops and the values of velocities, pressures and Mach numbers are printed at 9 points along the orthogonal. The output of the computer programme was used to obtain the velocity triangle at the outlet section and to plot a graph of pressure gradient ($\frac{dp}{ds}$) versus arc length (s)

where

$$\frac{dp}{ds} = \frac{P_i - P_{i+1}}{s_i - s_{i+1}}$$

here P_i = Pressure at i^{th} point

while s_i = Arc length from leading edge to i^{th} point.

If the input mass flow is greater than the choking mass flow, the programme obtains the value of the choking mass flow and prints out this information.

4.9 Loss Distribution Along the Passage

It will be observed that the present programme does not take into account any static pressure loss across the blade passage so that the flow is always isentropic. Once the preliminary blade design has been

obtained then additional work is required to survey the boundary layer flow over the blades in order to determine the pressure losses across the stage.

CHAPTER 5

RESULTS AND DISCUSSION

Figures (1, 2, and 3) show histograms, (i.e. history of curvature of the suction surface) which are plots of $\frac{b}{R_s}$ versus $\frac{x}{b}$ for three different total turning angles (115° , $128^\circ - 30'$, 140°) each with lift coefficients of .8, 1.0 and 1.2. As the total turning angle increases the area of rectangle formed between $\frac{b}{R_s}$ and $\frac{x}{b}$ increases and the same effect is observed by increasing the lift coefficient, keeping the turning angle constant. The area of the rectangle is given by

$$A = |\sin\beta_{S_1}| + |\sin\beta_{S_2}|$$

where $\beta_{S_1} = \alpha_1 + \Delta\alpha_1$

and $\beta_{S_2} = \alpha_2 + \Delta\alpha_2$

$$15^\circ \leq \Delta\alpha_1 \leq 20^\circ$$

(These are arbitrary limits placed on the design)

$$-10^\circ \leq \Delta\alpha_2 \leq -5^\circ$$

It should be noted that the selection of the histogram is entirely optional and that if one selects poorly, then losses may increase while the work output and efficiency decrease. If a histogram selected which has an area equivalent to the area represented by the

basic rectangle (as described in Chapter 4), such that the peak value of the diagram lies near the leading edge then the result will be a sudden drop of pressure within a very short axial chord length. Moreover the peak velocity point will also be very near the leading edge. Because of this the design will also feature a very large region of adverse pressure gradient and thereby might result in a severe loss in efficiency due to separation.

On the other hand, if the histogram selected is such that the peak of the diagram lies near the trailing edge then the pressure drop will be smooth but near the trailing edge the adverse pressure gradient will be quite severe, and the possibility of separation becomes more pronounced.

The histogram selected with an equivalent area should be such that the curvature variation is not abrupt and is in small steps. It should be observed that the peak velocity point is very near to the value of $\frac{x}{b} = \frac{1}{2}$. Figures 1, 2 and 3 show that an attempt has been made to keep the $\frac{b}{R_s}$ distribution reasonably symmetrical with each turning angle and that while the number of steps are finite, one is in fact approximating a continuous distribution of curvature from the leading to the trailing edge.

Figures 4(a, b, and c) show the profile shapes obtained as a result of the procedure shown in Chapter 4. It can be seen that the pitch (S) goes on increasing as the lift coefficient increases. The pitch (S) is given by the relationship

$$C_L = 2 \frac{S}{b} \cos^2 \alpha_2 (\tan \alpha_1 - \tan \alpha_2)$$

Moreover, keeping the lift coefficient constant as the total turning angle increases the pitch (S) also increases for symmetrical blades. Figures 5 and 6 show further theoretical profiles obtained for increased turning angles. If we examine Figures 4(a), 5(a) and 6(a) in which the lift coefficient is the same, it can be seen that as the total turning angle increases the peak value of curvature also increases for symmetrical blades. It also can be seen that the throat position with respect to the blade moves forward as one increases the turning angle with the lift coefficient held constant.

As the total turning angle increases, the area of inlet section increases while the outlet throat area decreases keeping the lift coefficient constant and the same effect is observed by varying the lift coefficient and keeping the total turning angle constant. It is to be noted that as the outlet angle increases the throat area reduces quite considerably, moreover, the inlet section area continues to increase making the distribution of curvature very difficult. The blade profile thickness is purely dependent on the curvature distribution given. The analysis will show regions of high velocity (greater than $M = 1.0$) on some portion of the blade surface and significant pressure changes both positive and negative. The length of the blade profile and length of the trailing edge portion are directly proportional to the total turning angle, the lift coefficient and the blade outlet angle.

If the curvature distribution varies widely from point to point, the profile obtained will likely be a discontinuous one. Good design should ensure that the radii of curvatures of the pressure as well as of the suction surface all have the same sign otherwise the flow passage cannot be of the converging type. Present analysis provides blade profiles see Figures 4(a), (b) and (c), 5(a), (b) and (C) and 6(a), (b) and which have very smooth variations in curvature on both surfaces.

It will also be observed that the curvatures given along the trailing edge portion of the pressure surface are very small indeed. In the final analysis it can be seen that the main area of blade design involves the suction surface from the throat location to the leading edge while the pressure surface is completely defined in the programme. As one increases the lift coefficient and/or the turning angle, the length of the suction surface under analysis becomes shorter. Great care must be taken in establishing the orthogonal lines, particularly when dealing with high turning angles especially so if it involves high lift coefficients.

Figures 7, 8 and 9 show plots of pressure distribution around turbine blades as a function of the turning angle and lift coefficient. In all the pressure distribution curves the point of minimum pressure lies between $.2 \leq \frac{x}{D} \leq .55$ which as mentioned depends on the histogram selected. The area enclosed by the suction and pressure surfaces goes on increasing as the turning angle increases keeping the lift coefficient constant and the same is true if one holds the turning angle constant and increases the lift coefficient. On the suction surface the pressure

drops very quickly over the first half of the blade chord and then rises gently over the last half of the section. On the pressure surface the pressure coefficient remains relatively constant over 70% of the chord and is negative over the remaining 30%.

Since one of the boundary conditions dictate the exit plane conditions, i.e., atmospheric pressure, then the pressure at the inlet increases with both turning angle and lift coefficient. The main point of the design is to keep the region of adverse pressure gradient as small as possible consistent with having a value as low as possible.

It can be concluded that the theoretical losses associated with these blades are small. The power output per blade goes on increasing as the total turning angle and the lift coefficient are increased. For instance, the increase in power per blade in the case of $128^{\circ}-30'$, $C_L = .8$ is approximately 10% higher than the power output for a blade with a turning angle of 115° and the same lift coefficient.

Figures 10, 11 and 12 show plots of the pressure gradient $(\frac{dp}{ds})$ versus profile length. It can be seen that there is a drastic rate of decrease of pressure near the inlet section to the point of minimum pressure. The slope of these curves goes on increasing for a turning angle and increasing the lift coefficient. The slope of the curve is very small once the point of minimum pressure is passed showing that the adverse pressure gradient is almost negligible. Figure 10 shows that the point of minimum pressure appears at a lower value of profile length (s) as the lift coefficient increases. The same can be said for an increase in the turning angle for symmetrical blades.

Finally, let us observe the effect of turning angle and lift coefficient on the velocity triangles. Figures 13, 14 and 15 show the velocity triangles at both the inlet and outlet sections. The total change in tangential velocities continue to increase as the lift coefficient increases for a particular turning angle. Secondly, the axial velocity at the outlet section continues to increase as the outlet angle decreases. Moreover, the axial velocity at the outlet section goes on increasing as the lift coefficient increases for a constant turning angle blade. The rate of change of momentum continues to increase with lift coefficient constant and if one holds the lift coefficient constant then the same is true for increase in the total turning angle.

In practice the angle of attack can not be exactly zero degrees. So while designing these blades any angle of attack from zero to five degrees has been taken into account. Finally let us observe the theoretical performance of these blades at other than zero degrees angles of attack. Figures 16 (a), (b) and (c), 17 (a), (b), and (c) and 18 (a), (b), and (c) show the pressure distribution for incidence angles of 3° and 9° . The pressure at points on the suction surface near the leading edge rises and then decreases causing the increase in magnitude of, and the region of, adverse pressure gradient. The pressure rises on the entire pressure surface by a very small amount. There is a net loss in power developed which can be observed by noting the net area under the curves of the pressure and the suction surface of the 9° angle of attack.

Figure 19 shows the plot of pressure distribution along an orthogonal for a blade having a total turning angle of 115° and a lift coefficient of .8. This curve clearly indicates that the pressure rises very quickly up to the first three or four streamlines position and then the rate of increase of pressure is much more gradual over the remainder of the orthogonal length.

CHAPTER 6

CONCLUSIONS

This study represents a set of nine blades designed for three different total turning angles (140° , $128^\circ-30'$, 115°) each with lift coefficients as defined by Zweifel of .8, 1.0, and 1.2. The angle of incidence of the flow was varied in a consistent manner from zero to nine degrees for each blade in order to observe the affect of such incidence changes on the blade performance.

The results of the present study indicate that the power developed increases with an increase of the total turning angle while keeping the lift coefficient constant. The same is true when the total turning angle is kept constant and the lift coefficient is increased from .8 to 1.2. It was observed that the adverse pressure gradient and the losses associated could be reduced considerably by developing an improved profile. This was achieved by suitably defining the curvature of the pressure surface, the curvature of the suction surface and the orthogonal length to minimize the adverse pressure gradient. The blades were designed without twist which will add to the ease of manufacture particularly for cascade testing.

This analysis allows the conclusion that the blade efficiency can be increased,

- (a) by using lift coefficients greater than .8.
- (b) by increasing the total turning angle.
- (c) by using the respective profile developed as shown in Figures 4, 5, 6, ((a), (b) and (c)) for the corresponding turning angles and lift coefficients.

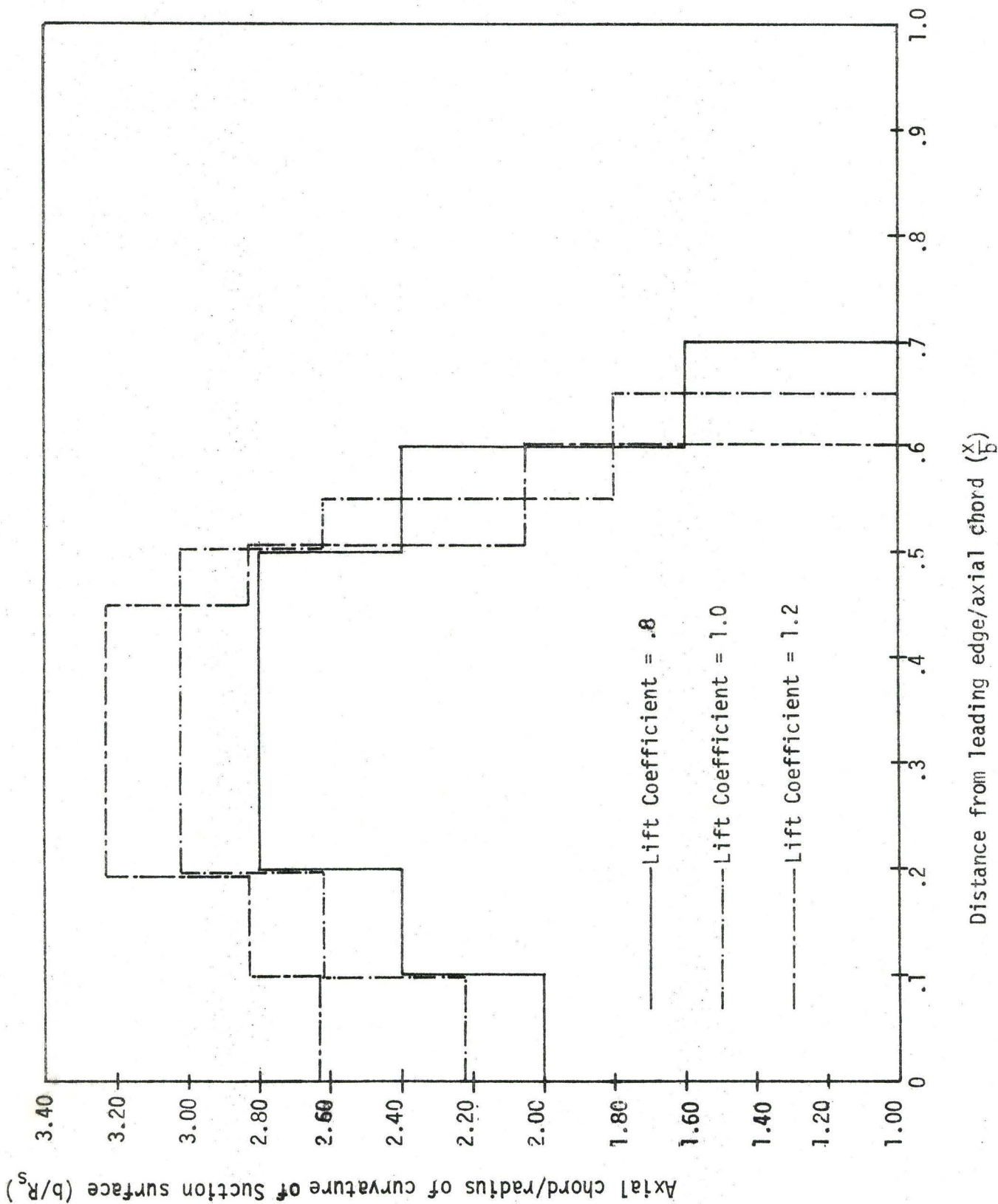
The use of high turning angle blades will allow an overall reduction in the number of blades and therefore reduce both the weight and the cost of a turbine of specified power.

REFERENCES

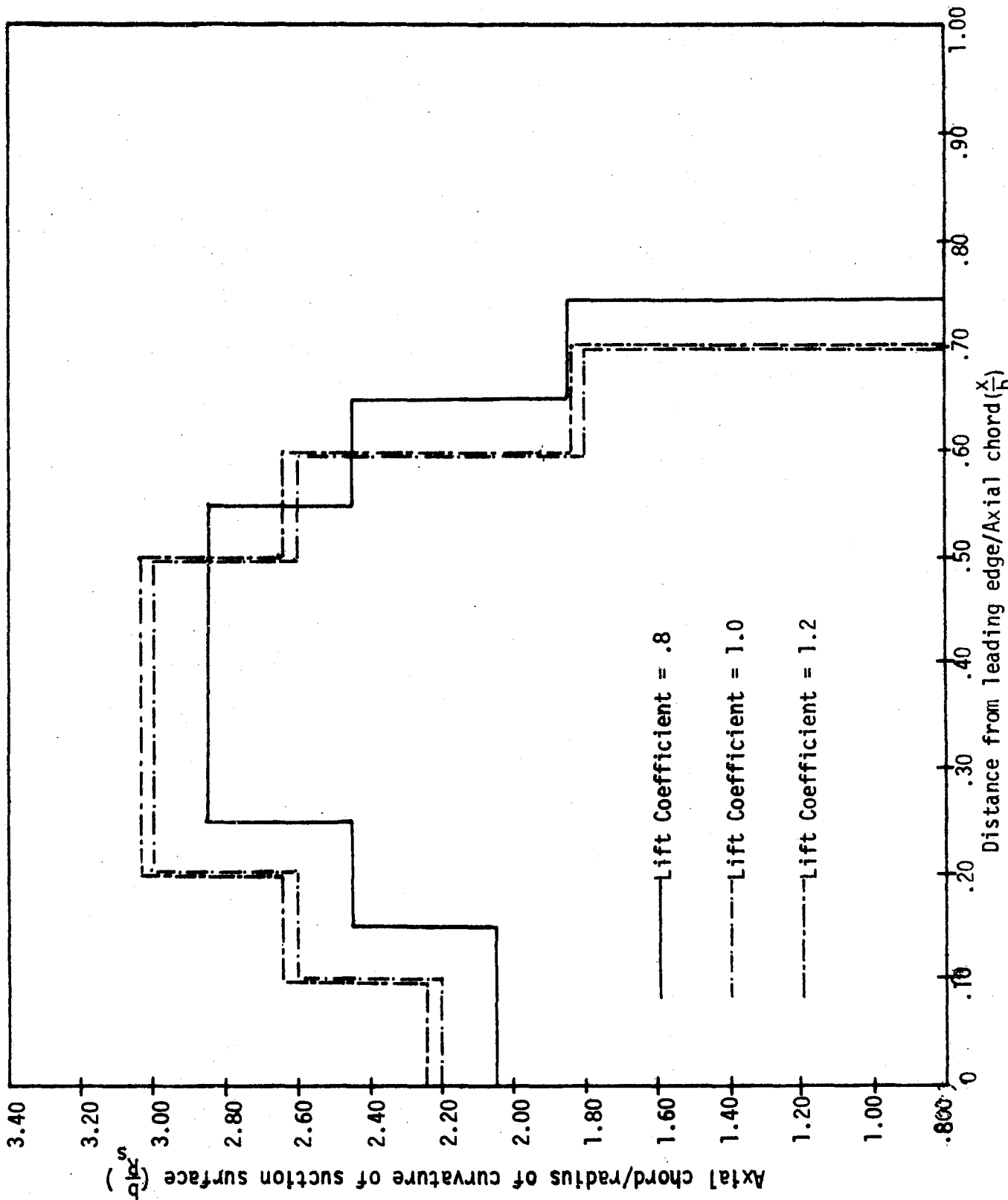
1. Tyler, R. A., Natl. Research Council of Canada Aero Note AN4; Ottawa, 1949.
2. Howell, A. R., J. Roy. Aeronaut. Soc. 52, 329 (1948).
3. Stodola, A., Steam and Gas Turbines, Translated by Loewenstein, New York, P. Smith, 1945.
4. Zweifel, O., The Spacing of Turbomachine Blading, especially with Large Angular Deflection, Brown Boveri Review, Dec., 1945.
5. Ainley, D. G., and Mathieson, G. C. R., A Method of Performance Estimation for Axial Flow Turbines; Brit. Aeronaut. Council Reports and Mem. 2974, 1957.
6. Stanitz, J. D., Design of Two Dimensional Channels with Prescribed Velocity Distribution along the Channel Walls, Part I, Relaxation Solution; NACA Tech. Note 2593, 1952.
7. Stanitz, J. D., Design of Two Dimensional Channels with Prescribed Velocity Distribution along the Channel Walls, Part II, Solution by Green's Function; NACA Tech. Note 2595, 1952.
8. George R. Costello, Robert L. Cummings and John T. Sinnette, Jr., Detailed Computational Procedure for Design of Cascade Blades with Prescribed Velocity Distribution in Compressible Potential Flows; NACA 1060, 1951.
9. George R. Costello, Robert L. Cummings and John T. Sinnette, Jr., Detailed Computational Procedure for Design of Cascade Blades with Prescribed Velocity Distribution in Compressible Potential Flows; NACA 1062, 1952.
10. Chung-Hua Wu and Curtis, A. Brown, A Theory of the Direct and Inverse Problems of Compressible Flow Past Cascade of Arbitrary Airfoils; J. Aero. Sci., 19(3), 1952 .
11. Kraft, H., The Development of Laminar Wing Type Turbine Bucket; Z. Angeio. Math. Phys., IX b, 1958 .
12. Martensen, G., Calculation of Pressure Distribution over Profiles in Cascade in Two Dimension Potential Flow by Means of a Fredholm Integral Equation; Archs. Ration. Mech. Analysis, 3, 3 1959 .

13. Baumgartner, F. and Amsler, R., Presentation of a Blade Design Method for Axial Flow Turbine Including Design and Test Results of a Typical Axial Flow Stage; Jour. of Engg. for Power, March, (1960).
14. Horlock, J. H., Axial Flow Turbines; Butterworths, 1966.
15. Dorman, T. E., Welna, H., and Lindlauf, R. W., Application of Controlled Vortex Aerodynamics to Advanced Axial Flow Turbines; ASME paper 68-GT-4, (1968).
16. Ainley, D. G., Performance of Axial Flow Turbines; Proc. Instn. Mech. Engrs., 159 (1948).
17. Emmert, H. D., Current Design Practices for Gas Turbine Power Elements; Trans. A.S.M.E., 72 (2), (1950).
18. United Aircraft of Canada Limited, Private Communication.
19. Hawthorne, W. R., Aerodynamics of Turbines and Compressors; Princeton Printing Press, 1964.
20. Horlock, J. H., Flow Disturbances due to Blade Thickness; J. Mech Eng. Science, VII, n 1, (1969).
21. Ainley, D. G., and Mathieson, G. C. R., An Examination of the Flow and Pressure losses in Blade Rows of Axial Flow Turbines; Brit. Aeronaut. Research Council, R and M 2891, 1955.
22. Sunder Rowtani, Vibration Analysis of Rotating Low Aspect Ratio Blades Idealized as Pretwisted Cantilever Plates; Ph.D. Thesis, Dept. of Mech. Eng., McMaster Univ., Hamilton, 1970.
23. Bury, K. V., A Method of Calculating and Designing for a Minimum Vibration Turbomachinery Blades; A.S.M.E. paper No. 67-Vibr-49, 1967.
24. Smith, J. E., The Vibration of Blades in Axial Turbomachinery; A.S.M.E. paper No. 66-WA/GT-12, 1966.
25. Armstrong, E. K., Recent Blade Vibration Techniques; A.S.M.E. paper No. 66-Wa/GT-14, 1966.
26. Mantell, C. L., Engineering Materials Handbook; McGraw Hill Book Company, 1958.
27. Whitehead, D., and Beavers, G. S., A Single Parameter Theory of Vortex Flow in Turbomachines; Aeronat. Research Council, R and M 3335, 1961.

28. Hilderband, F. B., Introduction to Numerical Analysis; McGraw Hill Book Company, 1956.
29. Miller, D. A. J., Faculty of Engineering, Carleton Univ., Ontario, Private Communication.
30. Vijay Kumar, The Design of Three Related Gas Turbines for an Experimental Investigation of the Effect of Blade Loading on Performance; Master Thesis, Dept. of Mech. Eng., Carleton University, Ottawa, Canada, (1968).



Histograms Showing the Proposed
 Figure 1. Variation of Curvature of Suction Surface
 Versus axial chord distance of turbine blade
 with turning angle 115° .



Histograms Showing the Proposed
 Figure 2. Variation of Curvature of Suction Surface
 Versus axial chord distance of turbine blade
 with turning angle $128^{\circ}-30'$.

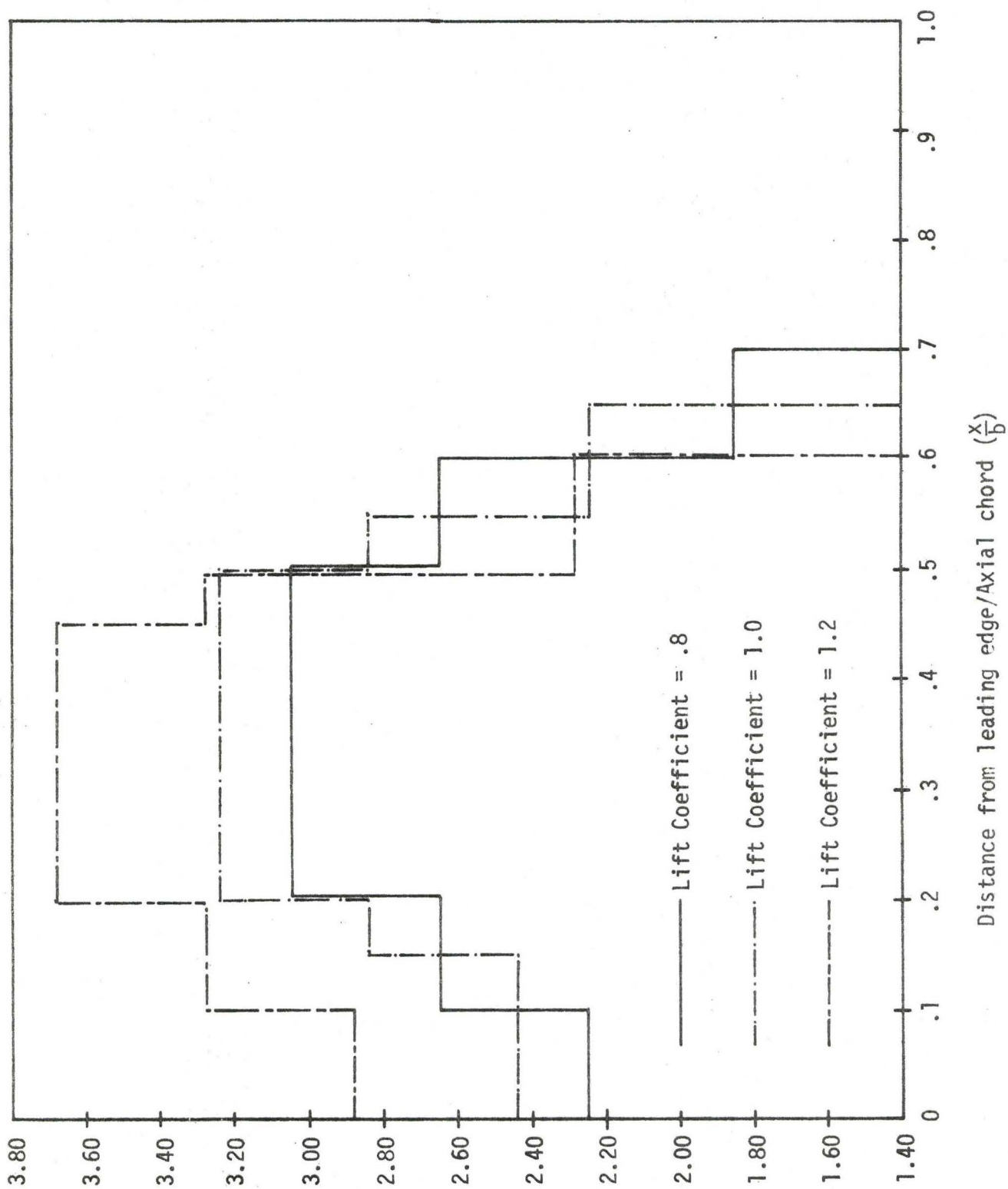


Figure 3. Variation of Curvature of Suction surface versus axial chord distance of turbine blade with turning angle 140° .

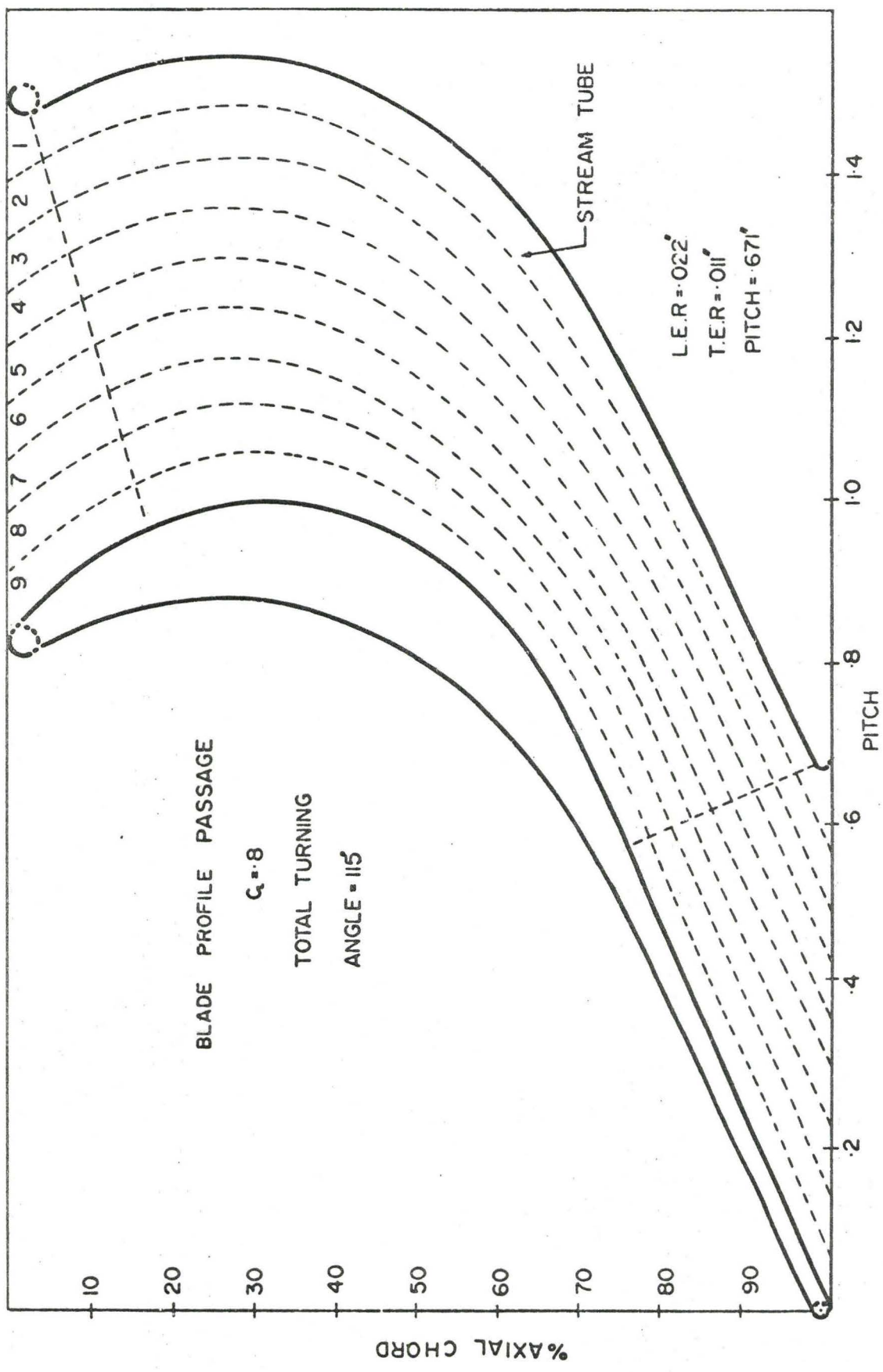


Figure 4(a) Blade Profile of Turning Angle 115° and Lift Coefficient .8.

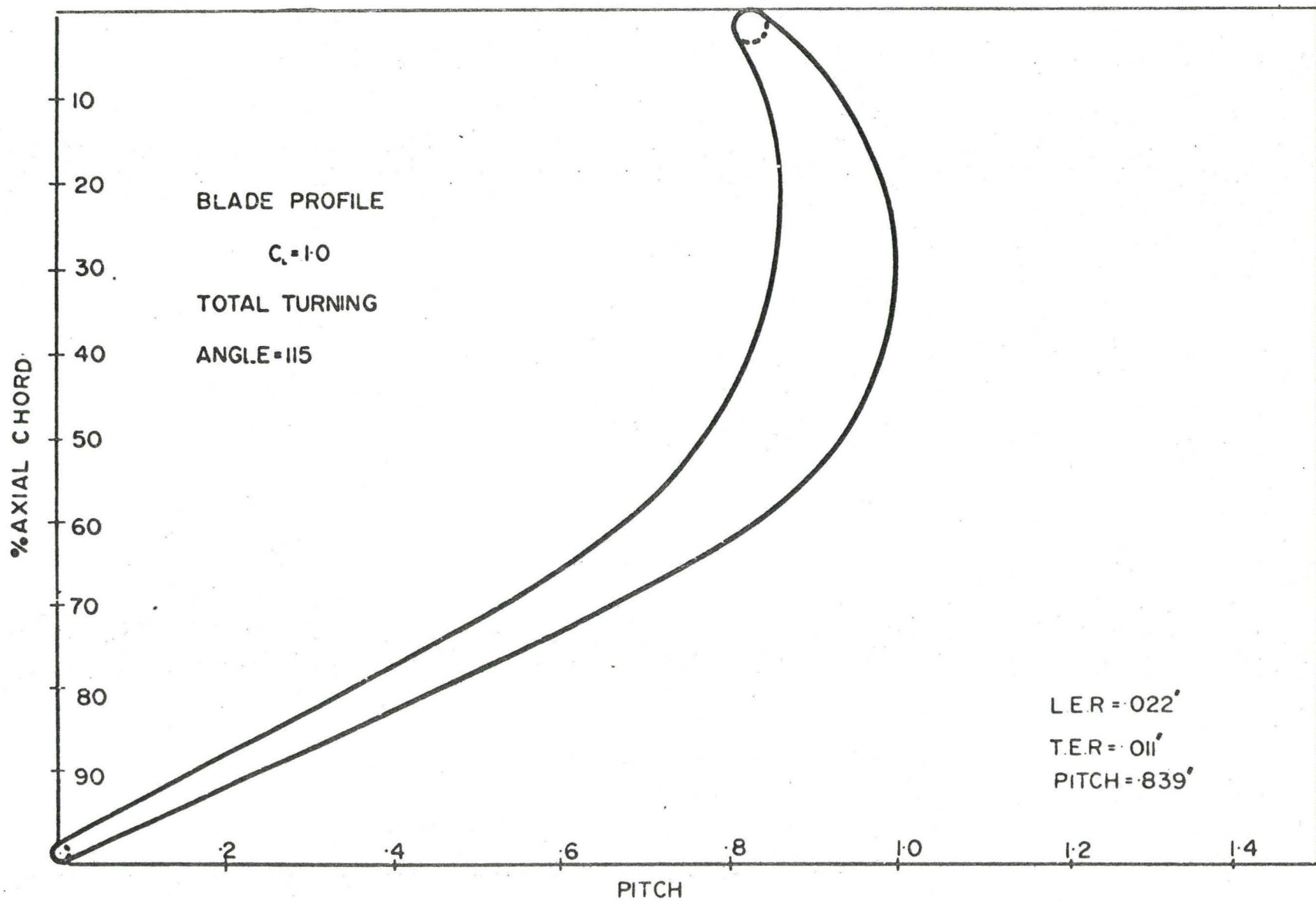


Figure 4(b) Blade Profile of Turning Angle 115° and Lift Coefficient 1.0.

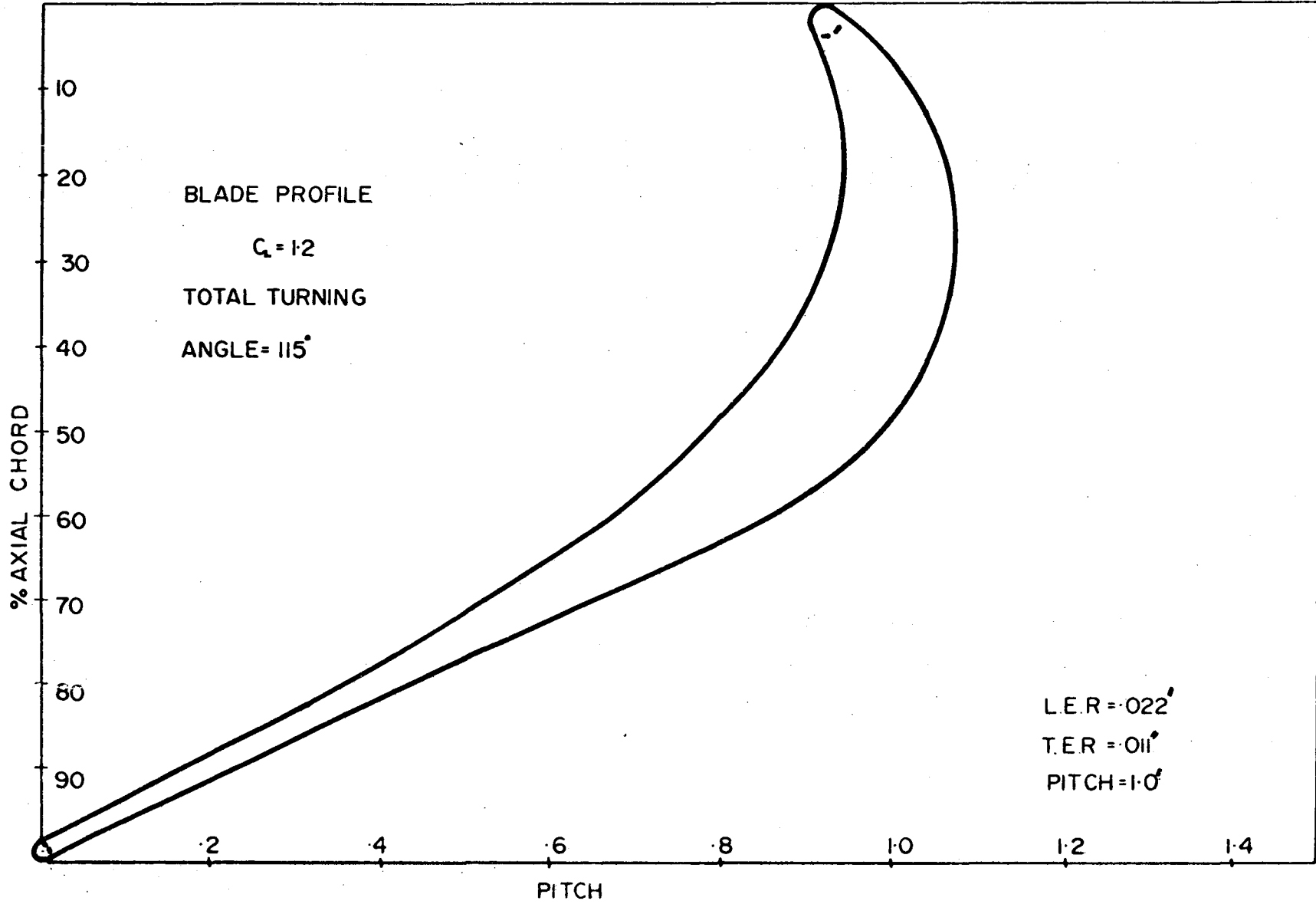


Figure 4(c) Blade Profile of Turning Angle 115° and Lift Coefficient 1.2.

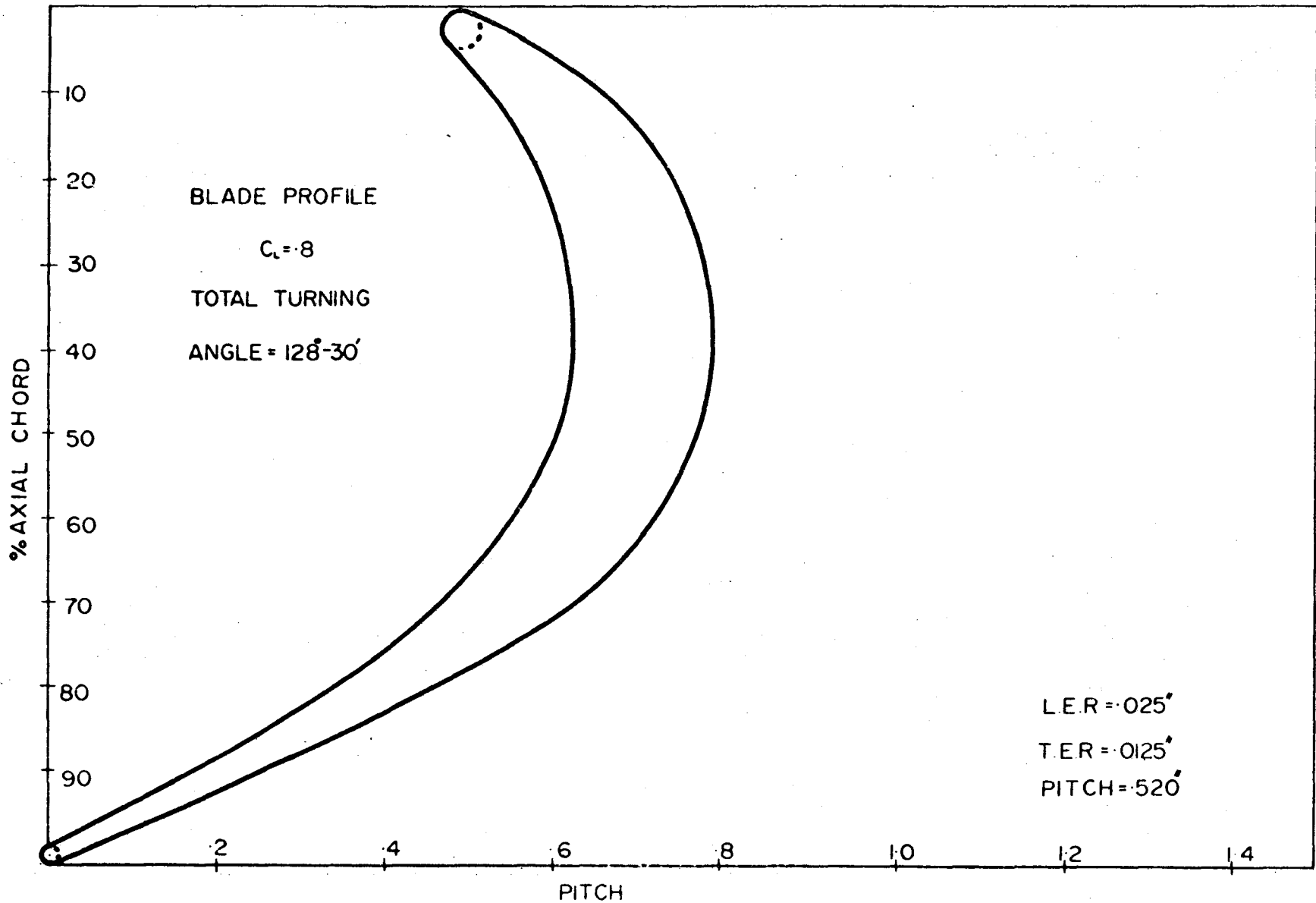


Figure 5(a). Blade Profile of Turning Angle $128^{\circ}-30'$ and Lift Coefficient .8.

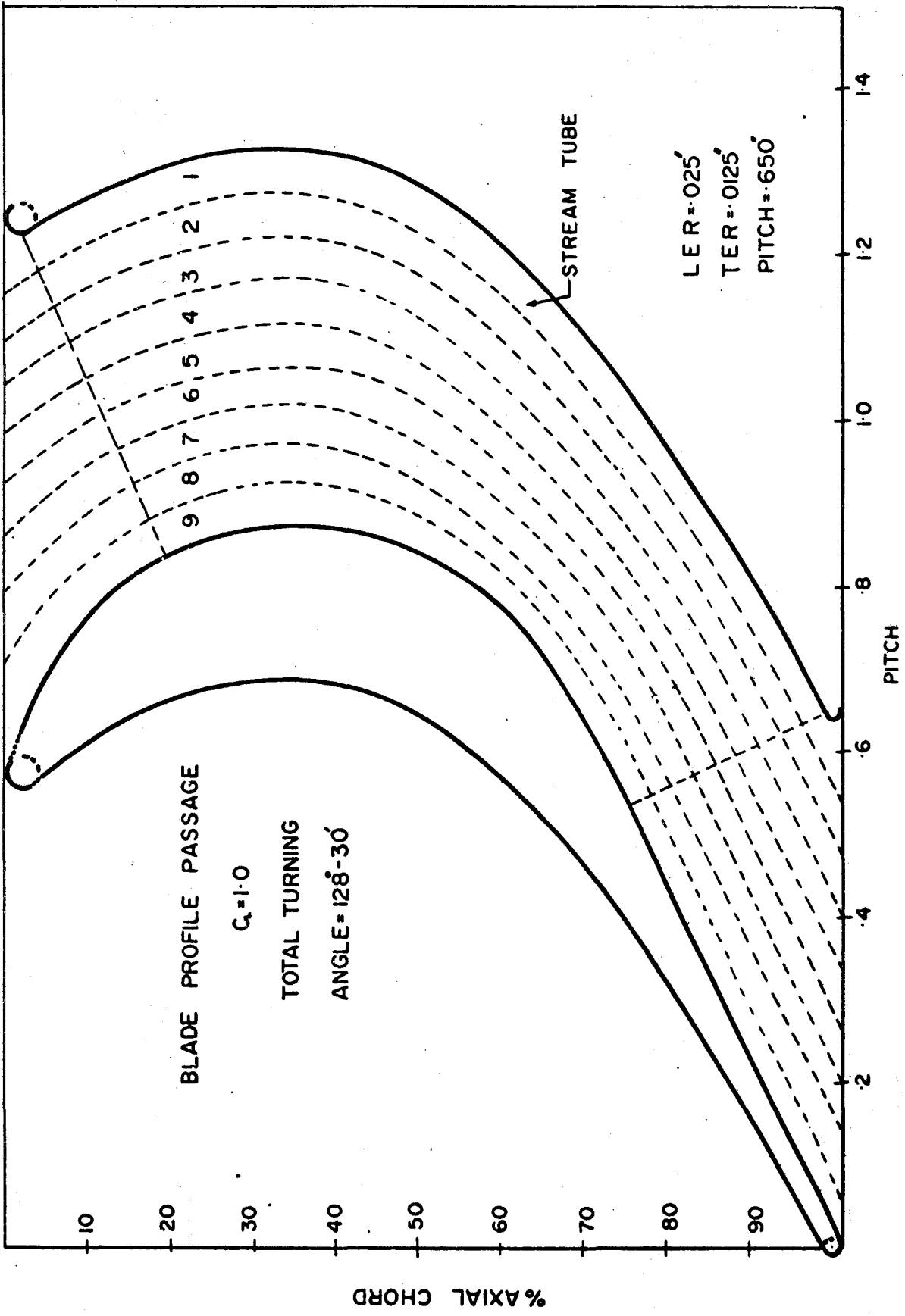


Figure 5(b). Blade Profile of Turning Angle $128^\circ-30'$ and Lift Coefficient 1.0.

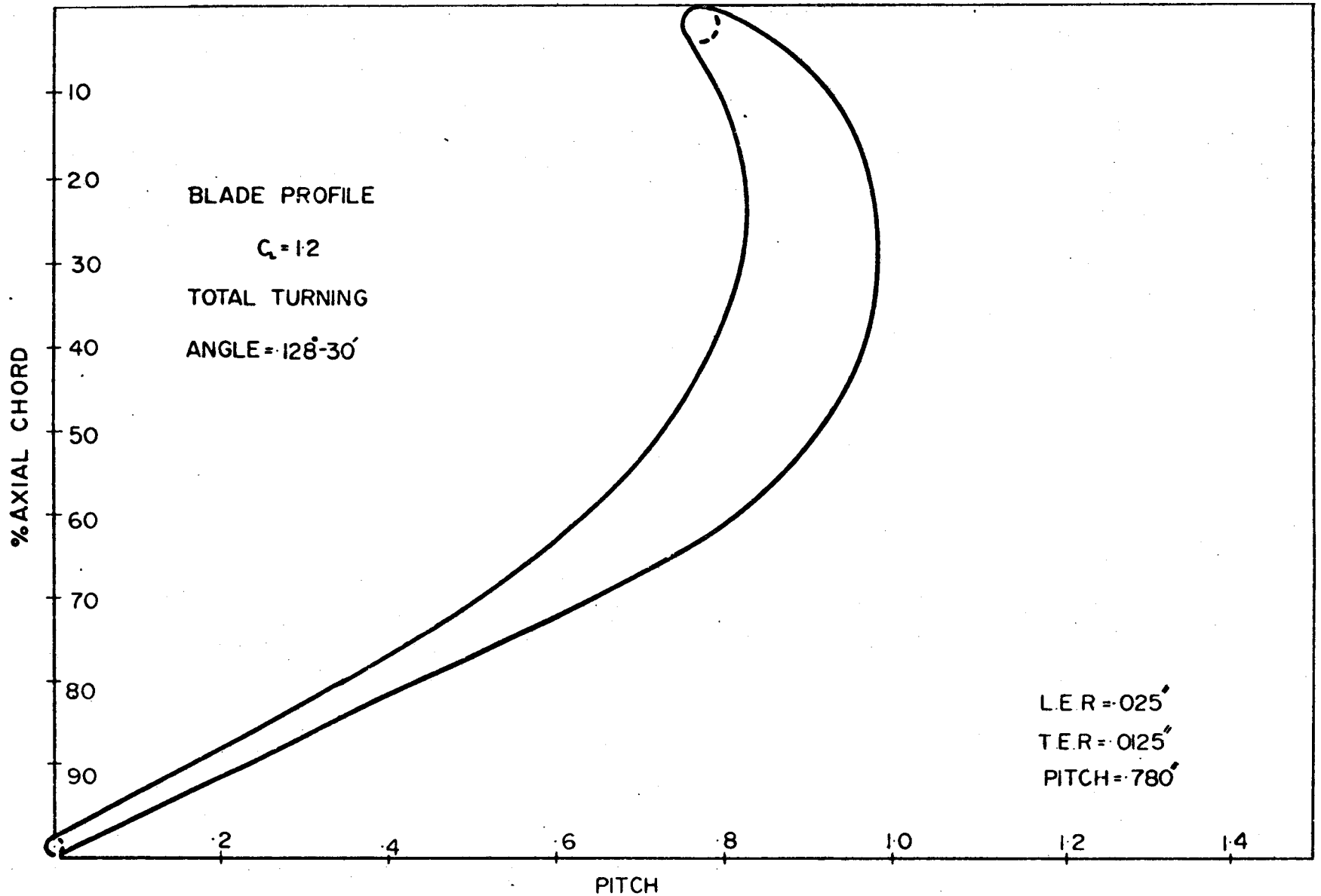


Figure 5(c). Blade Profile of Turning Angle $128^{\circ}-30'$ and Lift Coefficient 1.2.

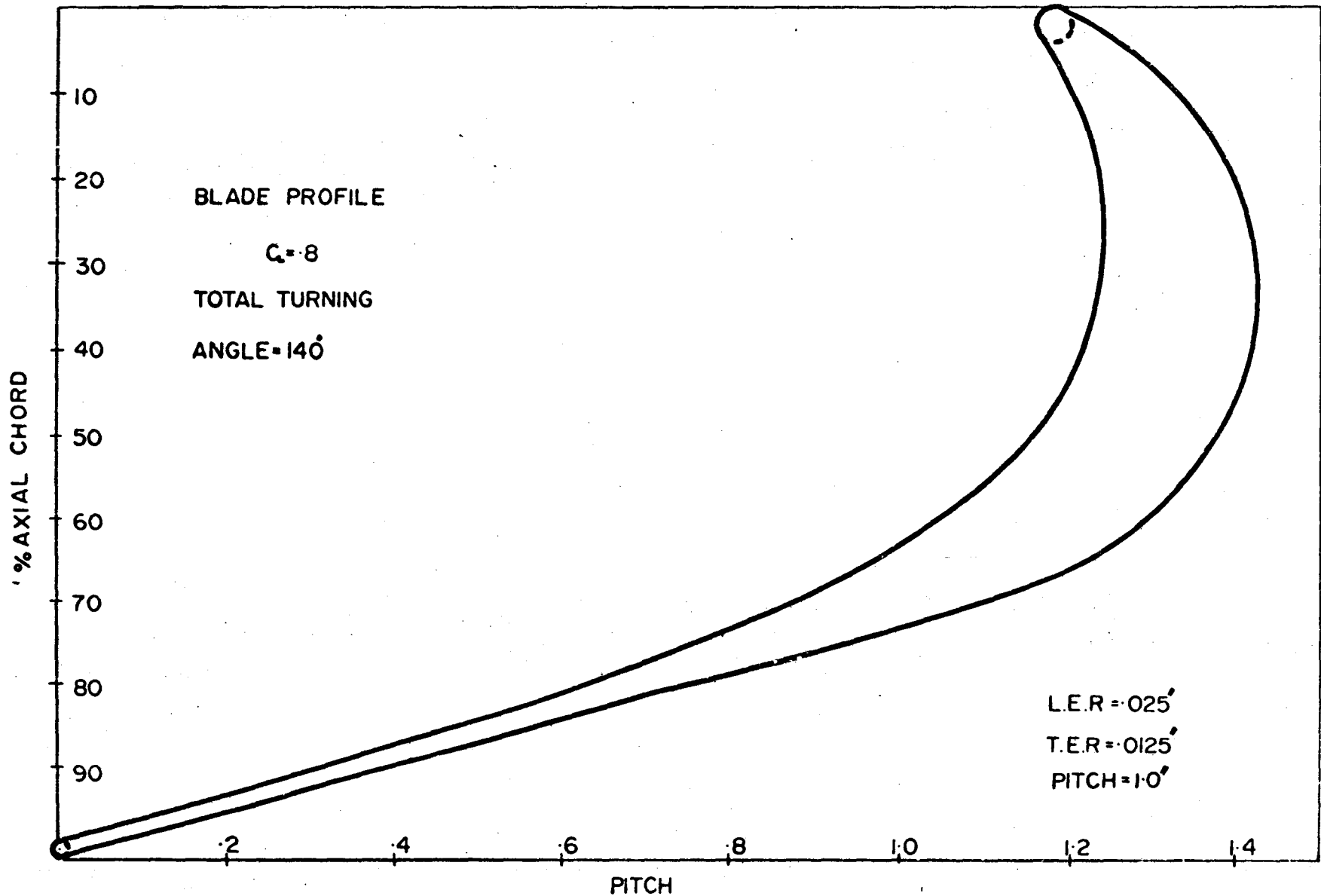


Figure 6(a). Blade Profile of Turning Angle 140° and Lift Coefficient .8.

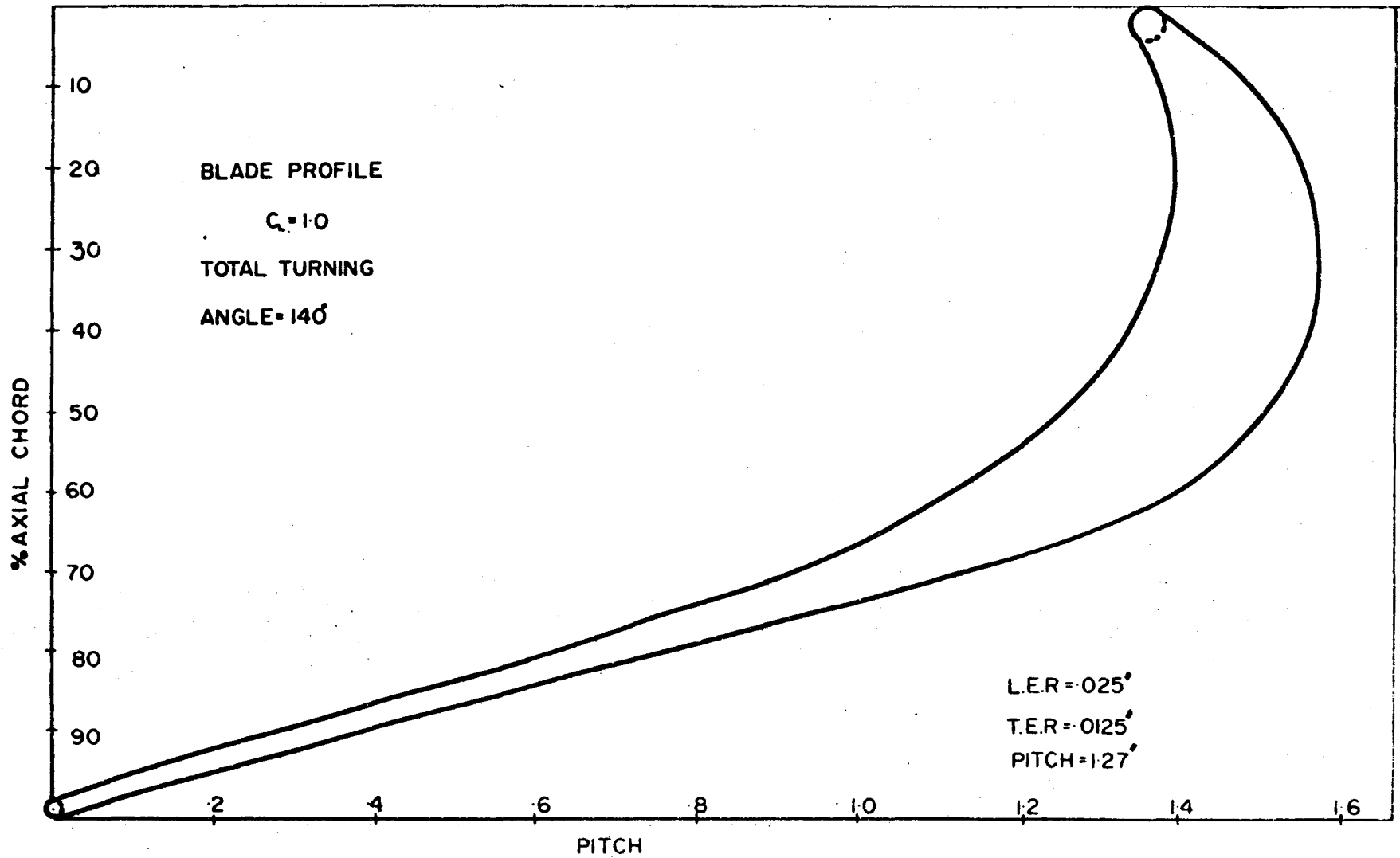


Figure 6(b). Blade Profile of Turning Angle 140° and Lift Coefficient 1.0

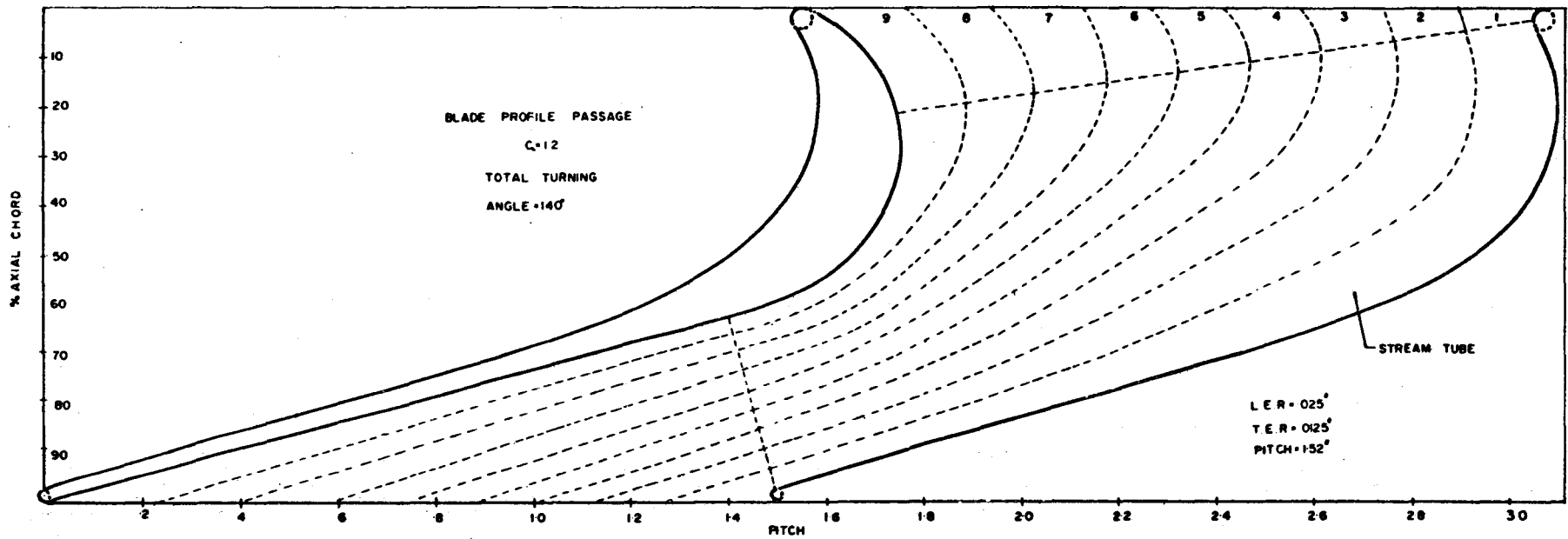


Figure 6(c). Blade Profile of Turning Angle 140° and Lift Coefficient 1.2.

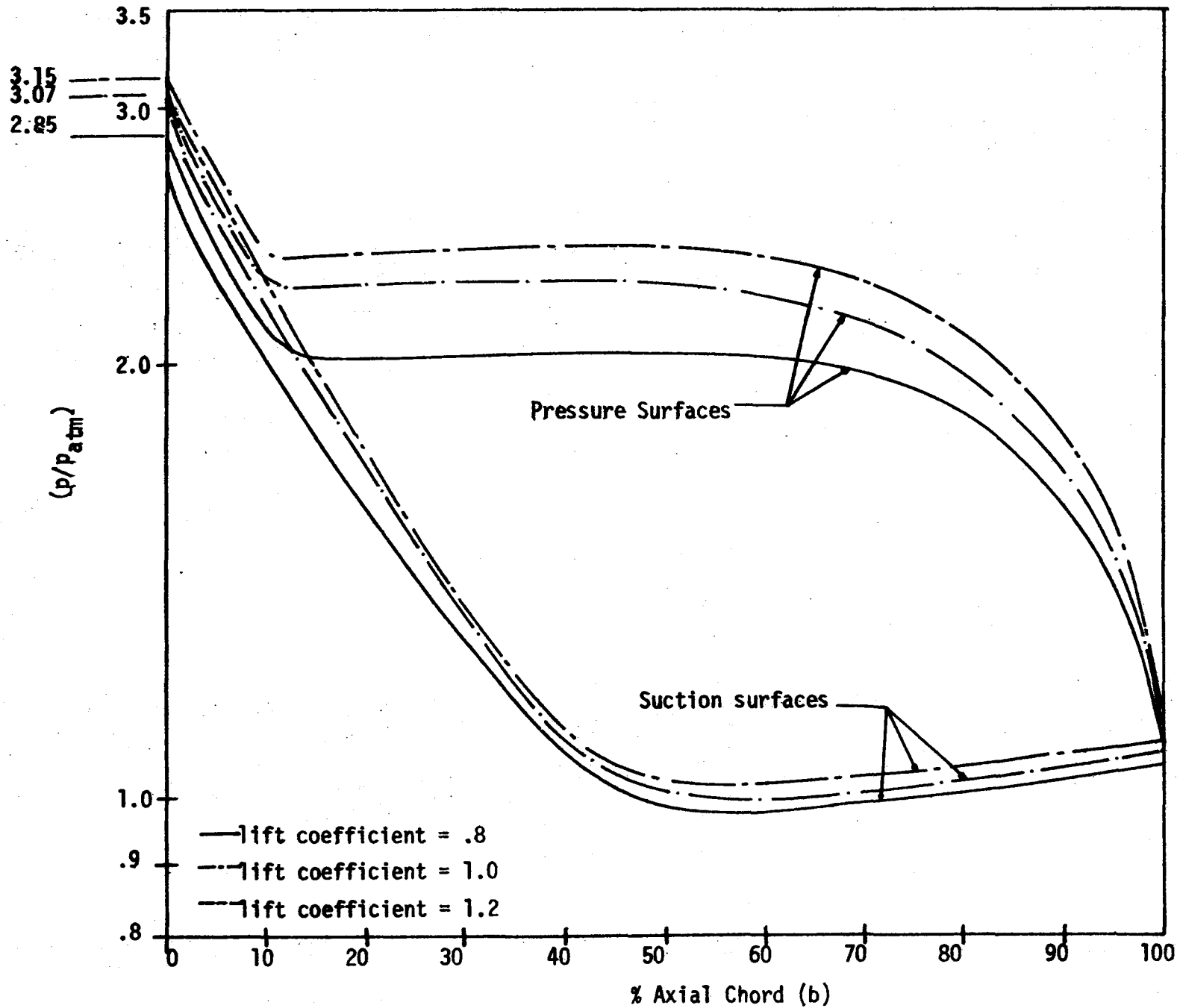
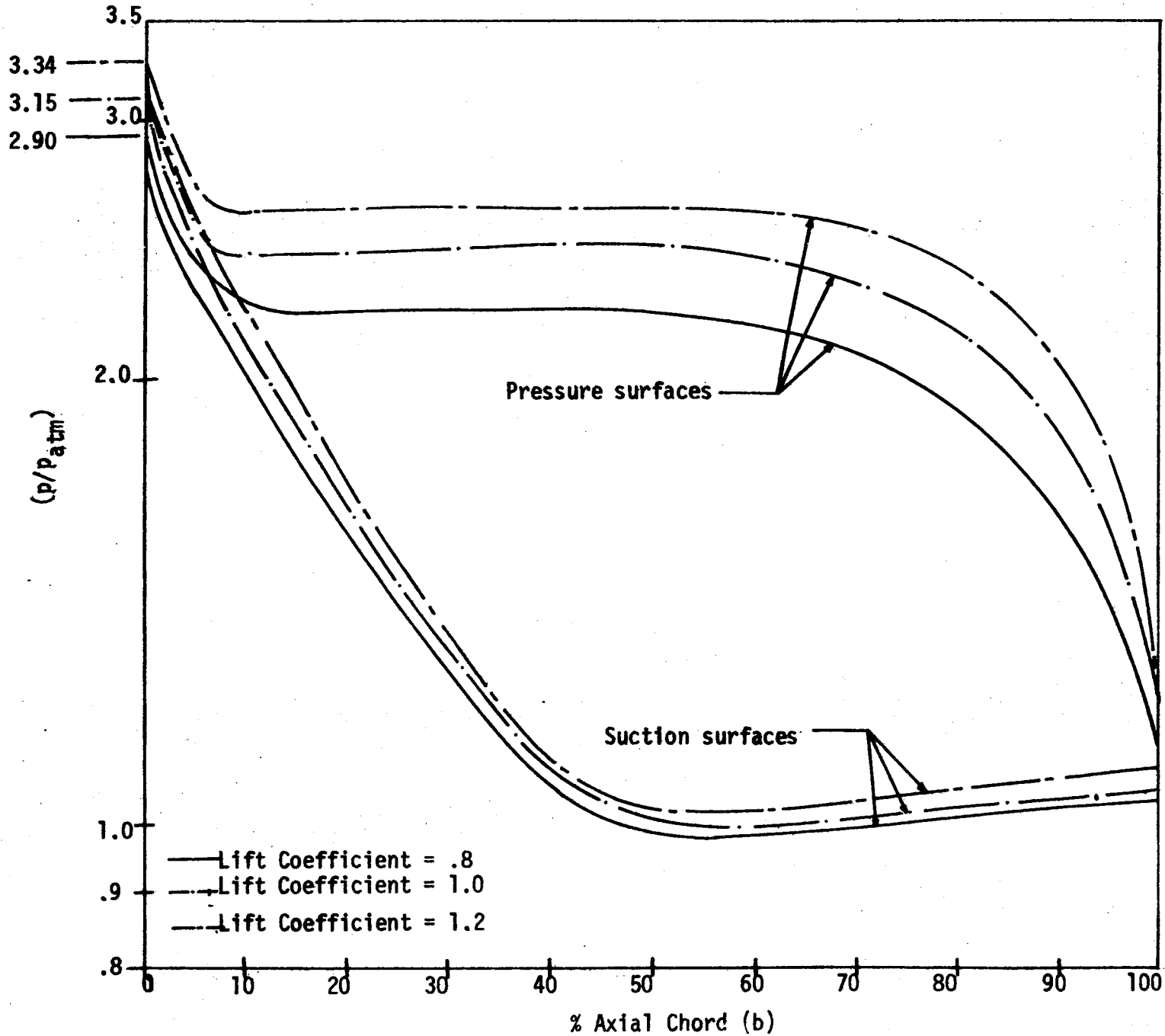


Figure 7 Pressure Distributions around turbine blades of turning angle 115° .



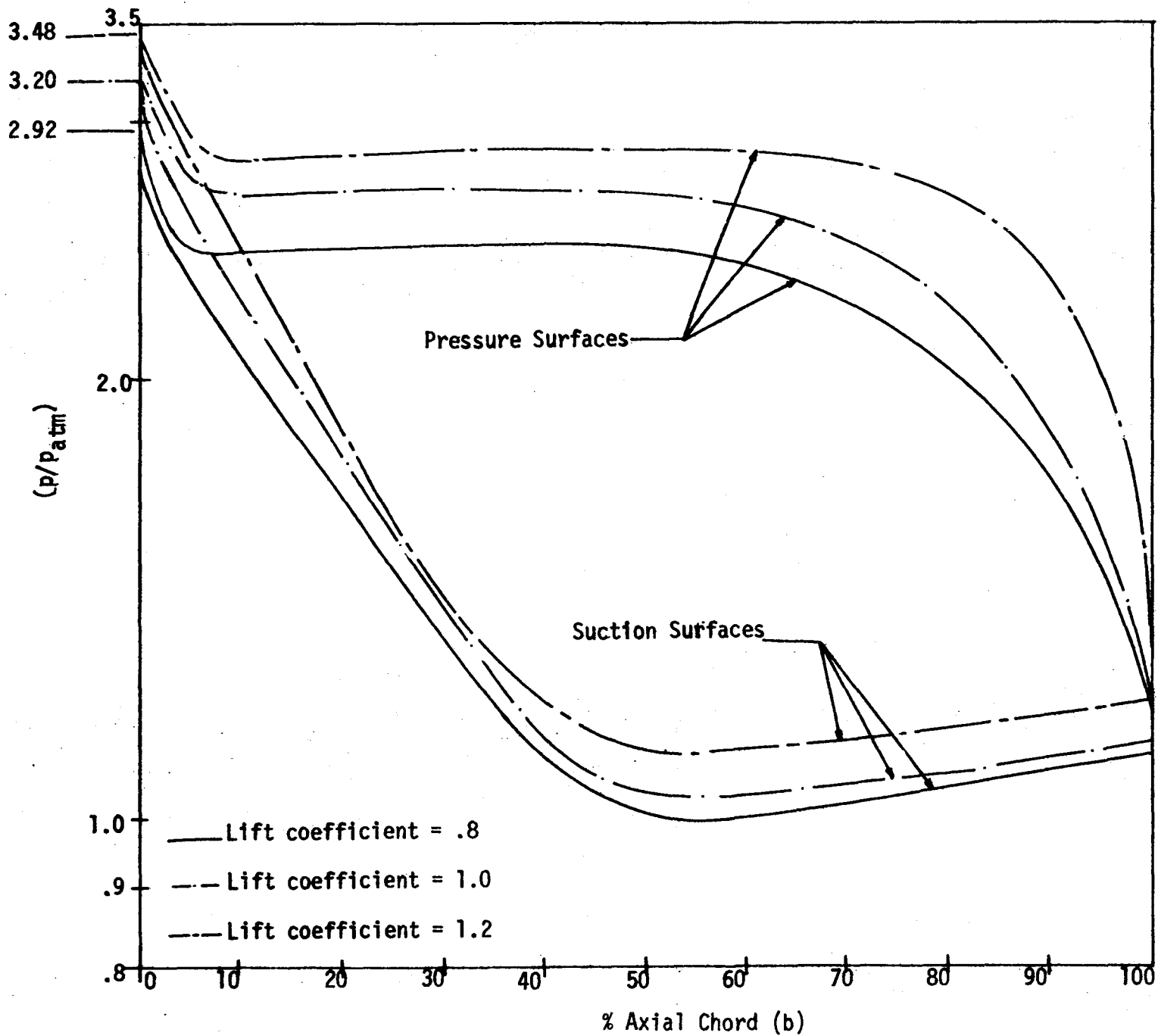


Figure 9 Pressure distributions around turbine blades of turning angle 140°.

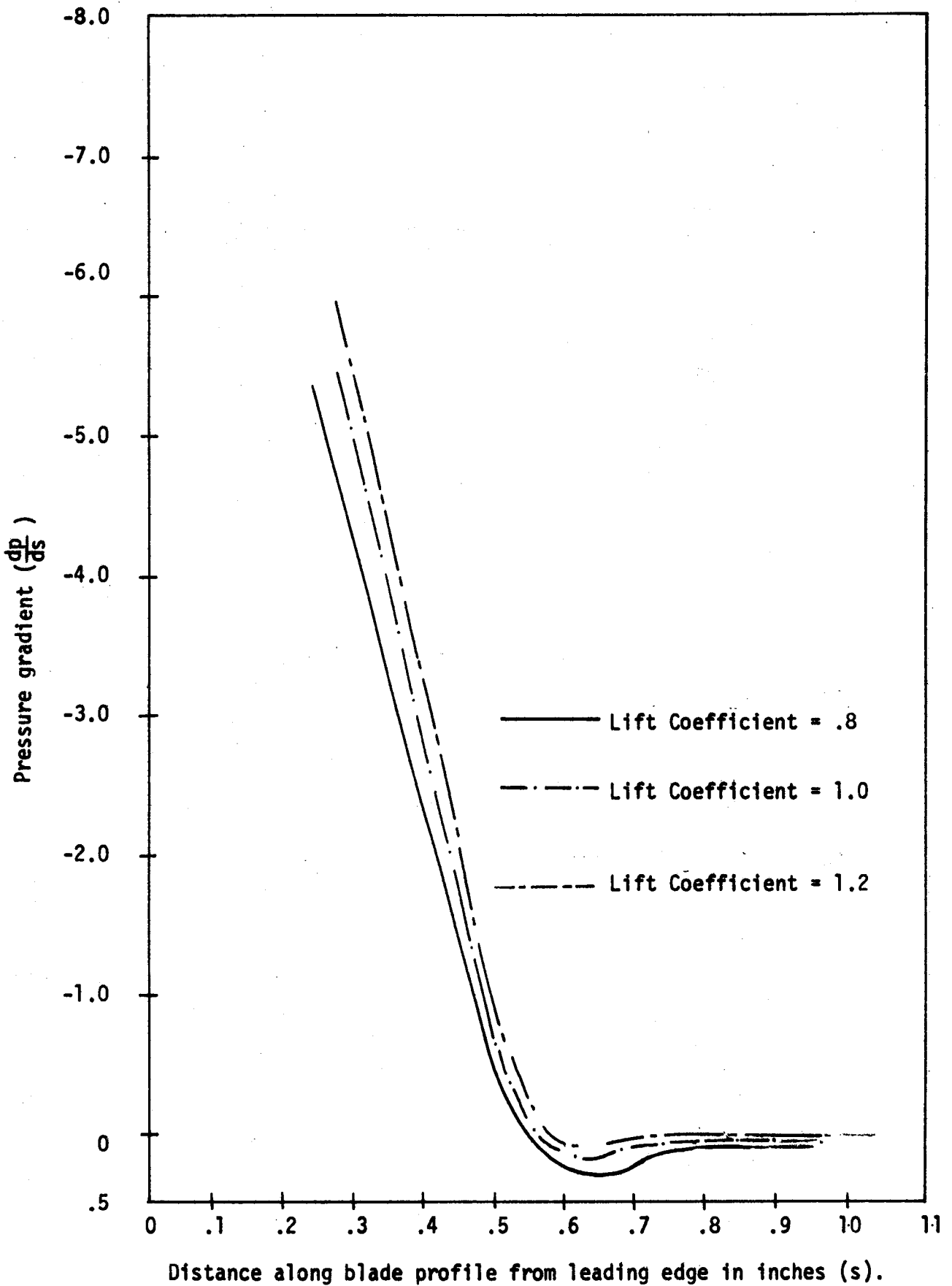


Figure 10. Variation of $\frac{dp}{ds}$ versus s of blade turning angle 115° .

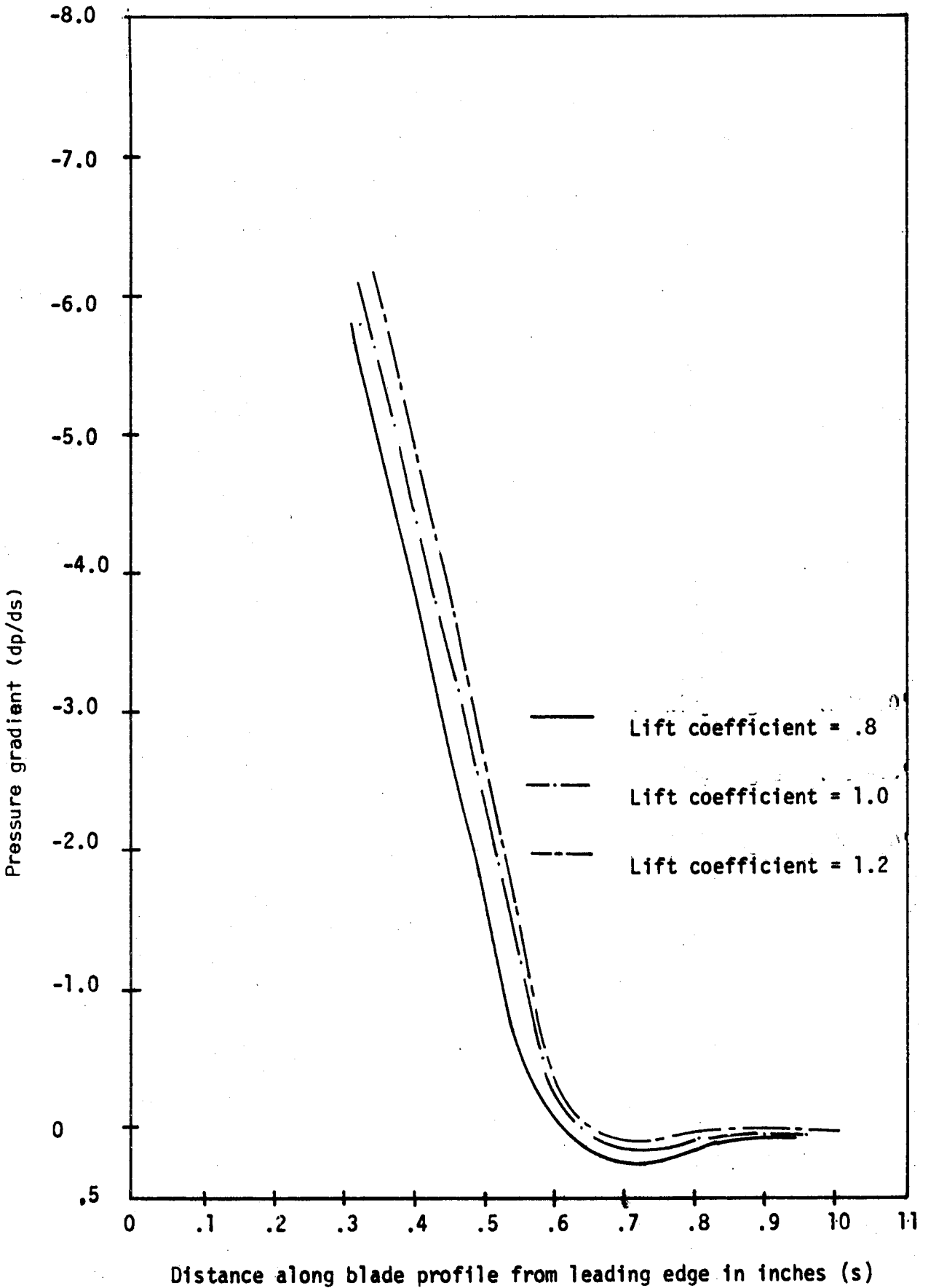


Figure 11. Variation of $\frac{dp}{ds}$ versus s of blade turning angle $128^\circ-30'$.

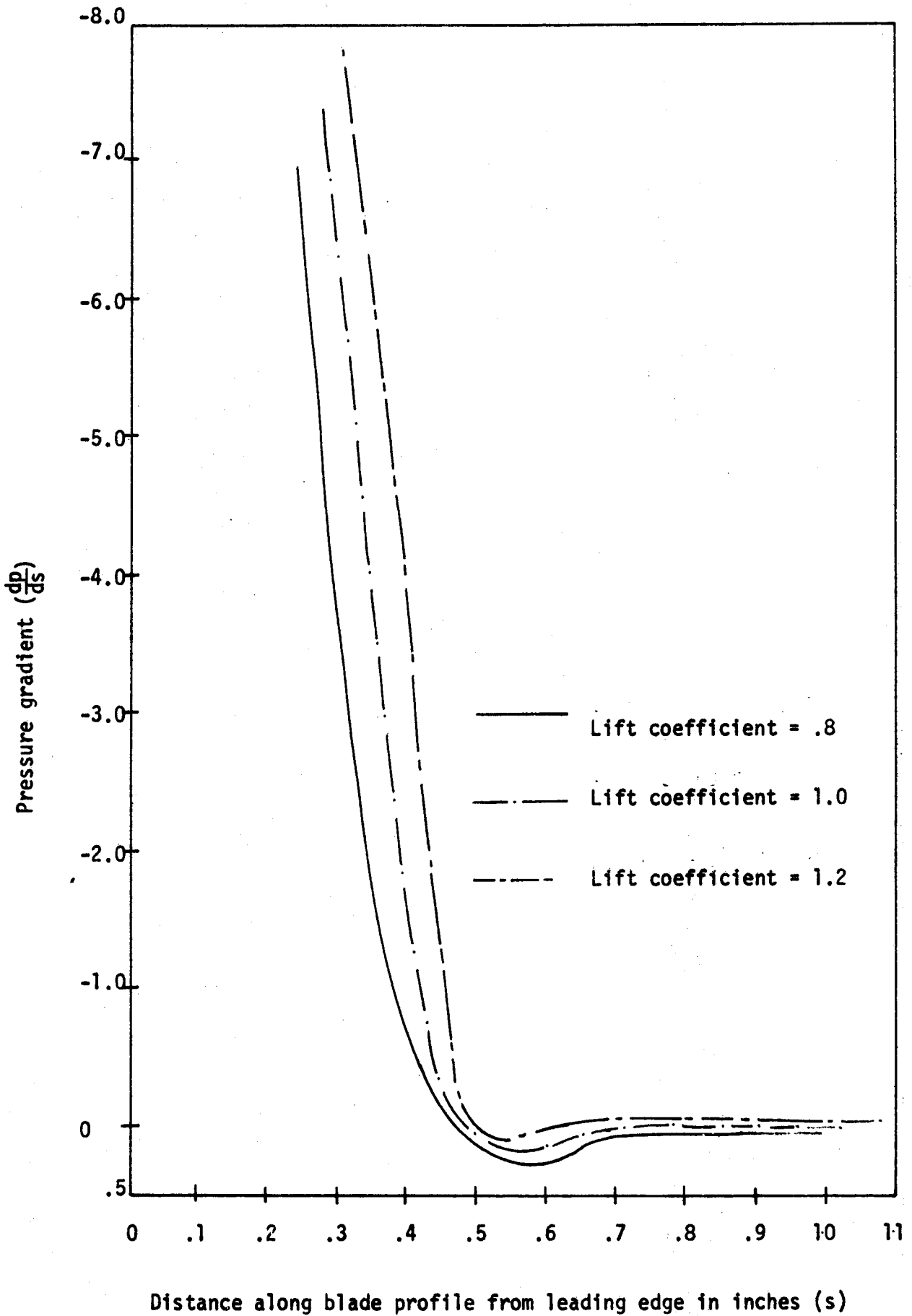


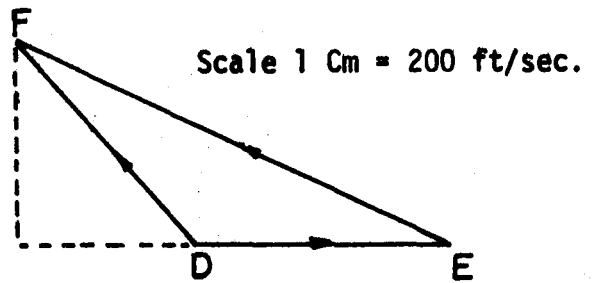
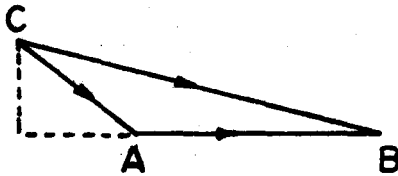
Figure 12. Variation of $\frac{dp}{ds}$ versus s of blade turning angle 140° .

$$AB = U, CA = W_1, CB = V_1$$

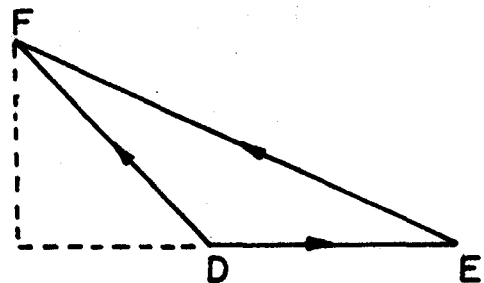
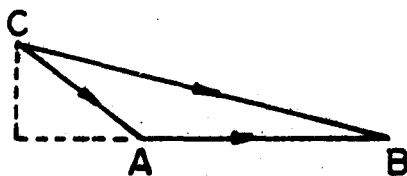
$$DE = U, EF = W_2, DF = V_2$$

$$U = 650 \text{ ft/sec}$$

(i) Lift Coefficient = .8



(ii) Lift Coefficient = 1.0



(iii) Lift Coefficient = 1.2

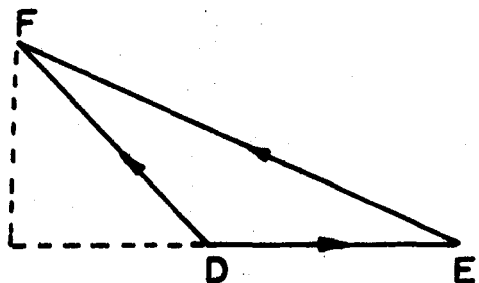
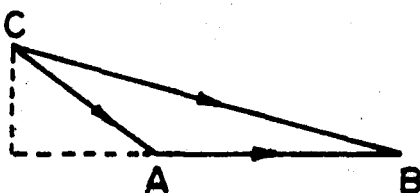
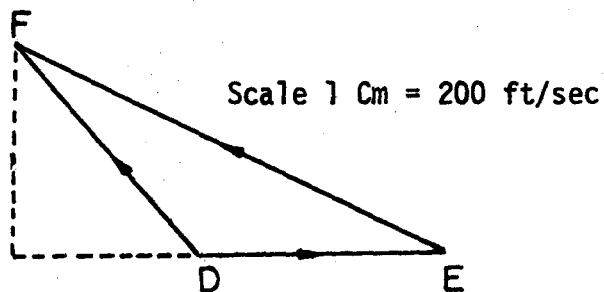
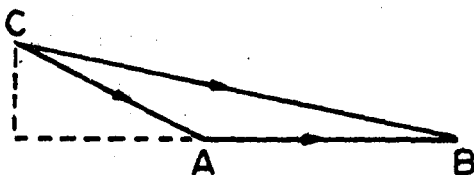


Figure 13. Velocity Triangles of Blade Turning Angle 115° .

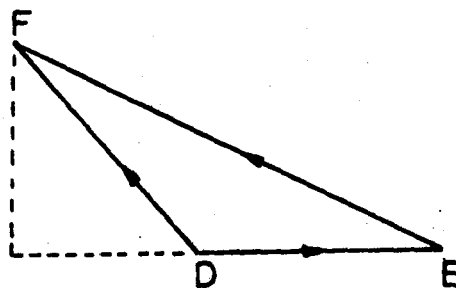
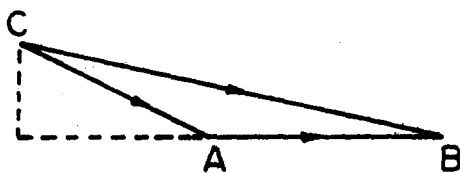
$AB = U, CA = W_1, CB = W_1$
 $DE = U, EF = W_2, DF = V_2$

$U = 650 \text{ ft/sec}$

(i) Lift Coefficient = .8



(ii) Lift Coefficient = 1.0



(iii) Lift Coefficient = 1.2

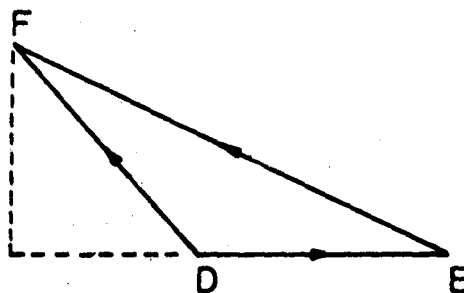
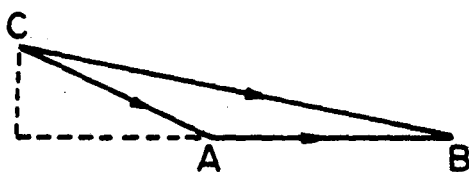


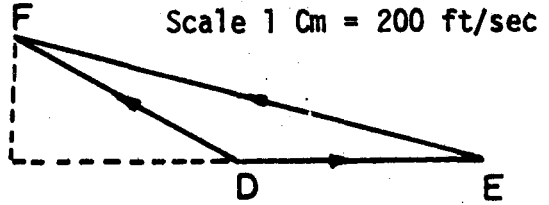
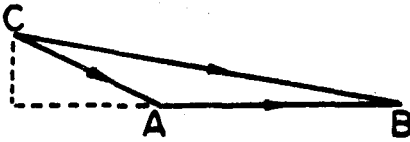
Figure 14 Velocity Triangles of Blade Turning Angle $128^{\circ}-30'$.

$$AB = U, CA = W_1, CB = V_1$$

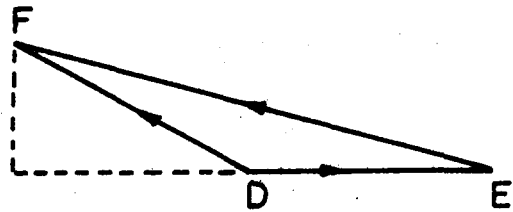
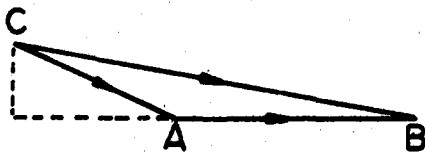
$$DE = U, EF = W_2, DF = V_2$$

$$U = 650 \text{ ft/sec}$$

(i) Lift Coefficient = .8



(ii) Lift Coefficient = 1.0



(iii) Lift Coefficient = 1.2

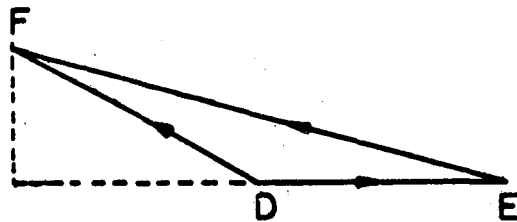
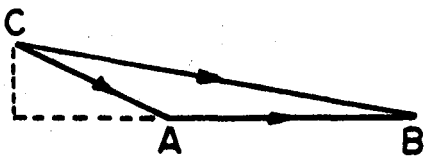


Figure 15 Velocity Triangles of Blade Turning Angle 140° .

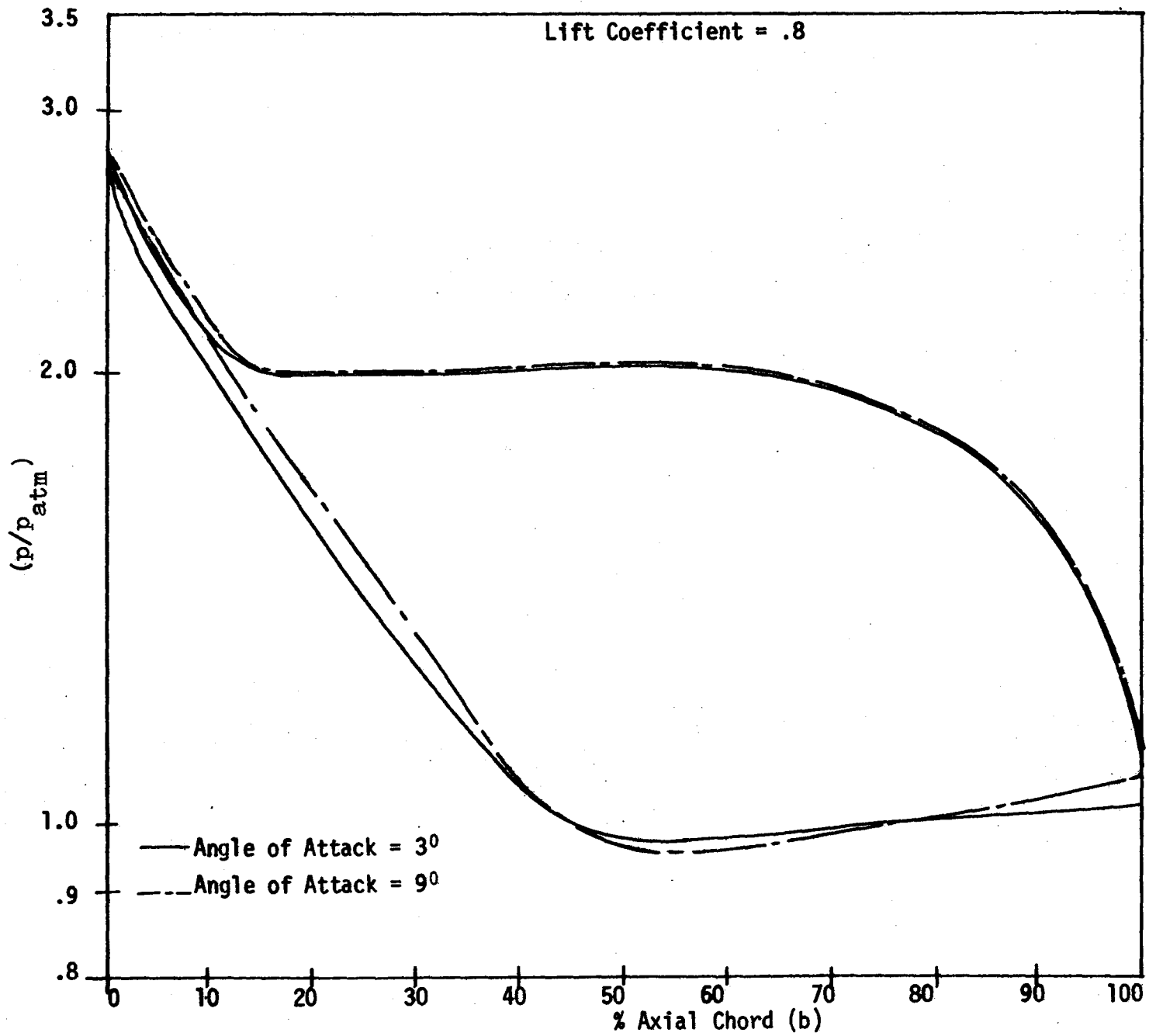


Figure 16(a). Pressure distributions around turbine blade of turning angle 115°, as a function of incidence angle for constant lift coefficient.

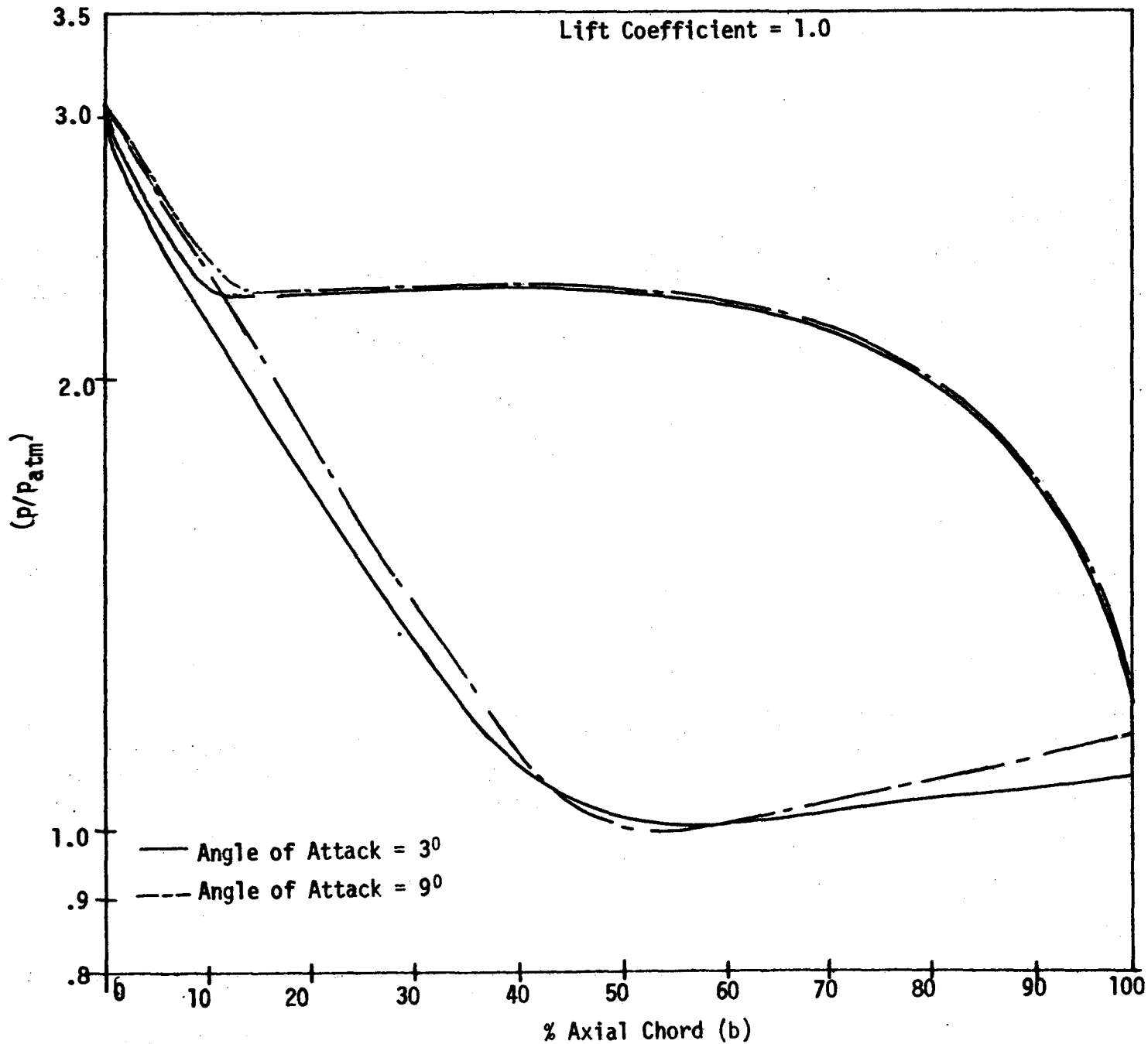


Figure 16(b) Pressure distributions around turbine blade of turning angle 115° as a function of incidence angle for constant lift coefficient.

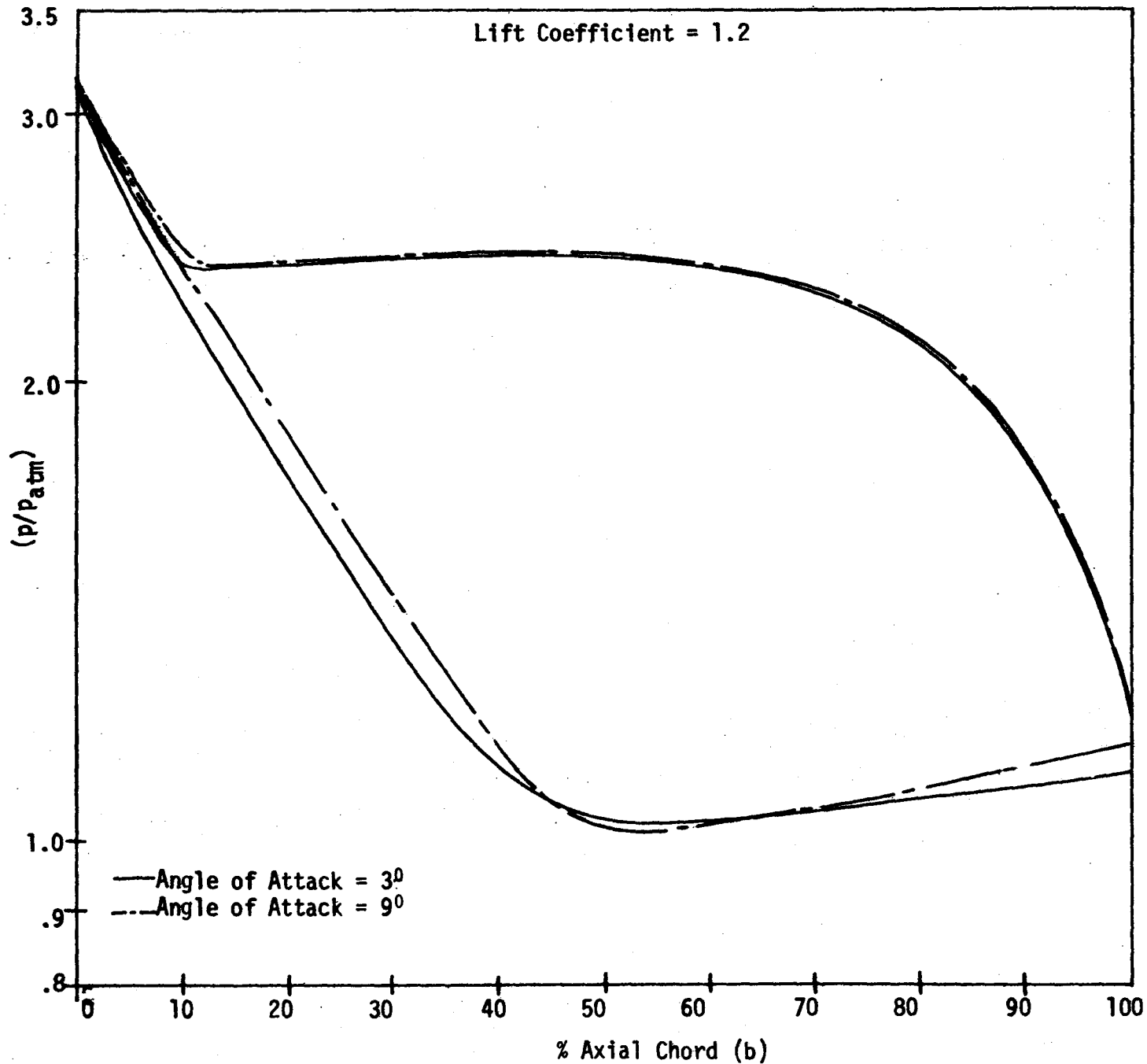


Figure 16(c) Pressure distributions around turbine blade of turning angle 115° as a function of incidence angle for constant lift coefficient.

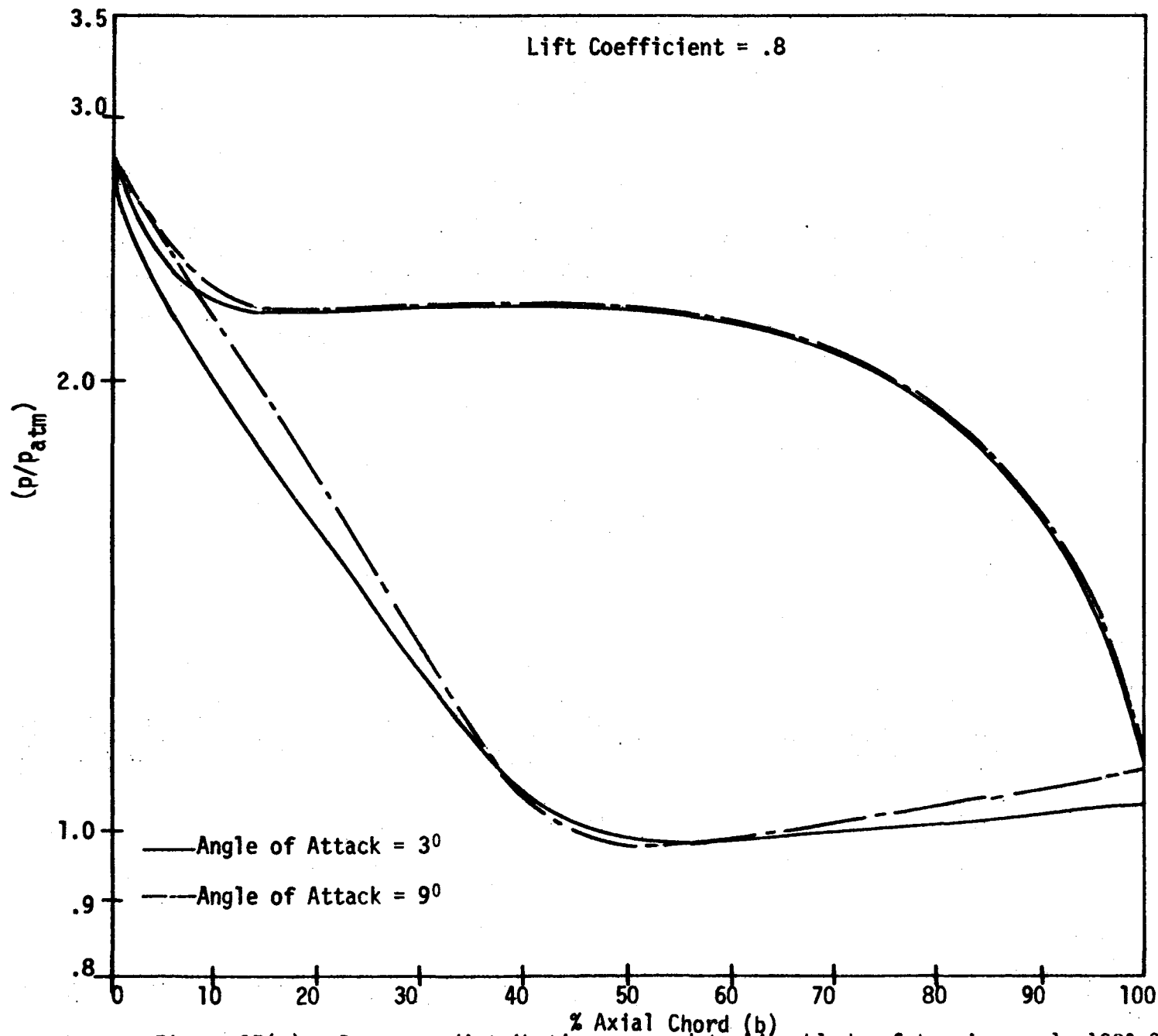


Figure 17(a). Pressure distributions around turbine blade of turning angle 128°-30' as a function of incidence angle for constant lift coefficient.

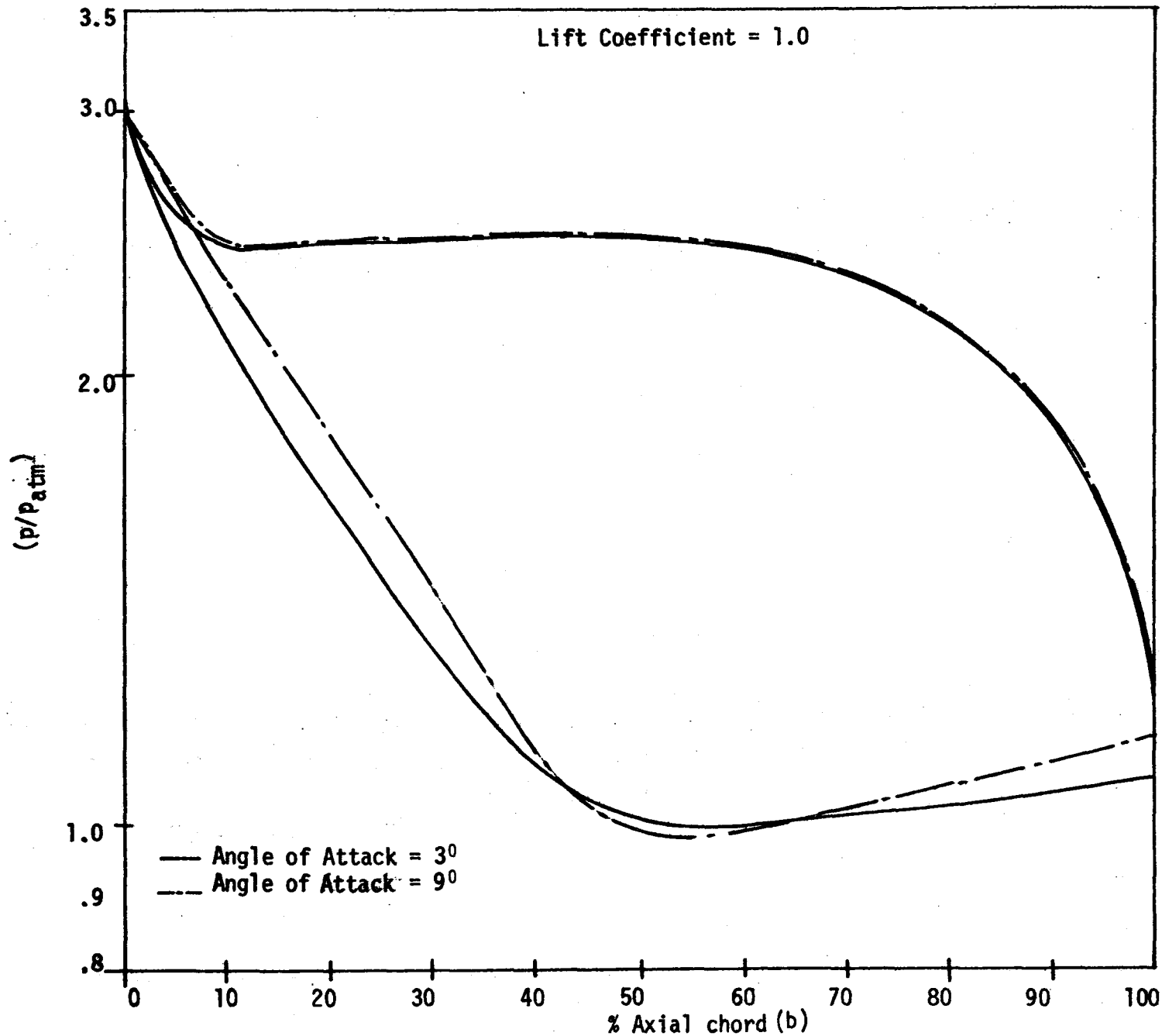


Figure 17(b). Pressure distributions around turbine blade of turning angle 128°-30' as a function of incidence angle for constant lift coefficient.

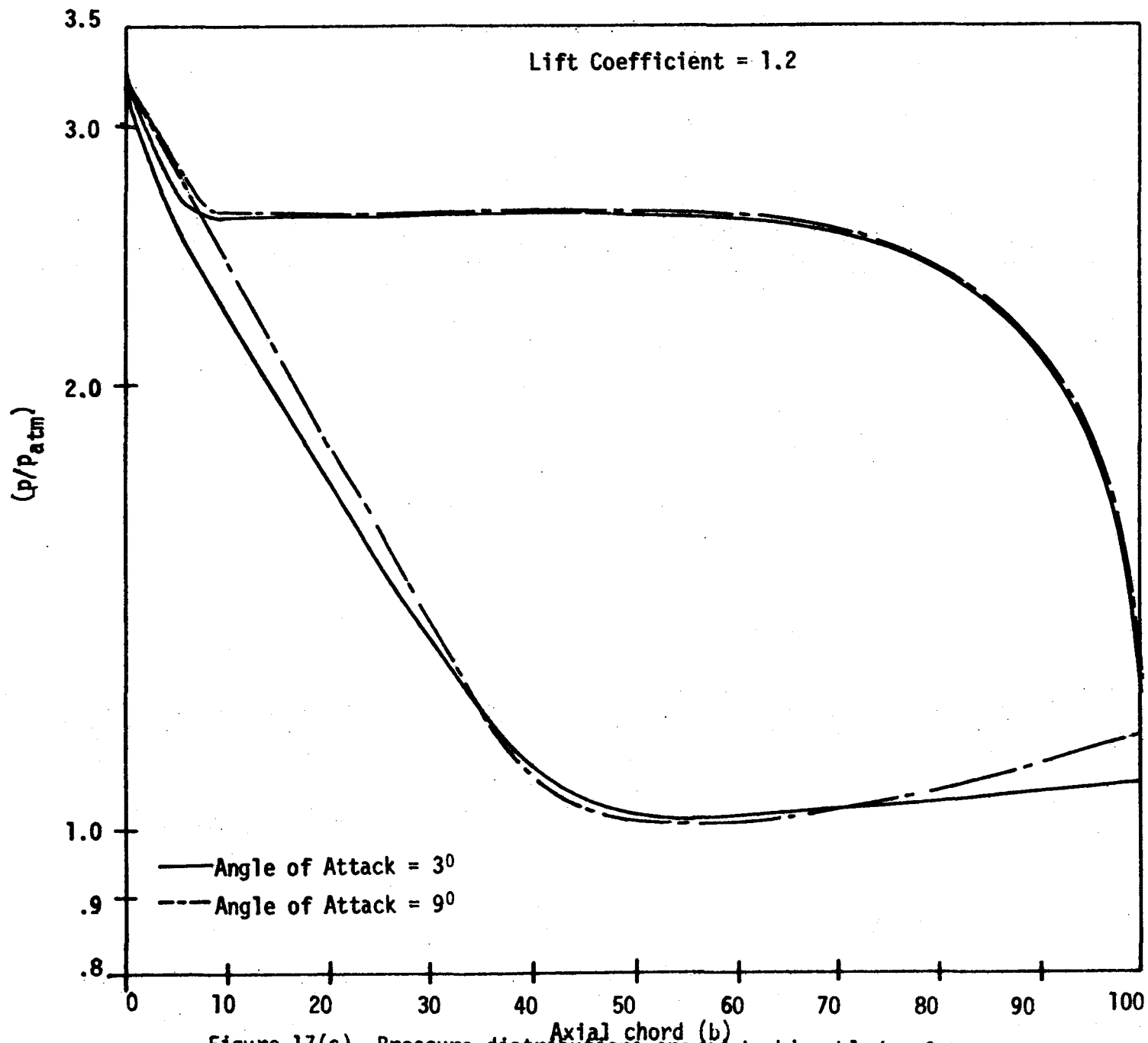


Figure 17(c) Pressure distributions around turbine blade of turning angle 128°-30' as a function of incidence angle for constant lift coefficient.

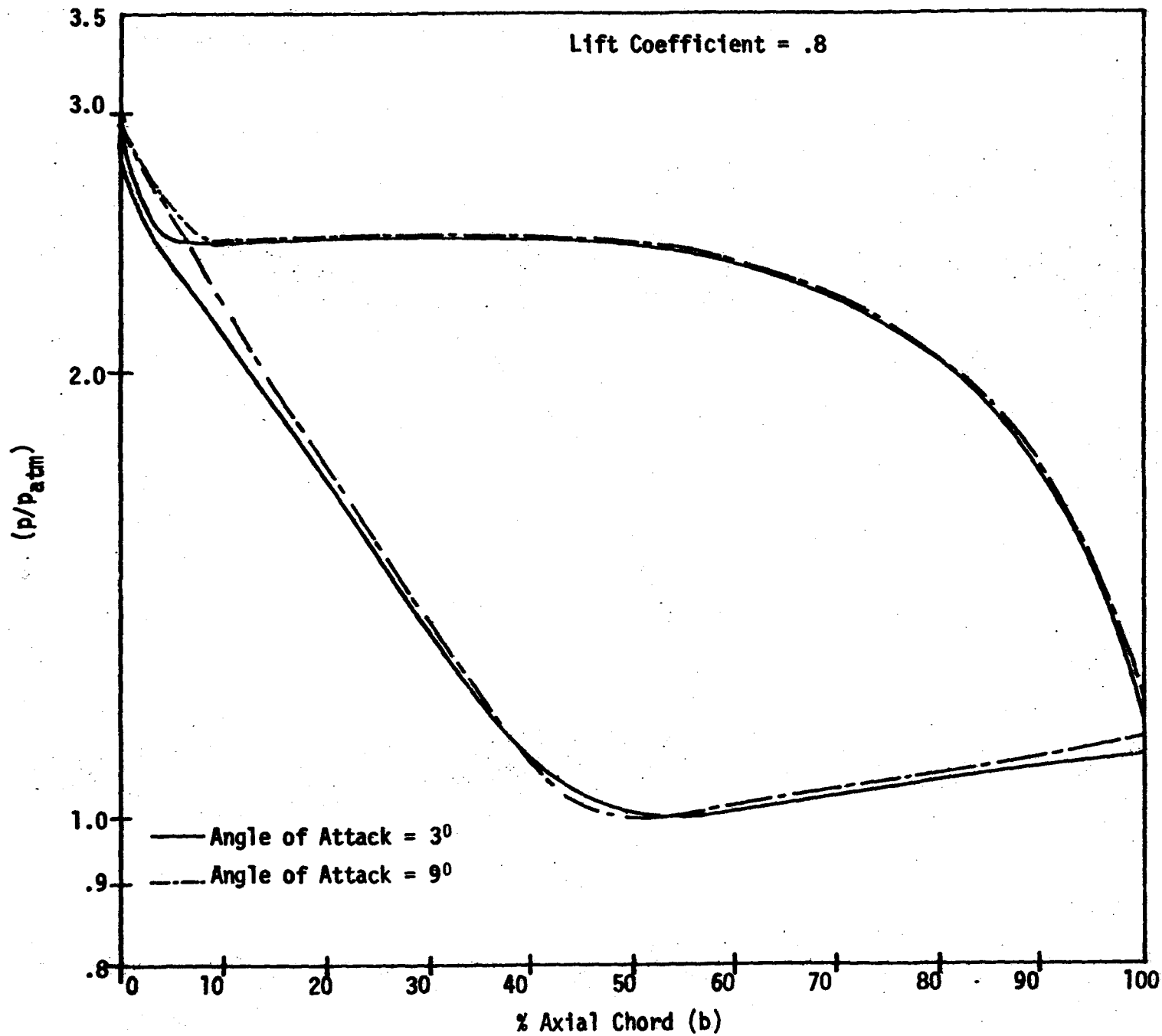


Figure 18(a) Pressure distributions around turbine blade of turning angle 140° as a function of incidence angle for constant lift coefficient.

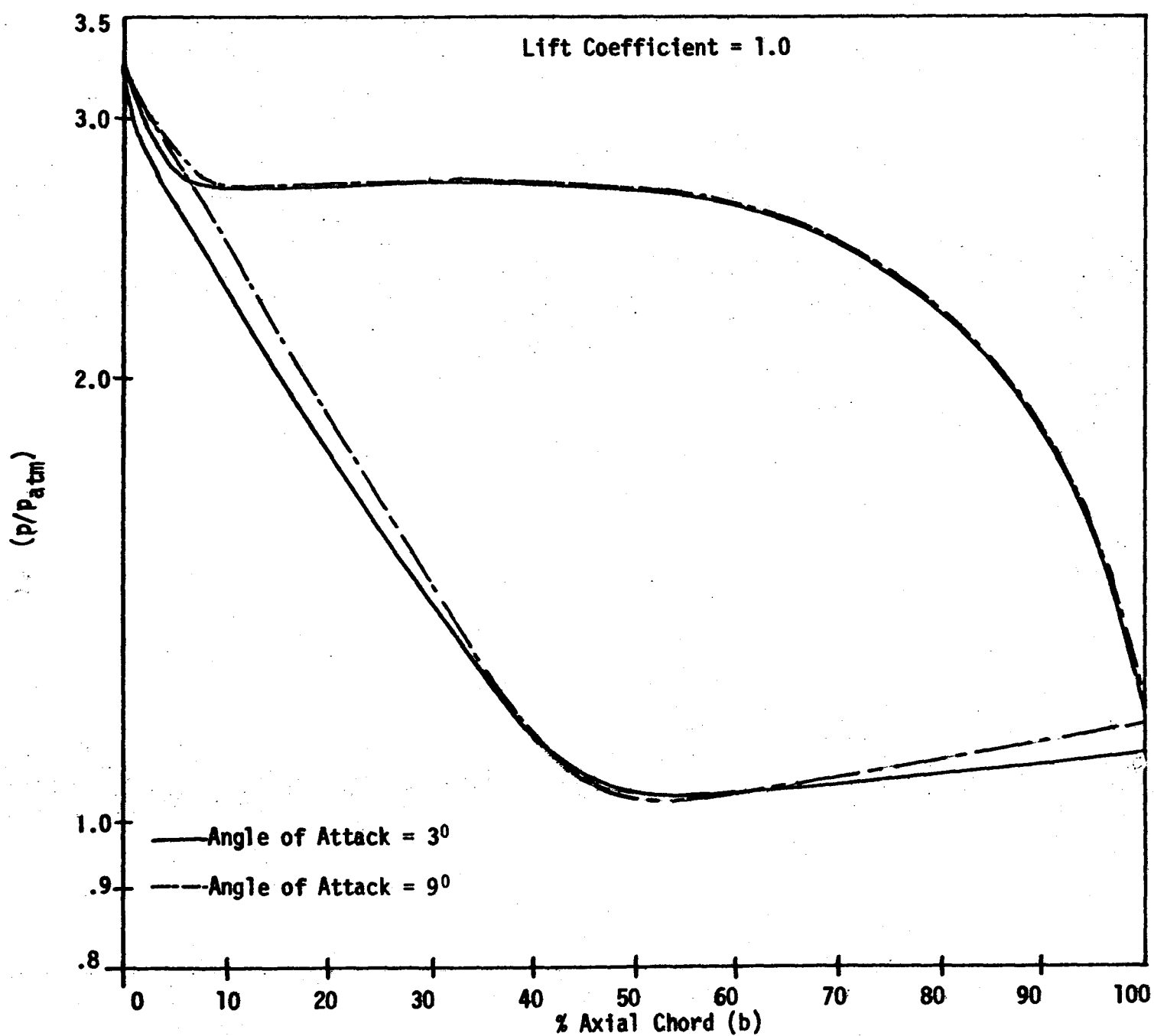


Figure 18(b) Pressure distributions around turbine blade of Turning angle 140°. as a function of incidence angle for constant lift coefficient.

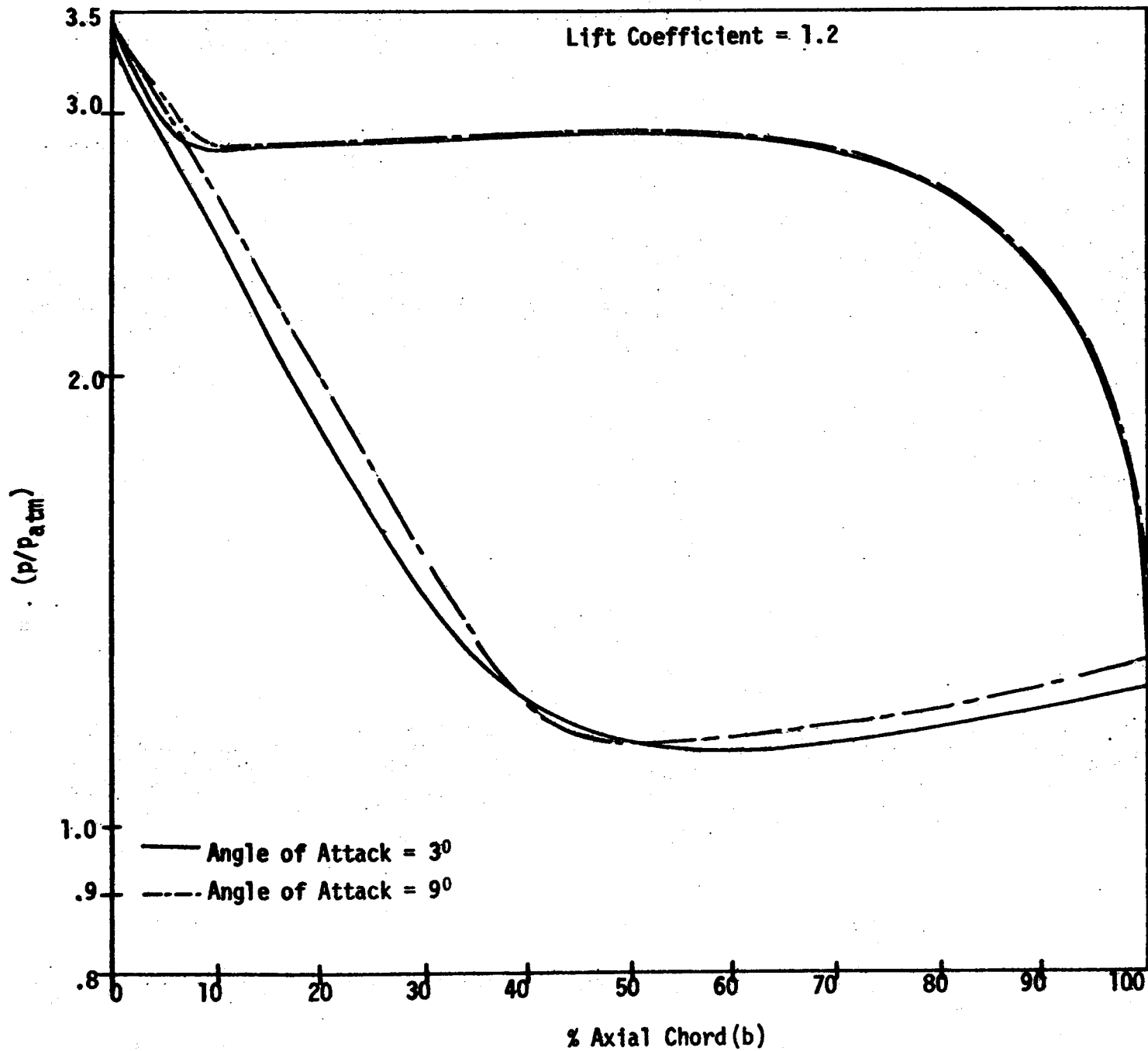


Figure 18(c) Pressure distributions around turbine blade of turning angle 140° as a function of incidence angle for constant lift coefficient.

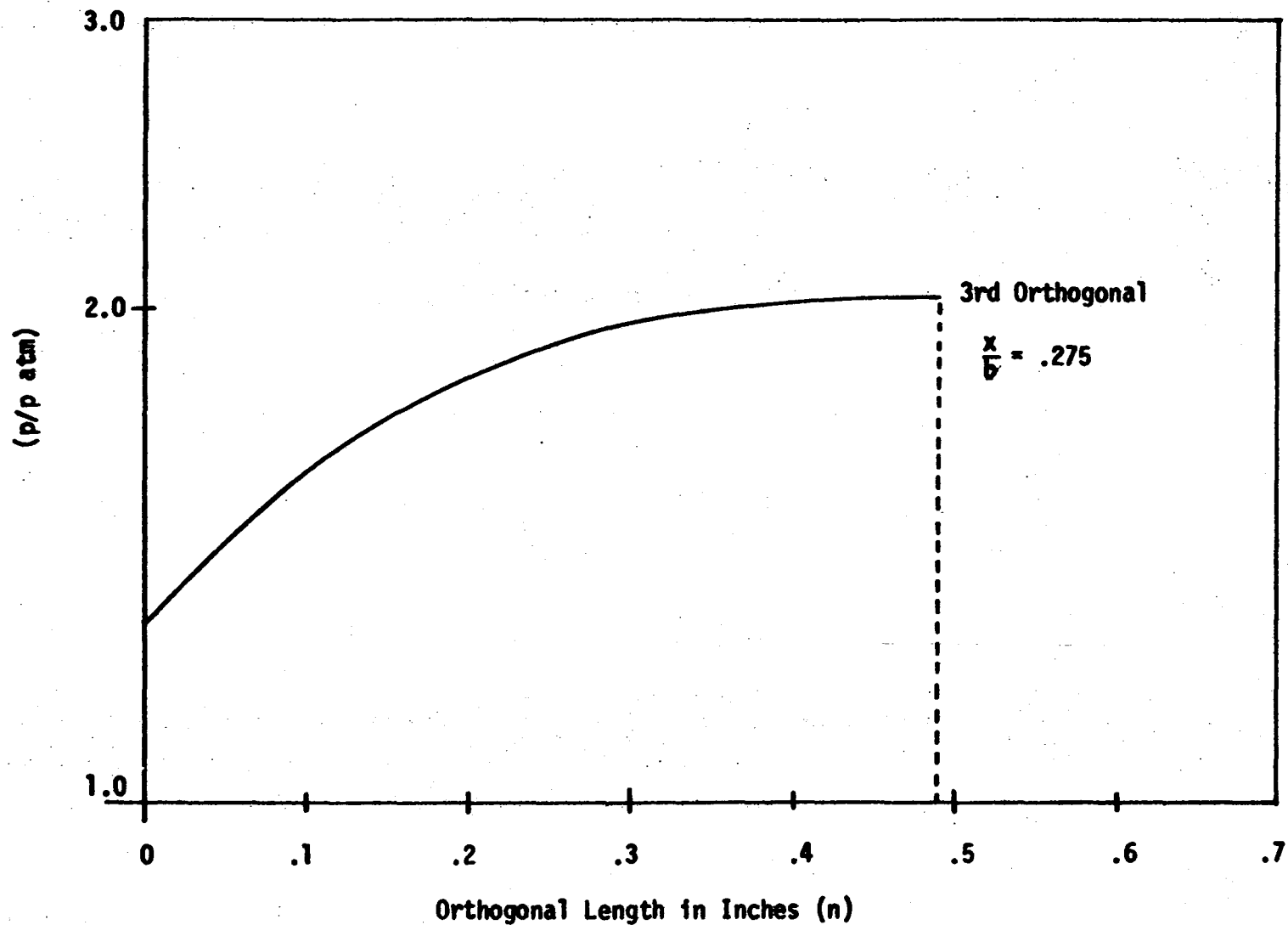
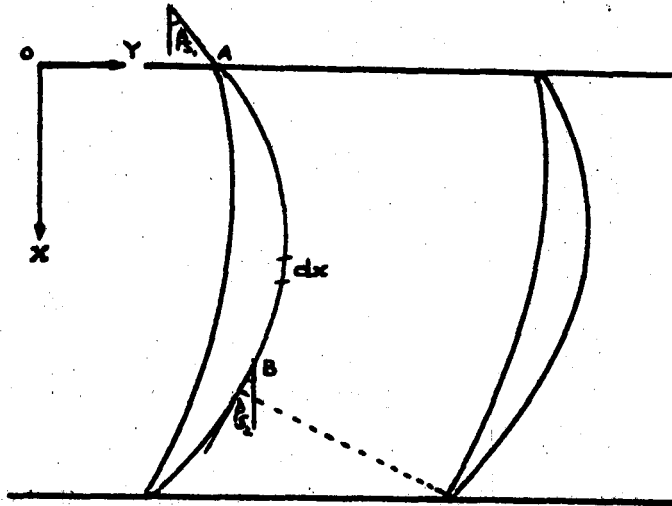


Figure 19. Pressure Distribution along an Orthogonal of Blade, Turning Angle 115° , Lift Coefficient = .8.

APPENDIX A

CURVATURE DISTRIBUTION AS A FUNCTION OF BLADE ANGLES



x, y are the co-ordinate axis.

Let R_s be the radius of curvature at any point (x, y) .

The area enclosed between the profile curvature (from A to B) and x-axis is given by

$$\text{Area} = \int_A^B \frac{1}{R_s} dx$$

as

$$R_s = \frac{[1 + (dy/dx)^2]^{3/2}}{d^2y/dx^2}$$

\therefore

$$\text{Area} = \int_A^B \frac{d^2y/dx^2}{[1 + (dy/dx)^2]^{3/2}} dx \quad (\text{A.1})$$

Putting $dy/dx = \tan \theta \quad \therefore \quad d^2y/dx^2 = \sec^2 \theta \, d\theta$

\therefore Equation (A.1) reduces to the following form

$$\text{Area} = \int_A^B \cos^3 \theta \, d\theta = \left| \sin \theta \right| \frac{B(\theta)}{A(\theta)}$$

As $A(\theta) = \beta_{S_1}$ and $B(\theta) = -\beta_{S_2}$

$$\therefore \text{Area} = \int_A^B \frac{1}{R_s} \, dx = \left| \sin \beta_{S_1} \right| + \left| \sin \beta_{S_2} \right|$$

APPENDIX B

DATA PERTINENT TO BLADES

Total Turning Angle (T.A) degrees	Blade Inlet Angle (α_1) degrees	Blade Outlet Angle (α_2) degrees	Lift Coefficient (C_L)	Pitch (s) inches	Axial Chord (b) inches
115	50	65	.8	.671	1
115	50	65	1.0	.839	1
115	50	65	1.2	1.0	1
128-30'	64	64-30'	.8	.520	1
128-30'	64	64-30'	1.0	.650	1
128-30'	64	64-30'	1.2	.780	1
140	65	75	.8	1.000	1
140	65	75	1.0	1.27	1
140	65	75	1.2	1.52	1

APPENDIX C

SAMPLE CALCULATIONS

For turning angle = 115° , Lift Coefficient = .8

$$\text{Let } \alpha_1 = 50^\circ$$

$$\therefore \alpha_2 = 65^\circ$$

$$\text{As } C_L = 2 \frac{S}{b} \cos^2 \alpha_2 (\tan \alpha_1 - \tan \alpha_2) \quad \text{C.1}$$

Putting values of C_L , α_1 , α_2 in equation C.1 one obtains

$$\frac{S}{b} = .671$$

$$\text{Let } b = 1''$$

$$\therefore s = .671$$

$$\frac{0}{S} = \cos \alpha_2 = .422''$$

$$\therefore 0 = .422 \times .671 = .284''$$

$$\beta_{s_1} = \alpha_1 + 15^\circ$$

$$= 50 + 15^\circ = 65^\circ$$

$$\beta_{s_2} = \alpha_2 - 10^\circ$$

$$= 65^\circ - 10^\circ = 55^\circ$$

$$\therefore |\sin \beta_{s_1}| + |\sin \beta_{s_2}| = 1.7$$

APPENDIX D

THE COMPUTER PROGRAM FOR PRESSURE DISTRIBUTION

This program determines the pressure distribution along an orthogonal line with the given values of gauging and radii of curvature at pressure and suction surfaces. Any number of sections can be fed along the blade surface and the values of pressure are obtained at nine points along each orthogonal and at every section. The program also gives the values of velocities and Mach numbers at all these points.

APPENDIX D.1

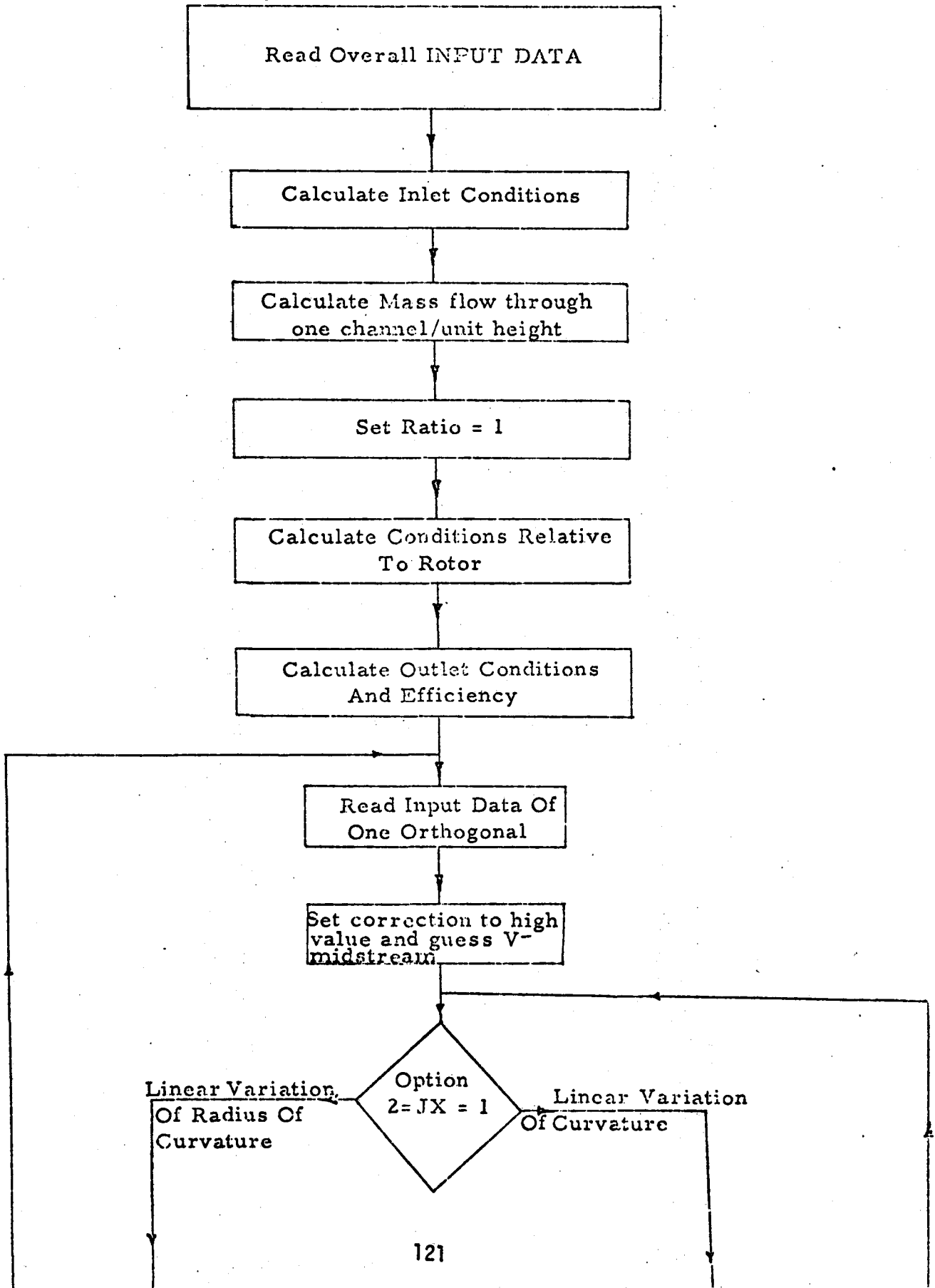
LIST OF SYMBOLS USED

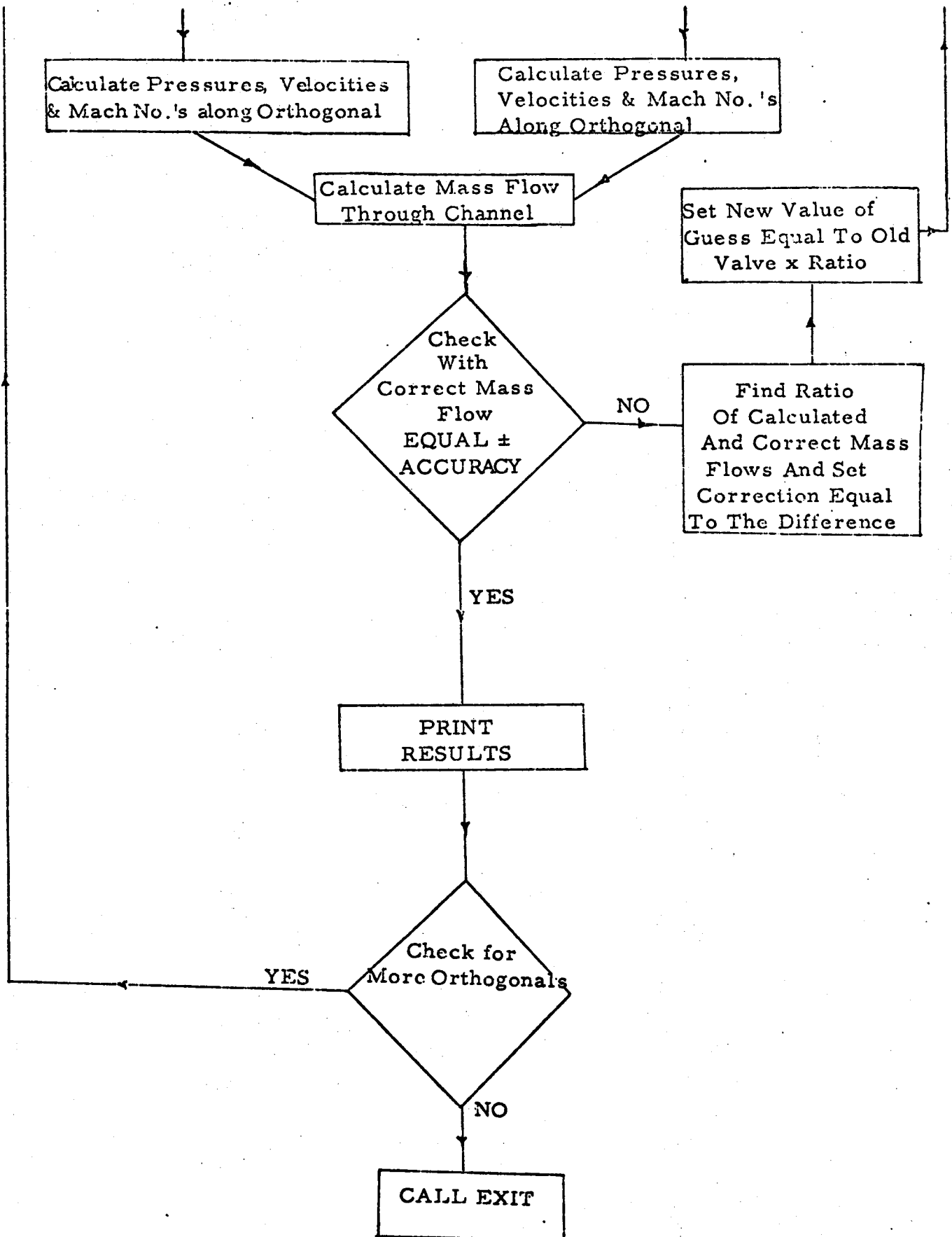
AMACH	Mach Number
AMAS	Design Mass Flow Through the Channel.
AP	Static Pressure.
AR	Density.
AT	Static Temperature.
AV	Resultant Velocity.
ACC	Allowable Difference between Design and Calculated Mass Flow.
COR	Correction for Iteration.
CP	Curvature of Pressure Surface.
CS	Curvature of Suction Surface.
D_1, D_2, D_3, D_4	Constants Containing gamma.
DELG	Distance between Two Adjacent Streamlines.
DELP	Pressure Loss through the Passage.
DIF	Difference between Two Assumed Velocities.
G	Gravitational Constant.
GAMMA	Ratio of Specific Heats.
GASC	Gas Constant.
GAUGE	Distance between Suction and Pressure Surfaces along an Orthogonal.
GUESS	Assumed value of Mid-channel Velocity at the beginning of Iteration.
GESS	Guess x Design Mass Flow/Calculated Mass Flow.

JX	An Input Index for the Choice of Type of Solution Needed.
POO	Total Inlet Pressure.
POW	$n_o (C_S (\frac{3}{8} - \frac{n}{n_o}) + \frac{1}{8} C_p \frac{1}{2} (C_p - C_S) \frac{n}{n_o})^2$
RATIO	Design Mass Flow/Calculated Mass Flow.
RELTOP	Relative Total Pressure.
RELTOT	Relative Total Temperature.
RETOPI	Relative Total Pressure at Entry.
RETOPO	Relative Total Pressure at Exit.
RO	Density.
RPR	Static Pressure.
RT	Static Temperature.
RVTI	Tangential Velocity at Inlet.
RVTO	Tangential Velocity at Exit.
SPACE	Spacing
TMAS	Calculated Mass Flow Rate in the Channel.
TOO	Total Inlet Temperature.
U	Blade Speed
VAX	Inlet Axial Velocity.
VCOR	Correction for Iteration.
W(1-9)	Velocity of Fluid at Streamlines, along the Orthogonal Line.
WCR	Velocity of Sound.
Z	Density x Velocity.

APPENDIX D.2

FLOW CHART





HVW2.

123

PUM(S)

SETINDF.

REDUCE.

LGO.

```
      6400 END OF RECORD
PROGRAM TST (INPUT,OUTPUT,TAPE5=INPUT,TAPE6=OUTPUT)
C      TOTAL TURNING ANGLE= 115 DEGREES, LIFT COEFFICIENT= .8
      DIMENSION W(9),RPR(9),Z(9),AMACH(9),DRPR(9)
      READ(5,14) U,VAX,RVTI
      READ(5,15) P00,EPO0,DELTA,T00
      READ(5,16) GASC,G,GAMMA,SPACE,JX
      READ(5,17) ACC
      READ(5,10) GAGE
10     FORMAT(F10.0)
14     FORMAT(5F8.2)
15     FORMAT(4F8.3)
16     FORMAT(4F8.4,I2)
17     FORMAT(F7.6)
      PATM=14.69
      D1=2.0*GAMMA*GASC*G
      D3=GAMMA-1.0
      D4=GAMMA+1.0
      D2=GAMMA/D3
      AV=(VAX**2+RVTI**2)**.5
      AT=T00-(AV**2)*D3/D1
      AP=P00/(T00/AT)**D2
      AR=144.0*AP/(GASC*AT)
      AMAS=AR*VAX*SPACE/12.0
      WRITE(6,24) AMAS
      RATIO=1.0
      RELTOT=T00-(2.0*RVTI*U-(U**2))*D3/D1
      RETOPI =P00*(RELTOT/T00)**D2
      RETOPO=RETOPI-DELTA
      DO 245 J=1,9
      READ(5,240) CP,CS,GAUGE
      COP=50.0
      GUESS=VAX*(GAUGE/GAGE)
```

```

48  VCOP=COP
    GESS=GUESS
    GUESS=GESS*RATIO
    W(5)=GUESS
52  IF(((W(5)**2)*D3/D1).LT.(RELTOT)) GO TO 51
    GUESS=GUESS/2.0
    W(5)=GUESS
    GO TO 52
51  CONTINUE
    D0235 I=1,9
    C=I
    DELG=(C-1.0)*GAUGE/8.0
    IF(JX.F0.1) GO TO 56
    IF(JX.F0.2) GO TO 57
56  POW=GAUGE*(CS*(3.0/8.0-DELG/GAUGE)+.125*CP-.5*(CP-CS)*(DELG
1/GAUGE)**2.0)
49  W(I) =W(5)*FXP(POW)
    GO TO 60
57  IF(CP-CS) 58,59,58
58  W(I)=W(5)*(2.0*(CP+(CS-CP)*DELG/GAUGE)/(CP+CS))*(GAUGE*CS
1*CP/(CP-CS))
    GO TO 60
59  POW=GAUGE*(.5-DELG/GAUGE)*CS
    GO TO 49
60  RELTOP=RELTOT
    RT=RELTOT-(W(I)**2)*D3/D1
    WCR=(D1/D4*RELTOT)**.5
    AMACH(I)=W(I)/WCR
    RPR(I)=RELTOT/(RELTOT/RT)**D2
    DRPR(I)=RPR(I)/PATM
    RO=144.0*RPR(I)/(GASC*RT)
235 Z(I)=RO*W(I)
    TMAS =(.03490*(Z(1)+Z(2))+.20760*(Z(2)+Z(8))- .03273*(Z(3)+Z(7))+
1.37023*(Z(4)+Z(6))- .16014*Z(5))*GAUGE/12.0
    COP =ABS(AMAS-TMAS)
    RATIO =AMAS/TMAS

```

```

        IF(COR-VCOR) 65,65,66
66      VCOR=10.0
        DIF=GUESS-GESS
90      RTMAS=TMAS
        GESS=GUESS
        GUESS=GESS+DIF/10.0
        W(5)=GUESS
89      IF(((W(5)**2)*D3/D1).LT.(RELTOT)) GO TO 86
        GUESS =GUESS/2.0
        W(5)=GUESS
        GO TO 89
86      CONTINUE
        DO251 I=1,9
        C=I
        DEL)=(C-1.0)*GAUGE/8.0
        IF(JX.F0.1) GO TO 46
        IF(JX.F0.2) GO TO 47
46      POW=GAUGE*(CS*(2.0/8.0-DELG/GAUGE)+.125*CP-.5*(CP-CS)*(DELG
1/GAUGE)**2.0)
50      W(I) =W(5)*EXP(POW)
        GO TO 200
47      IF(CP-CS) 281,291,281
291     W(I)=W(5)*(2.0*(CP+(CS-CP)*DELG/GAUGE)/(CP+CS))**((GAUGE*CS
1*CP/(CP-CS))
        GO TO 200
291     POW=GAUGE*(.5-DELG/GAUGE)*CS
        GO TO 50
200     RELTOP=RELTOT
        RT=RELTOT-(W(I)**2)*D3/D1
        WCP=(D1/D4*RELTOT)**.5
        AMACH(I)=W(I)/WCP
        RPR(I)=RELTOT/(RELTOT/RT)**D2
        DRPR(I)=RPR(I)/PATM
        RO=144.0*RPR(I)/(GASC*RT)
251     Z(I)=RO*W(I)
        TMAS =( .02480*(Z(1)+Z(9))+.20760*(Z(2)+Z(8))- .03273*(Z(3)+Z(7))+

```

```

1.37023*(Z(4)+Z(6))-0.16014*Z(5))*GAUGE/12.0
COR =ARS(AMAS-TMAS)
IF(COR-VCOR) 85,85,96
85  VCOR=COR
    GO TO 90
96  IF(ARS(RTMAS-TMAS).LF.ACC) GO TO 97
    GO TO 66
97  WRITE(6,28)TMAS
    DO 25 I=1,9
25  WRITE (6,29) I,RPR(I),AMACH(I),W(I),DRPR(I)
    GO TO 245
65  IF(COR-ACC) 61,61,48
67  VCOR=COR
61  WRITE(6,27)TMAS
    WRITE (6,30)
    DO 26 I=1,9
26  WRITE (6,29) I,RPR(I),AMACH(I),W(I),DRPR(I)
245 CONTINUE
24  FORMAT(1H1,40X,11HOUTPUT DATA/40X,11H----- // * DESIGN MASS
1FLOW RATE =*,F10.3)
27  FORMAT (1H0,5X,*CALCULATED MASS FLOW RATE =*,F10.3)
28  FORMAT (1H0,5X,*CHOKING MASS FLOW RATE =*,F10.3)
29  FORMAT (1H0,13,9X,F10.3,5X,X,F10.3,4X,F10.3,6X,F10.3)
240 FORMAT(3F10.0)
30  FORMAT (1H0,* I RPR(I) AMACH(I) W(I)
1 DRPR(I)*)
STOP
END
1 6400 END OF RECORD
650.1 260.03 962.1
42.2100 25.00 .000 816.0
53.30 32.20 1.40 .6710 1
.00020
.550
3.00 2.40 .550
5.6000 2.80 .520

```

6.76	2.800	.490
7.34	2.80	.420
6.00	2.80	.352
4.970	2.40	.320
3.86	1.60	.290
1.90	1.60	.283
.2	.2	.271

CD TOT 0153